AN INVESTIGATION INTO THE CONTAMINATION OF WSR-88D

VAD WIND PROFILE OUTPUT BY MIGRATING BIRDS

A Thesis

by

KARL WERNER SCHULZE

Submitted to the Office of Graduate Studies of
Texas A&M University
in partial fulfillment of the requirements for the degree of

MASTER OF SCIENCE

August 2003

Major Subject: Meteorology

AN INVESTIGATION INTO THE CONTAMINATION OF WSR-88D

VAD WIND PROFILE OUTPUT BY MIGRATING BIRDS

A Thesis

by

KARL WERNER SCHULZE

Submitted to Texas A&M University
in partial fulfillment of the requirements
for the degree of

MASTER OF SCIENCE

Approved as to style and content by:

John W. Nielsen-Gammon (Chair of Committee)	Richard E. Orville (Member)
Keith A. Arnold (Member)	Gerald R. North (Head of Department)

August 2003

Major Subject: Meteorology

ABSTRACT

An Investigation into the Contamination of WSR-88D

VAD Wind Profile Output by Migrating Birds. (August 2003)

Karl Werner Schulze, B.S., Northern Illinois University

Chair of Advisory Committee: Dr. John W. Nielsen-Gammon

The VAD Wind Profile (VWP), a time-height display of winds computed by the National Weather Service's WSR-88D radar, is known on occasion to have errors at night during the fall and spring seasons. Several studies, such Haro and Gauthreaux (1997), confirm that migrating birds often contaminate the VWP output. By means of telescopic observations of a full moon, birds were observed flying on two nights when VWP contamination was suspected. The nature of the VWP errors is consistent with migrating birds due to the seasonality, nocturnal nature, and the magnitude of the errors found (greater than 10 knots).

With careful selection of data, two clusters of points on the Velocity-Azimuth Display (VAD) are found to exist at certain altitudes when birds begin migrating. One cluster of points is due to radar sample volumes containing birds, and the other cluster is from radar sample volumes without birds. Being able to determine which cluster represents the wind could allow the wind to be calculated by the VWP.

Present limitations with the Radar Product Generator's processor and memory prohibit a very advanced detection algorithm. Two simple objective techniques to determine the existence of the two clusters, and determine the wind, were tested. While

they show some promise, these methods require further operational testing to determine their usefulness for real-time warning of bird contamination and the reporting of the true wind.

DEDICATION

I wish to dedicate this thesis to several very important people who have made it all possible in one way or another.

First of all, I wish to dedicate this thesis to my parents, Werner and Mary Schulze. Their many years of unconditional support, understanding, and love have given me the freedom and ability to pursue my dreams, even though I tended to stray way off course occasionally. Thanks for the love and support, Mom and Dad!

I also wish to dedicate this thesis to Jeanne Lambrecht. Her ability to succeed and her ability to love others, despite many obstacles, make her my role model. Her years of continued love and support have helped me to stay afloat during the tough times I have encountered. Despite our divorce, I am thankful that we have remained best friends. Thanks, Jeanne!

Last, but certainly not least, I wish to thank my fiancée - Larisa Timofeyeva! Without the hope and promise of starting things anew, it would have been more difficult to finally complete this thesis. My strong wish to be with her was the motivation to finally kick things into high gear, and she was the bright and beautiful light at the end of the tunnel. I love you very much, Larisa!

ACKNOWLEDGEMENTS

I would like to express my deep gratitude to my advisor, Dr. John W. Nielsen-Gammon. His support and understanding during the difficult times I faced allowed me to finish this thesis. His knowledge and expertise proved very useful as I worked on this thesis. I appreciate very much all your time and effort, John!

I also thank my other committee members, Dr. Keith A. Arnold and Dr. Richard E. Orville for their insight and assistance during the completion of this thesis. My thanks also go out to Dr. Michael I. Biggerstaff, who was on my committee before his departure to the University of Oklahoma. His radar knowledge and assistance was very valuable to me.

In my many years here at Texas A&M, I have come to know many fellow students with whom I have developed friendships. They are too numerous to mention; you know who you are. Their companionship both inside and outside the weather classroom has been a treasure, and I look forward to continuing my friendship with them in the years to come. In particular, I would like to thank Brandon Ely for his assistance with the IDL programming language, and Scott Steiger for his assistance with WATADS.

Finally, thanks go out to Paul Sirvatka for helping me get my foot in the door at the College of DuPage! Both he and his wife Cathy have provided me with a lot of support and encouragement to finish this thesis, and I thank them very, very much!

TABLE OF CONTENTS

LIST OF FIGURES

FIGURE Page

LIST OF TABLES

CHAPTER I

INTRODUCTION

Commencing in 1990, the United States National Weather Service began to replace their outdated weather radars, built in the 1950s through the 1970s, with a far more advanced Doppler radar: the WSR-88D. In addition to being able to detect the radial velocities of the targets, the newer radars were more powerful, more sensitive, had higher resolution, and possessed digitized output to allow computers to process and display computer algorithm products in real-time (Klazura and Imy 1993). The National Weather Service would be able to use radar for purposes beyond the simple detection of precipitation. The WSR-88D would allow computer algorithms to assist meteorologists in critical areas, such as detecting storm rotation that can precede tornadoes, calculating the amount of rainfall that fell over a given area in a certain period of time, and many other possibilities.

The National Weather Service office near Houston, Texas had one of the first WSR-88D units installed. Beginning in 1993, Mr. Steve Allen, the Science and Operations Officer at that office, periodically noticed something amiss with one particular algorithm product: the VWP, or VAD (Velocity Azimuth Display) Wind Profile (see Fig. 1). During the late summer and early fall months at night, the winds displayed on the VWP would be at large disagreement with the winds measured directly (by radiosondes) or inferred based on synoptic meteorological analysis. At times, Mr.

_____

This thesis follows the style and format of the *Journal of Atmospheric and Oceanic Technology*.
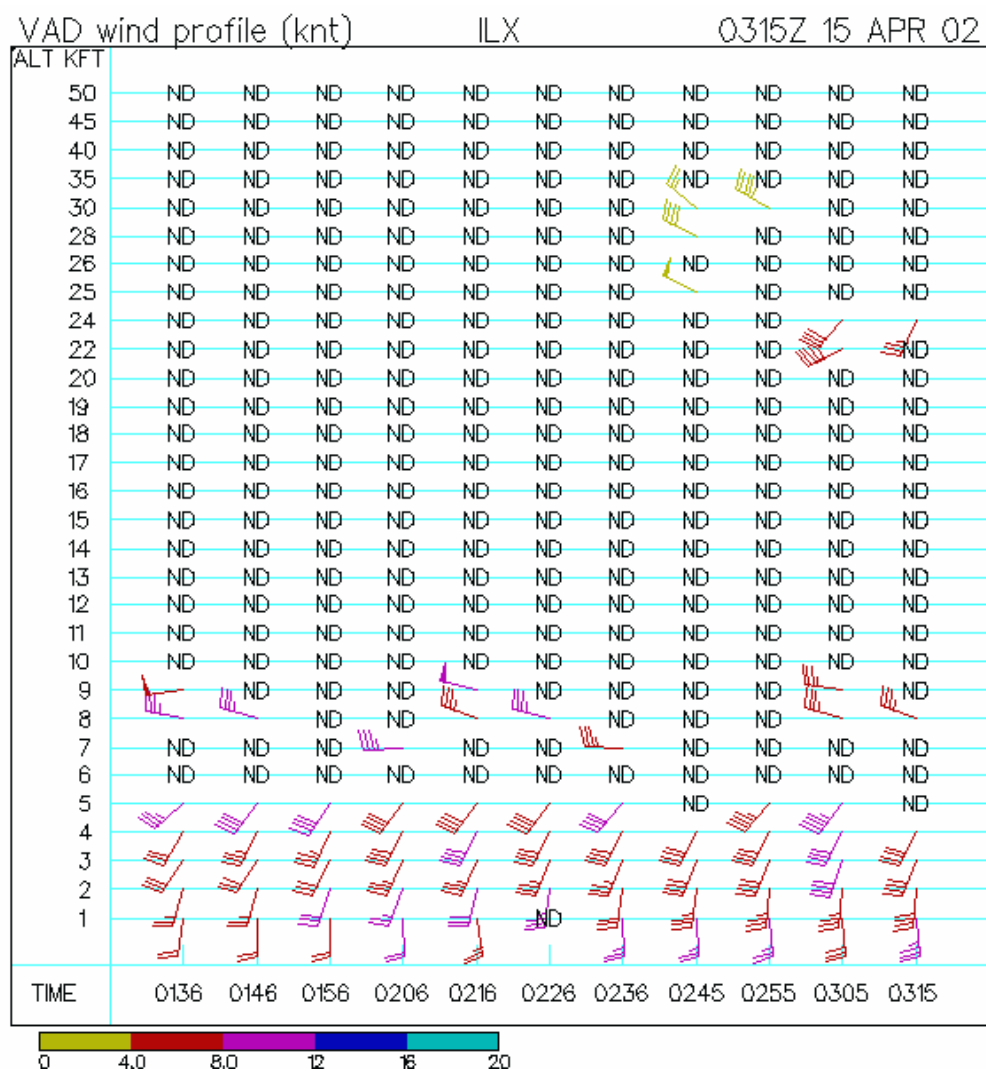
Fig. 1. Example of the VAD Wind Profile (VWP) output from the WSR-88D at Lincoln, Illinois (ILX) on April 15, 2002 at 3:15Z[1]. Time (Z) is plotted on the abscissa increasing from left-to-right. Height (in thousands of feet) is plotted on the ordinate. The wind barbs follow the standard meteorological format (barbs pointing towards the compass direction where the winds are blowing from; full flags are 50 knots, full barbs are 10 knots, and half barbs are 5 knots). The colors of the wind barbs reflect the root mean square error of the wind estimate according to the scale shown at the bottom. "ND" is written when no wind estimate can be computed.

---

[1]Universal Coordinated Time (abbreviated at UTC or simply Z); 5 hours ahead of Central Daylight Time.

Allen found the VWP-derived winds to be opposite in direction and double the speed of the geostrophic wind. During these times, there were radar echoes on the screen translating with velocities consistent with the VWP winds. Just prior to sunrise, these targets would disappear and the VWP-derived winds would return to agreement with the observed wind.

The fact that the VWP-derived winds can be erroneous at times is a significant problem. First of all, VWP output is used to initialize some atmospheric models, such as the RUC, or Rapid Update Cycle (Benjamin et al. 1994). The performance of such models could be hindered due to either the inclusion of erroneous data or to the omission of the valuable VWP data if the reason for the errors could be removed prior to being used in the model. Second of all, the faulty VWP output could lead the unsuspecting meteorologist to erroneous conclusions about the atmosphere, leading to incorrect forecasts. Steve Allen (1996, personal communication) noted an instance when a tornado watch was issued for the Houston area based primarily on the wind shear shown on erroneous VWP output. Aviation forecasters are also known to use the VWP output for pilot briefings and to forecast turbulence. Finally the echoes, if caused by targets other than hydrometeors, would cause the WSR-88D to produce false rainfall accumulations if the radar is running in precipitation mode.

I will be attempting to solve two problems with my research. The first problem is to identify the targets responsible for the VWP errors. The second problem is to determine whether or not the VAD algorithm can be amended (using methods and technology currently available with the WSR-88D) to warn the user of contaminated

data, and perhaps even allow the true wind to be determined by removing the spurious targets from inclusion in the VAD algorithm calculations.

Chapter II of this thesis will disclose the temporal and qualitative nature of VWP contamination, and will describe the method used to identify the targets causing the erroneous VWP calculations. Two early case studies will be discussed, showing the impact of VWP contamination. Chapter III will cover an overview of the many disciplines involved with this problem. Included in this literature review will be background information on the behavior of the targets, the relationship between their appearance and atmospheric conditions, the manner in which radar can detectable them, the VAD algorithm and how it computes the winds, and finally previous articles that have addressed contamination of the VWP product. Chapter IV will show my attempts at finding a solution to the problem using existing WSR-88D technology, and discuss the results. Chapter V will close this thesis with conclusions.

Much of the data shown in this thesis arose from the Texas Air Quality Study 2000 (hereafter referred to as TexAQS) project conducted in Houston between August 15, 2000 and September 23, 2000. While that project focused on the study of ozone concentrations in Houston, the resulting radar and weather balloon data collected during that project are valuable to this investigation. The operational dates of this project were over the time of year of interest (fall). Tapes of level-II archive data from the Houston WSR-88D during this study will be used in chapter IV to find solutions to the problem. As a result, this thesis will primarily focus on the anomalous VWP output from the

Houston/Galveston National Weather Service Office's WSR-88D, although the results of this research could possibly be used elsewhere.

While data were collected using the Aggie Doppler Radar (ADRAD) on top of the Eller Oceanography and Meteorology building on the Texas A&M campus, I have not included those data in this thesis. One reason is the data had many spurious echoes on the display that were not attributable to birds and most likely were caused by technical problems with the radar itself. The second and primary reason is the data from the ADRAD, which is a totally different radar system from the WSR-88D, would be superfluous. It is more important to focus on the data from the WSR-88D in order to understand the problem as it applies to its own data and VWP product.

CHAPTER II

PROBLEM

Steve Allen at the Houston National Weather Service office noted that the erroneous VWP output seemed to follow a certain temporal regularity (1996, personal communication). Such temporal characteristics included:

- The erroneous data only occurred in the late-summer to early-fall months. He did not report to me any occurrences that took place in the spring.

- Prior to sunset, the radar PPI would show typical daytime reflectivity characteristics owing to refractivity gradients, insects, dust, and other particulates in the atmosphere. The VWP output would be consistent with the observed wind field from weather balloons, aircraft, and meteorological analysis.

- The typical daytime reflectivity observed would diminish with time as evening approached and the sun disappeared below the horizon.

- Approximately 30 to 45 minutes after sunset, the radar screen would start to fill up with echo from targets that were moving at a different velocity than the observed wind field. This different velocity would be from the north to northeast, despite what the actual winds were. From this moment on, the VWP output would be in error with the observed wind field.

- The targets would increase as the night went on, often times filling up the radar PPI with echo. In addition, the heights at which the targets were

detected would continue to increase as time passed, causing the erroneous VWP winds to be reported at higher and higher altitudes.

- The targets producing the erroneous VWP data would disappear approximately 30 to 45 minutes prior to sunrise.

- After the targets disappeared off the radar screen, the VWP output would resume showing the correct winds.

Assuming that the targets detected by the radar during the erroneous VWP-derived winds actually exist, the conclusion that must be reached is that the targets are engaged in powered flight. The targets cannot be wind-borne, since weather balloons and synoptic weather analysis show the wind to be different from the targets' movement. Furthermore, because the VWP-derived winds are as much as 40 knots in error, the targets must be capable of flying at such speeds. Based on these velocity values, and based on the distinct seasonal and diurnal nature of the problem, the only obvious explanation is that the targets are migrating birds. The birds must be migrating because the observed erroneous VWP-derived winds in the fall over Houston are always from the NE or E, whereas random bird activity at night would produce random VWP-derived winds, if any conclusive direction at all. In the fall, bird migrations would certainly be heading south towards Mexico.

1. Proving Birds Are the Source of Anomalous VWP Winds

The first objective of my research was to show that birds were flying at the time of the VWP errors, and that their direction of flight could support the idea that they are

migrating. I started doing an extensive literature search in ornithological journals, looking for established methods of observing bird migrations, other than radar. Because the type of bird movements I hoped to observe were nocturnal, I had to find methods that could be performed particularly at night.

Fortunately, a method has been developed for not only observing bird migrations at night, but also quantifying them (Lowery 1951). This technique allows for the observation and quantification of night migrants, as well as information on the direction of movement, by looking for birds flying in front of a full moon through a telescope. Birds that fly through the volume of air being observed will appear as a dark silhouette against the bright disk of the moon (see Fig. 2). The path that the silhouette makes across the disk of the moon is recorded by noting the entry and exit point on the moon's face as it relates to the face of a clock (with 12 o'clock on top). There is a vertical limit to how high a bird can be observed visually through a telescope, and Lowery determined this flight ceiling to be one mile (in part to simplify the later calculations).

Several factors make this method a very complicated one. First, the cone of observation and its volume changes as the moon moves across the sky. When the moon is directly overhead, the volume observed will be of a smaller size than when the moon is low on the horizon. The differing volume affects the ease by which a bird is detected. It also affects any attempt to compare the number of birds flying from one hour to the next. More migrants observed at an hour when the moon is lower in the sky doesn't mean that there were more birds flying at that particular time. Fig. 2 illustrates the problem involved when the volume changes with time.
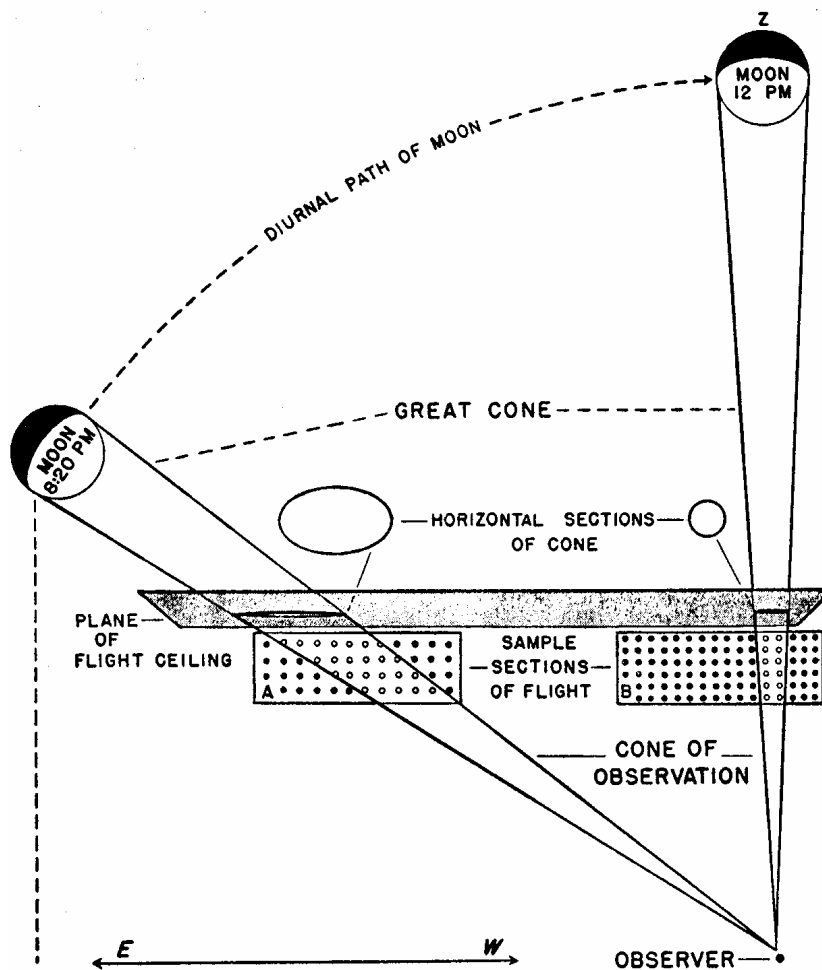
Fig. 2. Diagram of Lowery's moon-watching technique. (From Lowery 1951). The circles inside the rectangles represent birds, some of which are seen by the observer through the cone of observation.

Fig. 2 shows that while more birds are flying at 12 p.m. than are flying at 8:20 p.m., more are counted at 8:20 because of the larger observing volume size. Therefore, changes in the observation volume must be taken into account when performing any calculations.

The accuracy of determining the bird's true flight path also changes with the position of the moon. If the moon is directly overhead, a person observing a bird flying in front of the moon is directly below the bird and can determine the horizontal direction of flight very accurately (because there is no oblique viewing angle). If the moon is directly on the horizon, no accurate determination of the actual flight heading of the bird can be made. A bird seen moving from 9 o'clock to 3 o'clock with the moon on the horizon can be heading in any direction that has a component towards the south to it.

Lowery and his colleagues developed a method to take the observed flight path across the moon's face and attempt to convert it into the actual compass heading of the bird. They made the primary assumption that the birds fly along a horizontal plane. Bruderer (1997b) states that many small or medium passerines fly in what is described as undulating flight where there is alternating flapping (to gain altitude) and pausing phases (where altitude decreases and airspeed increases). Therefore, it is possible that the birds observed could have a vertical component to their apparent paths across the face of the moon. Any vertical component that exists will cause an error in the calculated compass heading of the bird. A second assumption that is made in the flight path calculation is that the Earth is flat, which for such a local area of observation is a reasonable approximation to make.

Because of the potentially large errors involved in Lowery's method of calculation, Nisbet (1959) greatly simplified Lowery's technique without introducing larger errors in the process. Nisbet's technique involves solving the following equation:

$$\tan (\tfrac{1}{2}\pi + \eta + Z) = \operatorname{cosec} A \tan B \tag{1}$$

where η is the bird's actual flight direction, Z is the azimuth angle of the moon, A is the altitude angle of the moon, and B is the angle of apparent direction that the bird's path across the moon took. B is measured counterclockwise from the 9 o'clock to 3 o'clock line. Nisbet made the mathematical solution quite simple by printing various tables, thereby eliminating the need to solve equation 1 by hand.

Lowery also offers a technique to quantify the number of migrants flying. Lowery decided to express the quantity flying in terms of the number of birds flying past a mile front (line) per hour. For this calculation, Lowery assumed that the birds flying below the one-mile ceiling are evenly distributed, and that no birds are flying above the ceiling.

Calculating the density crossing a one-mile front is not as simple as just multiplying the number of birds observed through the cone of observation by the number of cones that would fit in one mile. Fig. 3 illustrates this problem. In Fig. 3a, the observer sees three birds crossing the square observational area. If the observer multiplies their number of observations by sixteen (the number of observational areas that would fit in the desired square mile), their result is forty-eight birds per square mile. From Fig. 3a, it is clear that the actual number crossing that square mile is either four or eight, depending on the orientation of the front.
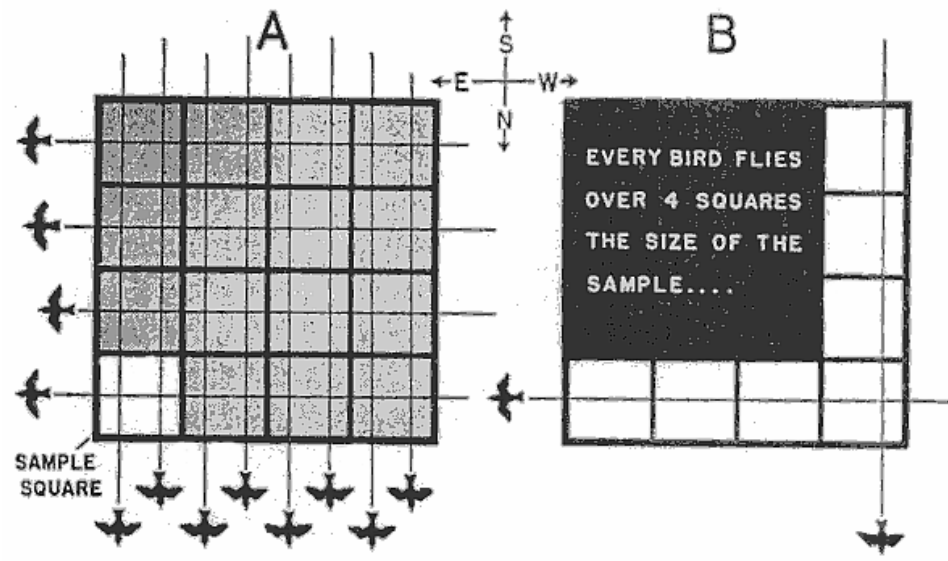
Fig. 3. (a) Illustration that the area of observation is not the simple ratio to the larger area sought. (b) Reason why simply converting the sample area to the total area fails (From Lowery 1951).

The problem lies in the fact that the birds are flying in different directions and the same bird can be counted more than once by this simple method, as shown in Fig. 3b. The solution to this problem that Lowery developed was to separate the birds observed into sectors of 22 ½ degrees wide. By doing this, we can calculate the number of birds crossing a mile front for each sector, and Lowery called this number the sector density. The total density of birds flying past the mile front would be the sum of the sector densities.

The number of birds observed in each sector would be multiplied by a correcting factor, given by the following equations:

$$X = 240 \sin^2 A, \text{ and} \tag{2}$$

$$Y = 240 \sin A \tag{3}$$

where A is the altitude angle of the moon (Nisbet 1959). Because the altitude angle of the moon changes throughout the night, Lowery and Nisbet both require that this calculation be performed for each hour of observation separately, with the angle A to be used at the middle of the observational hour involved. The correction factor X is to be used when the flight paths across the moon is more or less horizontal (i.e., 8 o'clock to 3 o'clock), whereas the correction factor Y is to be used when the flight paths are more or less vertical.

Just as with the calculation of flight directions, the calculation of flight density can be prone to many errors. Liechti et al. (1995) highlighted many of the errors that can happen which will affect the flight density calculations (and the flight directions as well). Observations made by a human observer were compared with observations that

were made by both radar and a passive infrared system, which were observing the same sample volume as the human observer. Results from Liechti et al. (1995) show that observers missed half of the birds that flew at a distance of 1.5 kilometers away. Many of the birds were missed because they flew along the edge of the moon and weren't noticed, or were flying too high to be observed by the naked eye. Fatigue (including eye strain), inattentiveness, and other human factors also cause some birds crossing the observer's field of view to be missed.

The study from Liechti et al. (1995) also showed differences between human observers based on prior experience; inexperienced observers missed half of the birds. I would certainly consider myself as inexperienced, so my flight density results are most likely on the conservative side.

Despite serious accuracy concerns, the moon-watching technique is the only method available to me to directly observe birds migrating at night. Even if the quantitative results of the moon-watching technique are questionable, the qualitative nature of the observations (whether birds were seen at all) is valuable to confirm that birds were flying on evenings when the VWP is in error.

2. Case Studies

a. August 19-20, 1997

My first attempt to visually identify birds being airborne using the moon-watching technique was on the full-moon evening of August 19th and 20th, 1997. For this task, I used telescopes furnished by the Department of Physics at Texas A&M

University. Because I was working alone, I made use of a video camera with the time stamp running to record the time of observation, and to record my voice as I announced the entry and exit points of the birds that I observed fly across the moon's face, as well as any additional comments I felt important to make. Data regarding the moon's azimuth and altitude angle at the time of observation were obtained from the website of the Naval Observatory, which provides this information for any locality in the United States in five-minute intervals (USNO 1997).

Using my observations and the moon data on this evening, I computed the flight heading of the bird according to Nisbet's technique. Results of my observations for this night are summarized in Table 1. The total flight density for the period of observation (approximately two and a half hours) was 900 birds per mile.

From the observation results listed on Table 1, one can see that there was no consistent flight heading of the birds observed on this evening. Breaking down the observations in regards to the size of the silhouette observed, small silhouettes were observed flying towards the north whereas large-sized silhouettes were generally flying towards the south.. The remarks indicate that some of the large silhouettes I observed had flight paths that changed as they passed across the face of the moon.

The size of the silhouettes depends on both the size of the bird and the distance between the bird and my position. Assuming that all the birds were of the general songbird size, their size corresponds directly to the altitude that they are flying at. The larger the silhouette was, the faster they moved across the face of the moon. Therefore, it is entirely possible that the larger silhouettes were caused by nocturnal bird species not

Table 1. Moon-watching results from the night of August 19-20, 1997. Time is given in Z. The columns "In" and "Out" refer to the position of a clock face where the birds were observed entering and exiting the moon's disk, respectively. The remarks column contains any additional comments that were made during the observation. The flight heading column lists the bird's compass flight heading calculated using the procedures outlined by Nisbet (1959).

Time (Z)	In	Out	Remarks	Flight Heading (Towards)
2:58			Began Observations	
3:01	2:00	10:30		39
3:02	4:00	12:00	Odd flight path – curved upwards	97
3:04	8:00	2:30	Large silhouette (low), fast	246
3:22	7:30	4:00	Large silhouette, curved upwards	219
3:25	5:00	6:00	Small	54
3:30	9:30	2:00	Large	221
3:35			Stopped Observations (break)	
3:48			Resumed Observations	
4:03	4:30	9:00	Small	354
4:10	4:30	10:30	Very small	2
4:18	11:30	3:30	Large, fast	155
4:55			Stopped Observations (break)	
5:03			Resumed Observations	
5:03	6:00	9:00		349
5:03	9:30	1:00		254
5:04	10:00	4:00	Large, fast	185
5:04	8:00	2:00	Small	263
5:08	12:00	1:30	Medium-sized	195
5:28			Concluded Observations	

migrating (owls), or other flying animals such as bats. The very quick travel across the face of the moon did not allow me to observe any features which would identify the silhouette as a bat, rather than a bird, so they can not be discounted as a cause for some or all of the larger silhouettes.

Because the larger silhouettes may not be birds, and because birds observed may not be migrating at the time, we should treat the large silhouette observations with suspicion. Because the remainder of the silhouettes observed were flying in a seasonally inappropriate direction, a thorough review of bird migratory behavior will be required. This will be done in chapter III, and an attempt to explain this odd behavior will be made at that point.

We now need to consult with surface and upper-level weather charts in order to determine if the VWP product for this evening was in error. Fig. 4 shows the surface weather conditions for the Texas area nearest to the time of moon-watching observations (3Z). For College Station, it was a warm night (87 degrees Fahrenheit) with light winds (5 knots) from the south-southeast.

The winds aloft were also quite light. Fig. 5a shows the weather conditions at the pressure level of 850-millibars (hereafter abbreviated as mb), and Fig. 5b shows the weather conditions at the pressure level of 700-mb, both at a time of 0Z. At Corpus Christi, Texas (the nearest radiosonde location to New Braunfels), the height of the 850-mb level was 1551 meters (or approximately 5090 feet) above mean sea level, and the wind was from the south-southwest at 10 knots. The height of the 700-mb surface at Corpus Christi was 3204 meters (or approximately 10,510 feet), and winds were
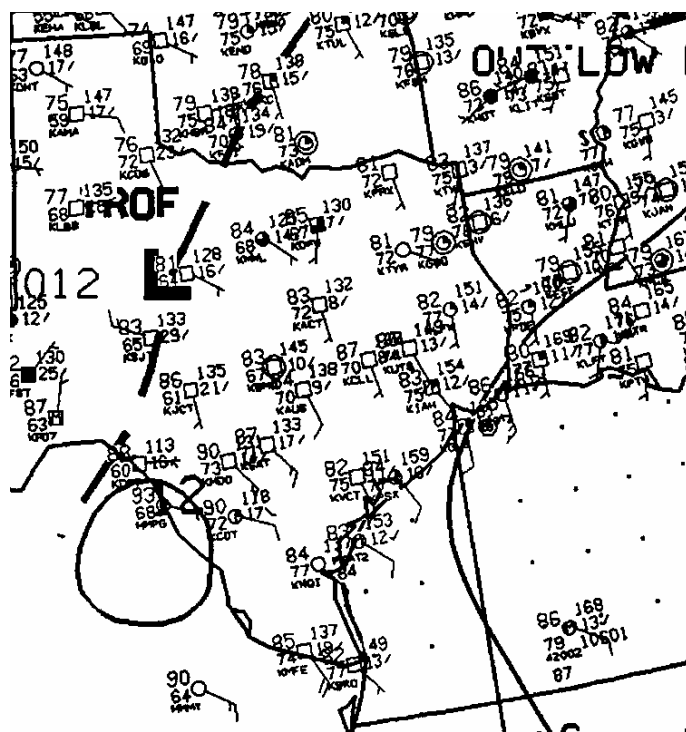
Fig. 4. Surface weather chart from 3Z on August 20, 1997. Wind is depicted in the same manner as the VWP example in Fig. 1. The number at upper-left from the circle is the temperature (Fahrenheit), the lower-left number is dew point temperature (Fahrenheit), the four letters found below the dew point is the station four letter identifier (KCLL = College Station), the upper-right number is sea-level pressure (in millibars, with leading 10 and decimal point between last two digits omitted; 145 = 1014.5-mb). The station circle will be filled according to cloud cover (filled circle for overcast, empty for clear skies, etc.). The dashed line denotes a pressure trough (marked TROF) and the solid lines are isobars (drawn every 4-mb; the line near Houston is the 1016 isobar). The large L denotes a developing low pressure area.
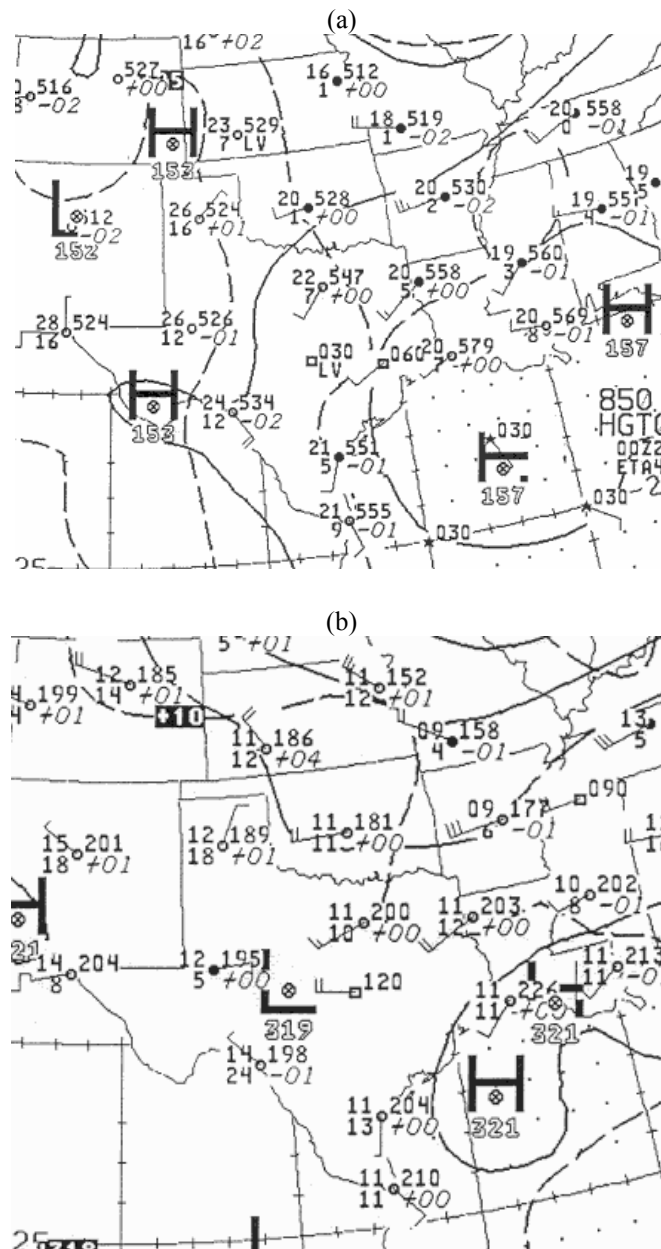
Fig. 5. Upper-air weather charts from 0Z on August 20, 1997 for the (a) 850-mb pressure surface, and (b) 700-mb pressure surface. Wind is depicted in the same manner as Fig. 1. The stations denoted with circles are radiosonde launch sites; those denoted with squares are from aircraft and are ignored. The upper left number for each radiosonde station is the temperature (in Celsius), the lower left number is dew point depression (in Celsius), the upper right number is the height of the pressure surface (in meters; leading 1 omitted in Fig. 5a, leading 3 omitted in Fig. 5b. Station circles are filled if the dew point depression is 5 degrees or less. Dashed lines are isotherms (drawn every 5 degrees Celsius) and solid lines are isoheights (drawn every 30 meters). H and L signify relative high heights and low heights, respectively.

measured at 5 knots from the south. These are the winds that one would expect from the VWP for that evening. However, the WSR-88D was calculating winds that were quite different from these observations.

Fig. 6 is the VWP produced by the WSR-88D Algorithm Testing and Display Software, hereafter referred to as WATADS (NSSL 1997). The algorithm and output appearance is not an exact replication of the WSR-88D VWP, but it is a close approximation. Fig. 6 shows the VWP from New Braunfels beginning at 1:10Z. Sunset on this date was at 1:09Z. Beginning at 1:59Z, winds above 8000 feet started to appear from the north on the VWP, and these winds proceeded to be reported from a higher and higher altitude with time. Winds below 8000 feet remained with their directional heading, but increased from 10 knots up to 20 to 25 knots by 2:39Z.

Fig. 7 is a continuation in time of the VWP output from Fig. 6. The same feature can be seen in the reported winds: from the north above 8000 feet, and strong out of the south below 8000 feet. Winds between 8000 and 11,000 feet were calculated to be light out of the west. The altitude of VWP reported winds increases up to 25,000 feet in this figure.

Fig. 8 is VWP from a bit later in the night, from 4:27Z to 5:55Z. The winds reported by the VWP remain consistent from the prior figures. This remains to be the case until sunrise. Fig. 9 is VWP output from 11:41Z to 12:34Z. Sunrise occurred at 12:03Z on this day. The height of the reported winds drops to a maximum of 11,000 feet, and the wind speed above 4000 feet reduces to 5 to 15 knots at 12:05Z. Some winds from the north remain on the VWP after sunrise, but they aren't as strong.
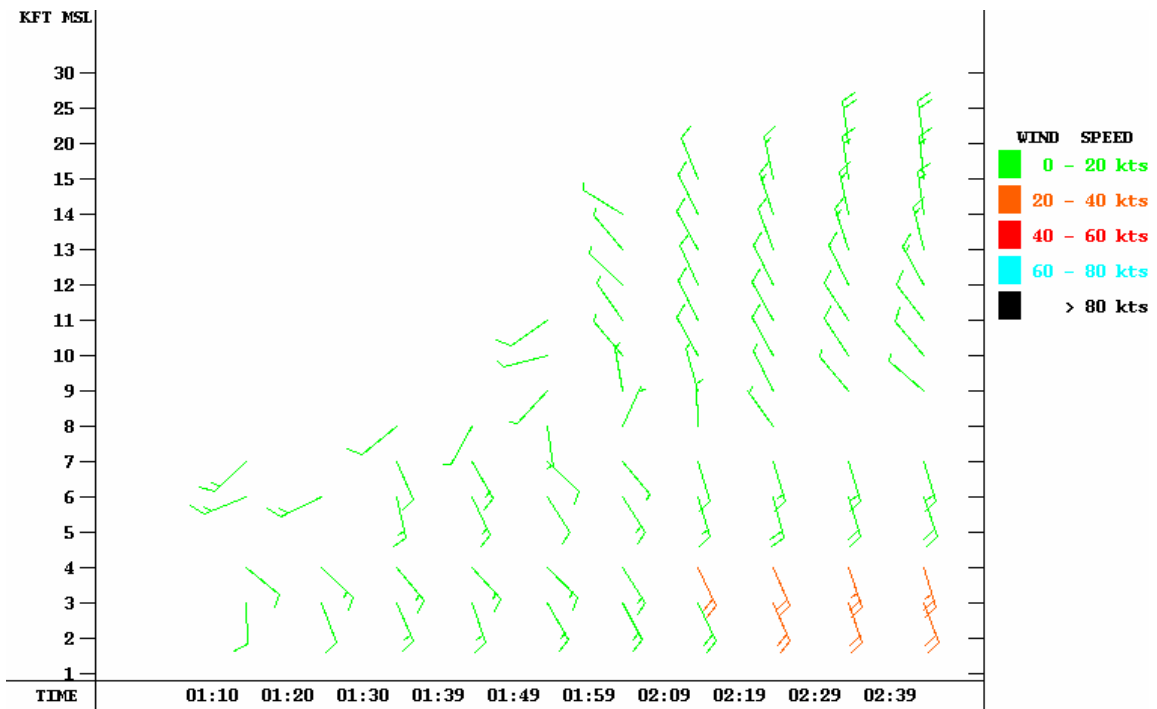
Fig. 6. WATADS VWP for New Braunfels, TX on August 20, 1997 between 1:10 Z and 2:39Z. Format is identical to Fig. 1, except that the colors displayed denote the wind speed range as indicated by the scale on the right (RMS error is not given) and "ND" is omitted from points where winds cannot be calculated.
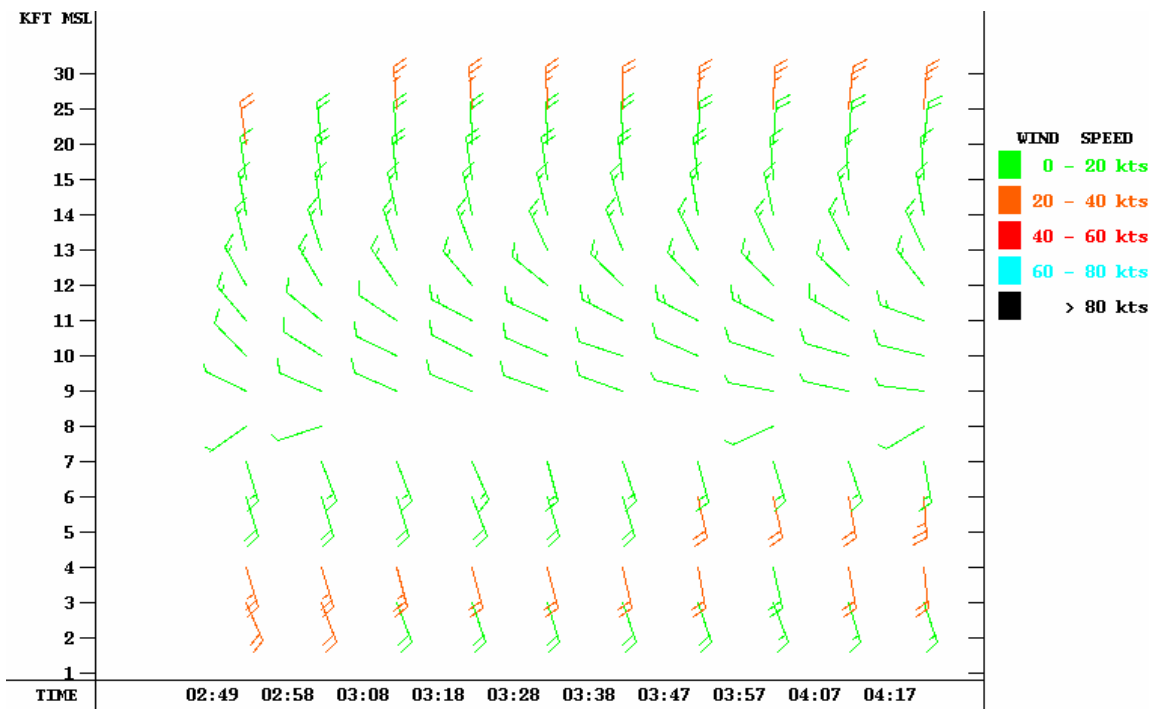
Fig. 7. WATADS VWP for New Braunfels, TX on August 20, 1997 between 2:49Z and 4:17Z. Format is identical to Fig. 6.
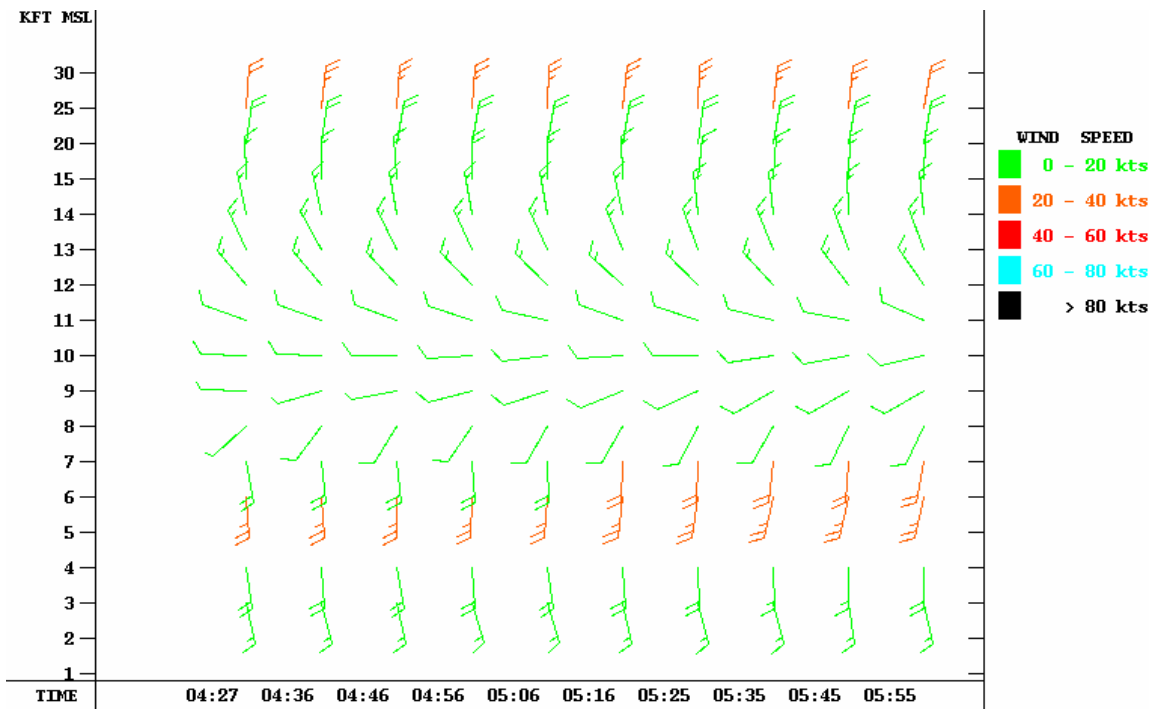
Fig. 8. WATADS VWP for New Braunfels, TX on August 20, 1997 between 4:27Z and 5:55Z. Format is identical to Fig. 6.
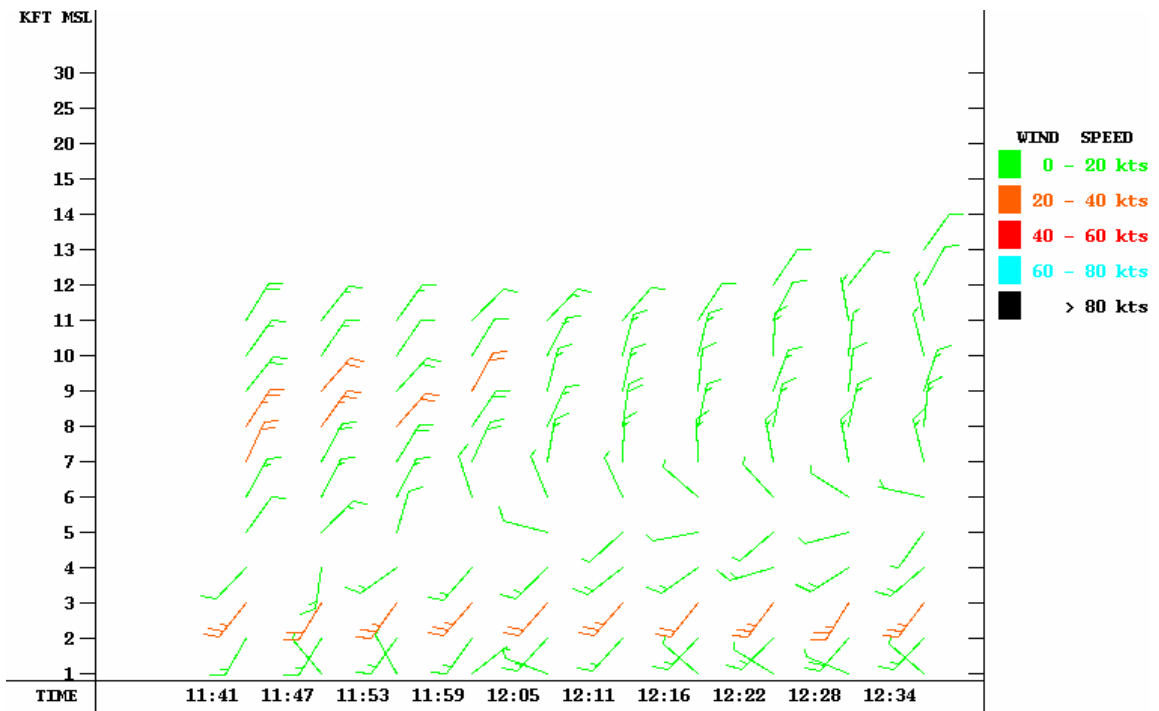
Fig. 9. WATADS VWP for New Braunfels, TX on August 20, 1997 between 11:41Z and 12:34Z. Format is identical to Fig. 6.

Fig. 10 shows the surface weather chart for 12Z. Fig. 11a shows the 850-mb chart and Fig. 11b shows the 700-mb chart for 12Z on August 20. These do not differ appreciably from the earlier maps from 0Z (Fig. 4 and Fig. 5). The winds on both sets of weather charts are consistent with the pressure distribution shown on them.

Because the VWP-derived winds extend up to rather high altitudes, examination of the winds at a higher pressure surface should be done as well. The 500-mb surface is located at approximately 18,000 feet. Fig. 12a is the 0Z map of the 500-mb surface from August 20, 1997 and Fig. 12b is the 12Z map of the 500-mb surface. Both maps depict high pressure located in the Gulf of Mexico region, and show the corresponding wind flow (in a clockwise fashion) around the high pressure center; winds at Corpus Christi were from the south, and winds farther north at Fort Worth were from the west. There are no winds with a component from the north anywhere near New Braunfels. We can, therefore, exclude with absolute certainty the strong winds from the north depicted on the New Braunfels VWP around 18,000 feet.

No meteorological explanation exists for the sudden strong winds out of the north to appear and disappear between the times of the weather charts. With the exception of the weak winds around 10,000 feet in Fig. 7 and Fig. 8, the VWP output is at odds with the actual weather observations: winds too strong in the low levels and both the strength and direction of winds are erroneous above 10,000 feet. Clearly, the VWP is not reporting the actual wind. What the VWP reports must be the vector sum of the bird velocity and the wind velocity for the levels at which the birds are flying.
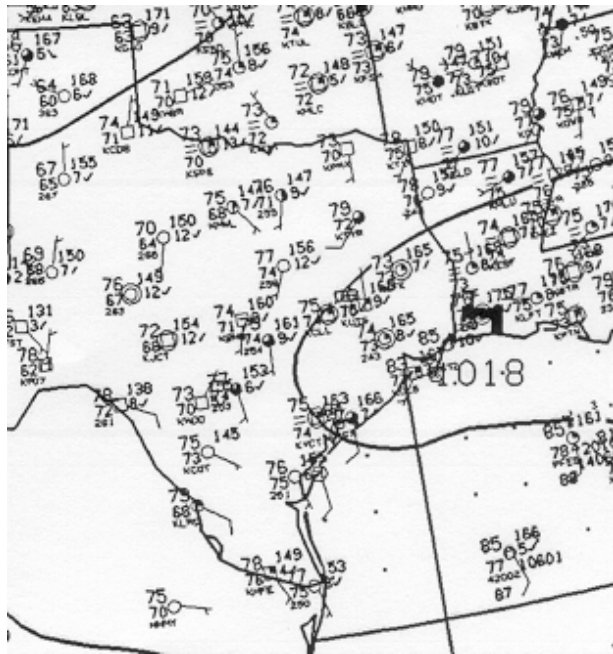
Fig. 10. Surface weather chart from 12Z on August 20, 1997. Data format is the same as Fig. 4.

(a)

(b)
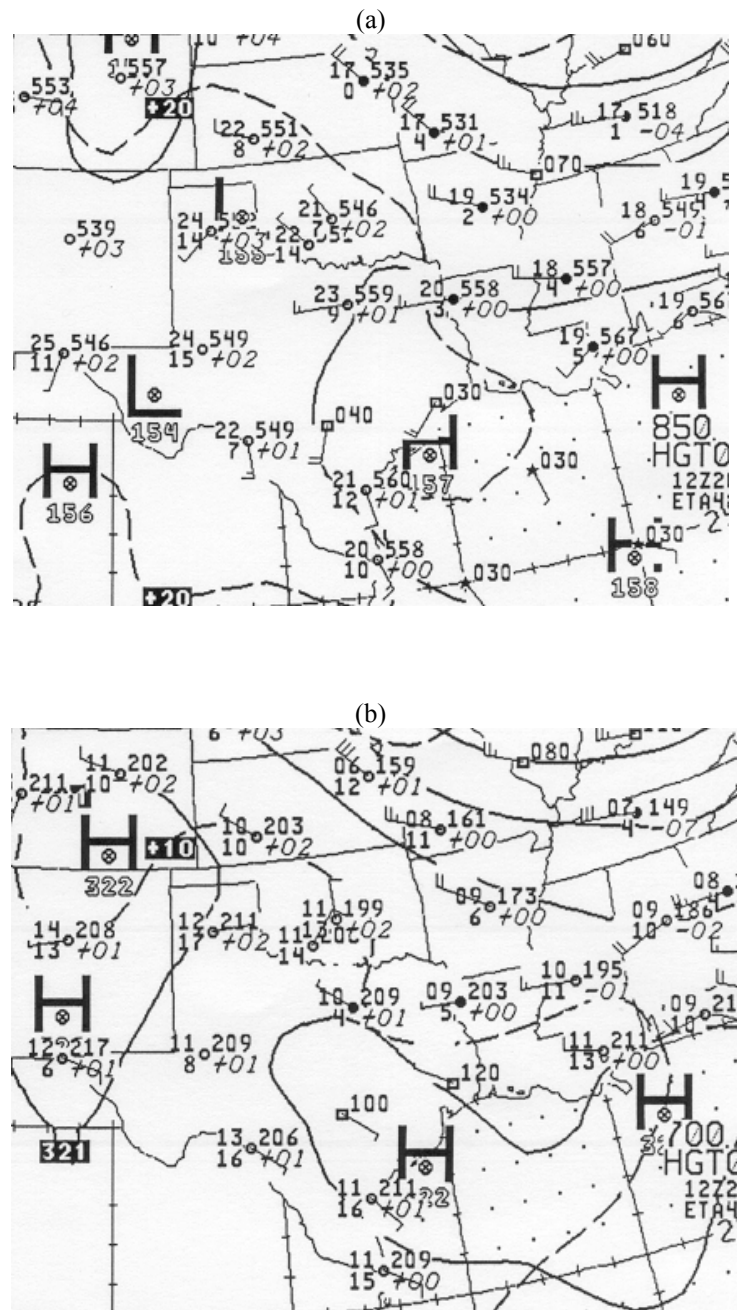
Fig. 11. Upper-air weather charts from 12Z on August 20, 1997 for the (a) 850-mb pressure surface and the (b) 700-mb pressure surface. Data format is the same as Fig. 5.

(a)

(b)
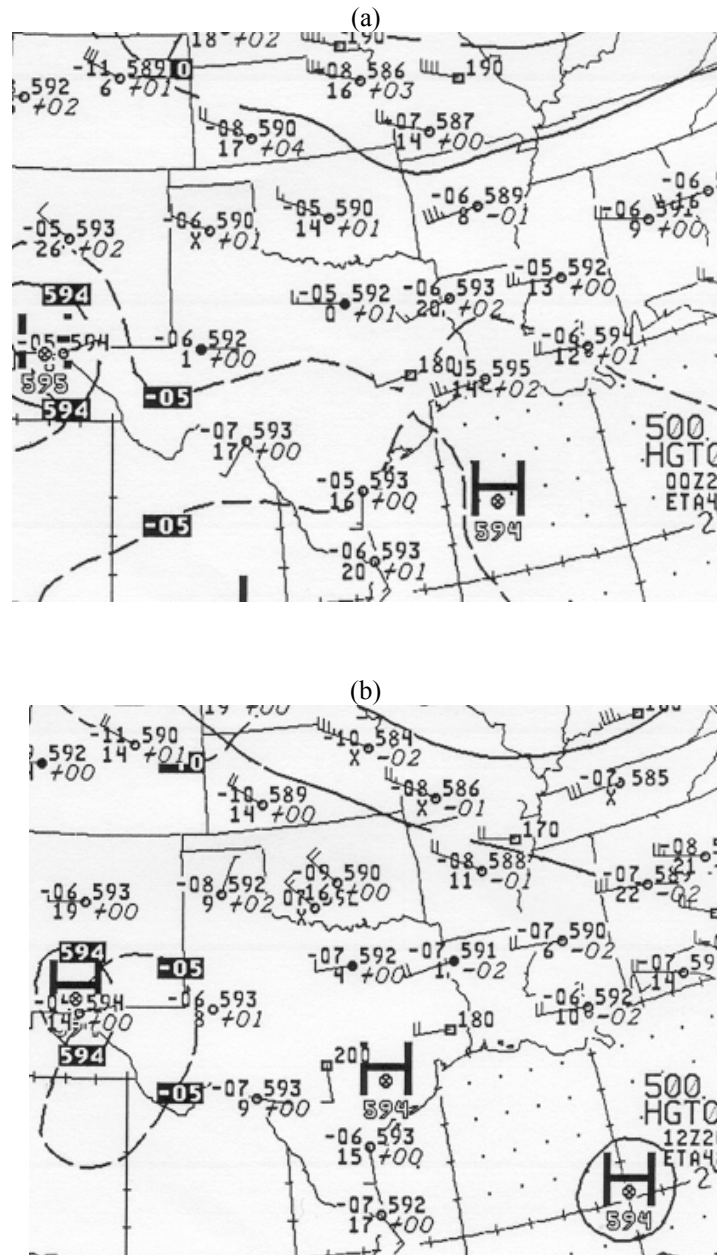
Fig. 12. 500-mb pressure surface charts for August 20, 1997 at (a) 0Z, and (b) 12Z. Data is plotted in a similar manner to Fig. 5, with the exception that the height of the pressure surface at each station is written without the trailing zero at the end (593 at Corpus is 5390 meters), and the isoheights are drawn at intervals of 60 meters.

The appearance of the birds can also be seen on other WSR-88D products besides the VWP. Fig. 13a through Fig. 13d show the reflectivity display for the 0.5-degree elevation angle. Fig. 13a is the reflectivity image at 1:30Z, or roughly 20 minutes after sunset. Few targets can be seen on the display. Fig. 13b shows the reflectivity display one hour later. Clearly, the screen has filled up with echo up to 18 dBZ. Fig. 13c, from 10:37Z, shows a continuation of the expansive area of echo. A weakness or total absence of reflectivity at close ranges to the radar suggest that the majority of birds were flying at a particular range of higher altitudes and not flying at lower altitudes. Finally, sunrise occurred at 13:03Z. Fig. 13d, from 13:04Z, shows that the majority of echoes have disappeared from the radar screen. The very strong echoes to the south and southwest of the radar are a result of anomalous propagation of the radar beam (beam bent down strongly towards the earth at a distant range, resulting in ground clutter).

Fig. 14a through Fig. 14d are the radial velocity images at the same time as the corresponding lettered images from Fig. 13. Fig. 14a shows that the low-level winds were from the southeast just after sunset. The appearance of the birds in Fig. 14b shows that while the low-level targets continued their movement from the southeast, targets at distant ranges (or higher altitudes) were generally flying from north to south. Fig. 14c shows this trend in clearer detail, although a mixture of inbound and outbound velocities can be seen together in the same general area. The low-level wind has veered to the southwest since the prior images. Finally, with the sunrise, most targets have disappeared. The near zero velocities of the strong echoes seen to the south and
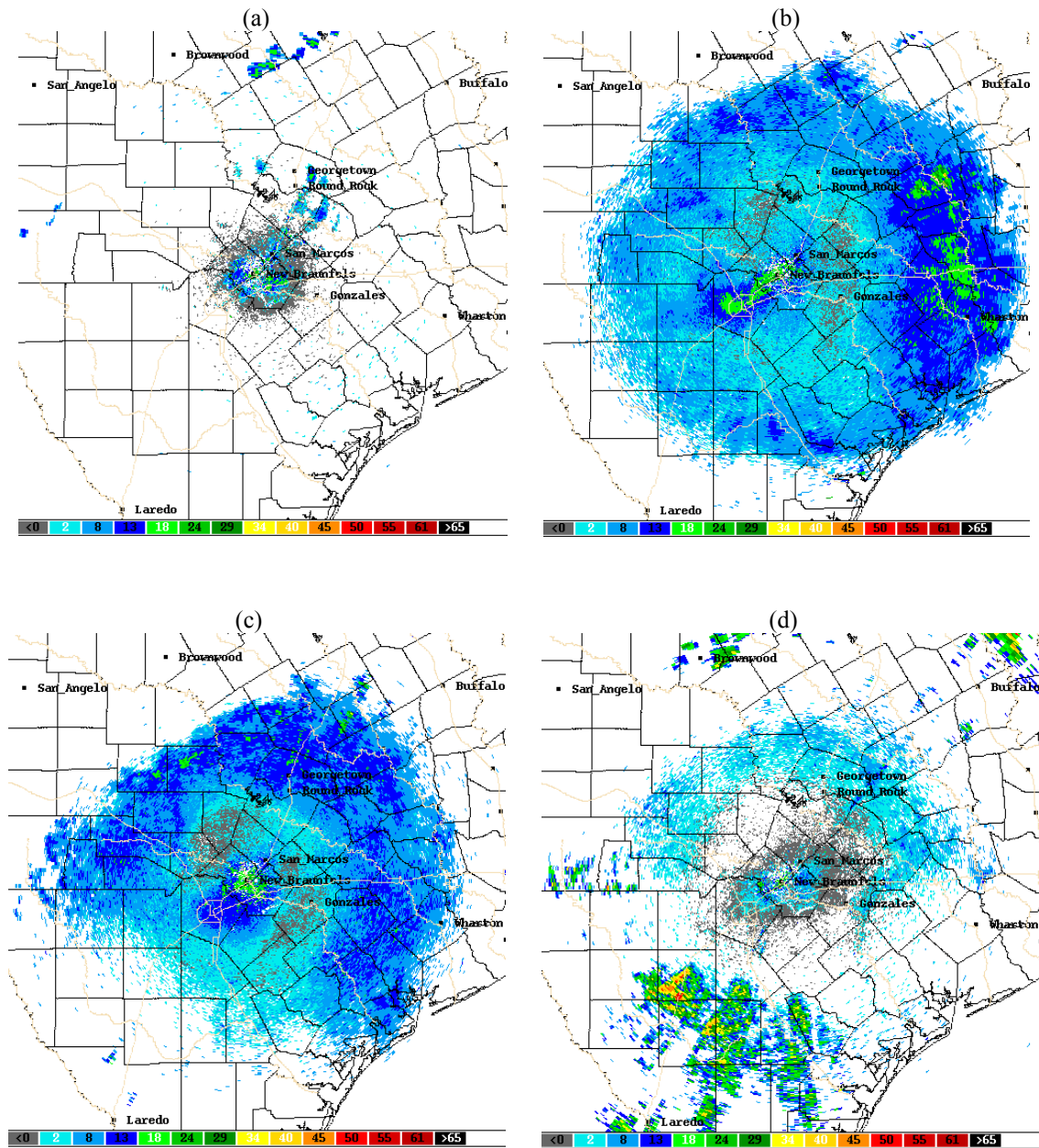
Fig. 13. 0.5 degree reflectivity images from KNWX on August 20, 1997 at (a) 1:30Z, (b) 2:29Z, (c) 10:37Z and (d) 13:04Z. Reflectivity values (dBZ) are according to the color code on the bottom of each image: from left to right, grey is < 0 dBZ, light blue is 2 dBZ, medium blue is 8 dBZ, dark blue is 13 dBZ, light green is 18 dBZ, medium green is 24 dBZ, dark green is 29 dBZ, light yellow is 34 dBZ, medium yellow is 40 dBZ, dark yellow/gold is 45 dBZ, light red is 50 dBZ, medium red is 55 dBZ, dark red is 61 dBZ, and black is >65 dBZ.
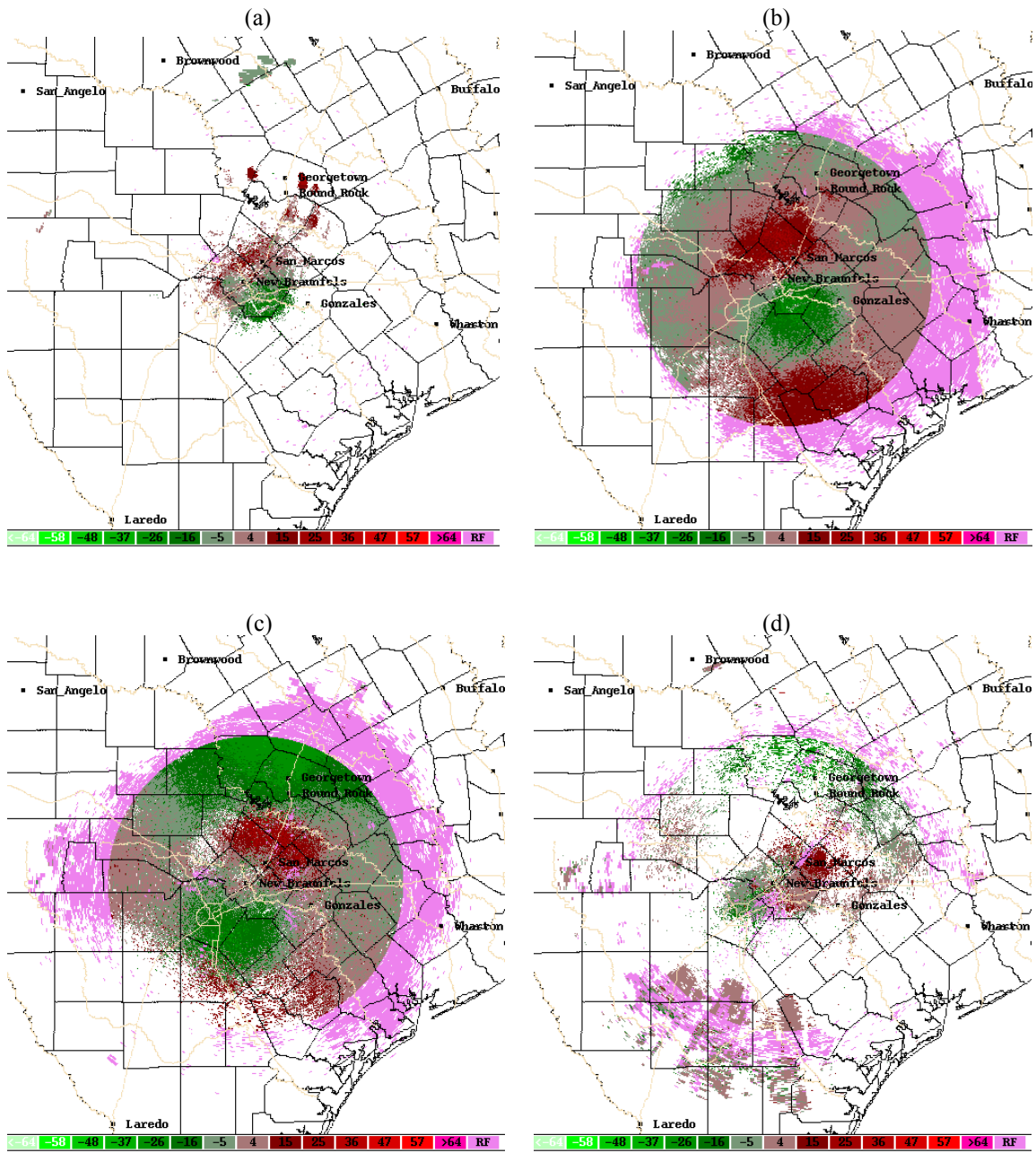
Fig. 14. 0.5 degree radial velocity images from KNWX on August 20, 1997 at (a) 1:30Z, (b) 2:29Z, (c) 10:37Z and (d) 13:04Z. Velocity values (knots) are according to the color code on the bottom of each image; negative values for inbound velocities and positive values for outbound velocities. Green values, from left to right on the scale at the bottom are: <-64, -58, -48, -37, -26, -16, and -5 knots. Red values, from left to right on the scale are: 4, 15, 25, 26, 36, 47, 57, >64 knots, and RF, which denotes range-folded velocity data.
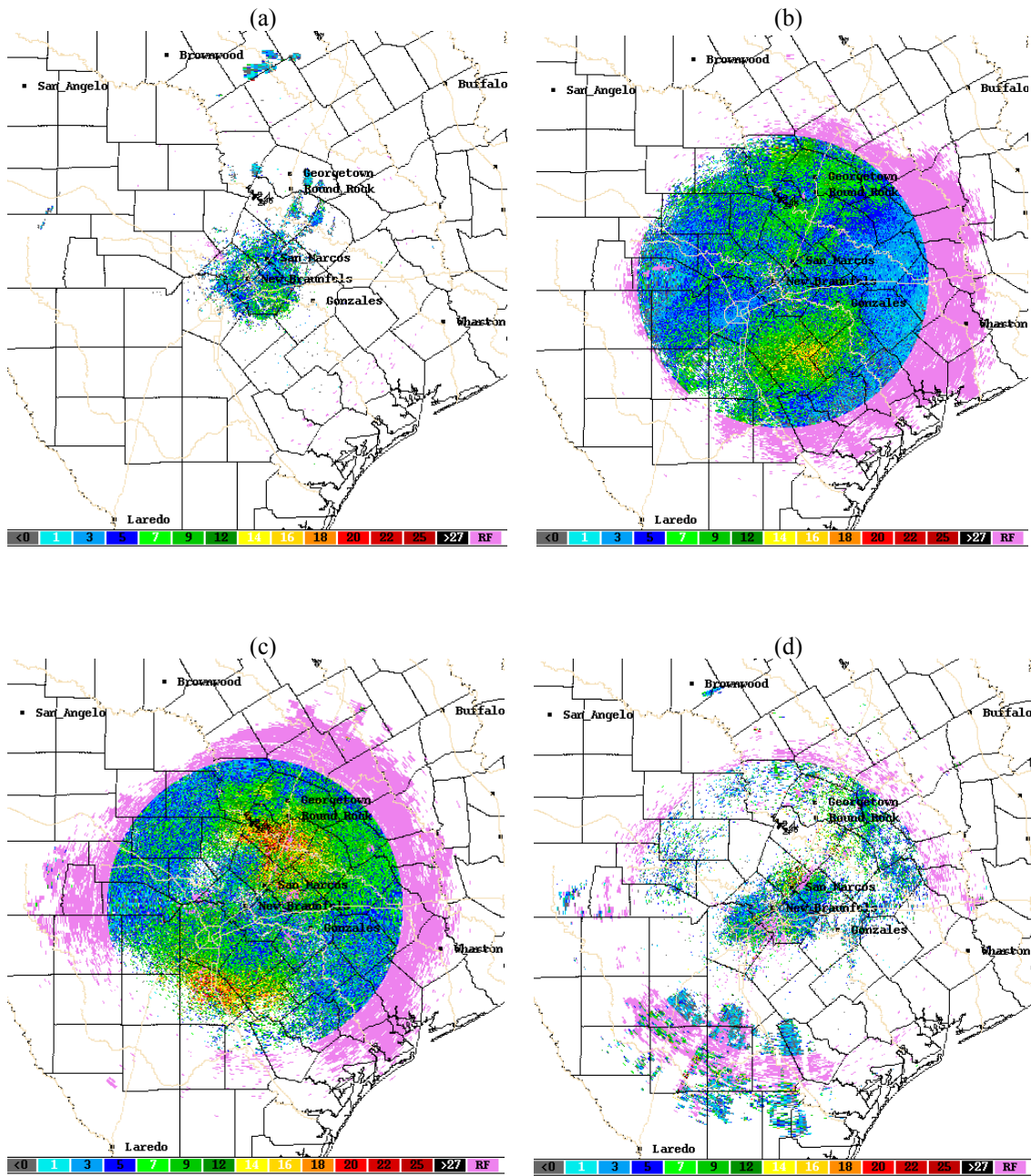
Fig. 15. 0.5 degree spectrum width images from KNWX on August 20, 1997 at (a) 1:30Z, (b) 2:29Z, (c) 10:37Z and (d) 13:04Z. Spectrum width values (knots) are according to the color code on the bottom of each image: grey is < 0, light blue is 1 knot, medium blue is 3 knots, dark blue is 5 knots, light green is 7 knots, medium green is 9 knots, dark green is 12 knots, light yellow is 14 knots, medium yellow is 16 knots, dark yellow/gold is 18 knots, light red is 20 knots, medium red is 22 knots, dark red is 25 knots, and black is >27 knots. Light purple (RF) denotes range-folded data.

southwest of the radar confirm anomalous propagation to be the cause of those echoes. One can see that the velocity images support the VWP data; unfortunately, the velocity of the targets was not a result of the wind, which is the underlying assumption when meteorologists consult the VWP product.

Finally, the spectrum width images from the same corresponding time as the preceding two figures are shown in Fig. 15a through Fig. 15d. One can see that the spectrum width product usually has a speckled appearance; no recognizable difference exists between the spectrum width products without birds (Fig. 15a and Fig. 15d) and those with birds (Fig. 15b and Fig. 15c). While there does seem to be a reduction in spectrum width when the beam is pointed orthogonal to the path of the birds, such a trademark doesn't seem to offer much of a solution to the problem of identifying birds. The spectrum width is normally smaller when the velocity values are small to begin with, so this feature is not uncommon when the beam is orthogonal to the path of the target.

b. September 16-17, 1997

I repeated the moon-watching technique on the next full-moon evening available, September 17, 1997. I used the same tools and methods that were used for the first case study. The observation results for this evening (shown in Table 2) depict a much more consistent flight heading of all the birds observed on this evening. Only the two birds that had large silhouettes had a flight direction not in agreement with the flight headings towards the west or southwest of the others. Using the same argument regarding large

Table 2. Moon-watching results from the night of September 16-17, 1997. Format is identical to Table 1.

Time (Z)	In	Out	Remarks	Flight Heading (Towards)
22:29			Began observations	
22:41	8:30	2:30	Small and quick	244
22:47	3:30	7:30	Large	44
22:48			Stopped observations (break)	
23:01			Resumed observations	
23:07	2:30	8:00	Large and fast	77
23:08	9:30	1:00	Small	257
23:11	8:30	1:30	Small	275
23:15	10:00	2:00	Small	
23:23	10:00	2:00	Small	
23:23			Stopped observations (break)	
23:35			Resumed observations	
23:38	9:00	1:00	Small	276
23:41	8:00	2:00	Medium, flying with bird below	277
23:41	8:00	2:00	Medium, flying with bird above	288
23:44	10:00	3:30	Very Small	216
23:56	10:00	2:00		282
23:56			Concluded Observations	

silhouettes made in the first case study, we can perhaps exclude those two silhouettes from the results. The total flight density for the period of observation (just one hour) on September 17 was 1720 birds per mile.

Now, the VWP output from the Houston WSR-88D (hereafter called KHGX) needs to be examined between the hours of sunset and sunrise. Sunset on this particular evening was at 0:24Z. Fig. 16 is WATADS VWP output from 0:29Z and 1:14Z, similar to Fig. 6 through Fig. 10 for the previous case study. As with the previous case study, additional altitudes of velocities are reported past sunrise. Also in accordance with the previous case study, the winds aloft are from the north (with a component from the east more than KEWX) at 15 to 20 knots. Fig. 17 continues in time from Fig. 16, and shows a continuation in what Fig. 16 was presenting.

Fig. 18 is from later that night, from between 3:22Z and 4:51Z. As with the previous case study, the winds reported by the VWP strengthened and increased in altitude. Winds are now calculated at 25,000 feet to be from the northeast at 25 knots.

Sunrise on this date occurred at 12:06Z. Fig. 19 is the VWP from that time period, and it shows that the altitude of the reported winds has decreased since the time of Fig. 18, and the wind speeds have reduced.

The comparison between my moon-watching results and the VWP seems to be in good agreement, except that my results would expect more of a component from the east to their velocity. An explanation to why there might be a difference will be offered in chapter III when I discuss issues relating to the direction of travel chosen by migrating birds.
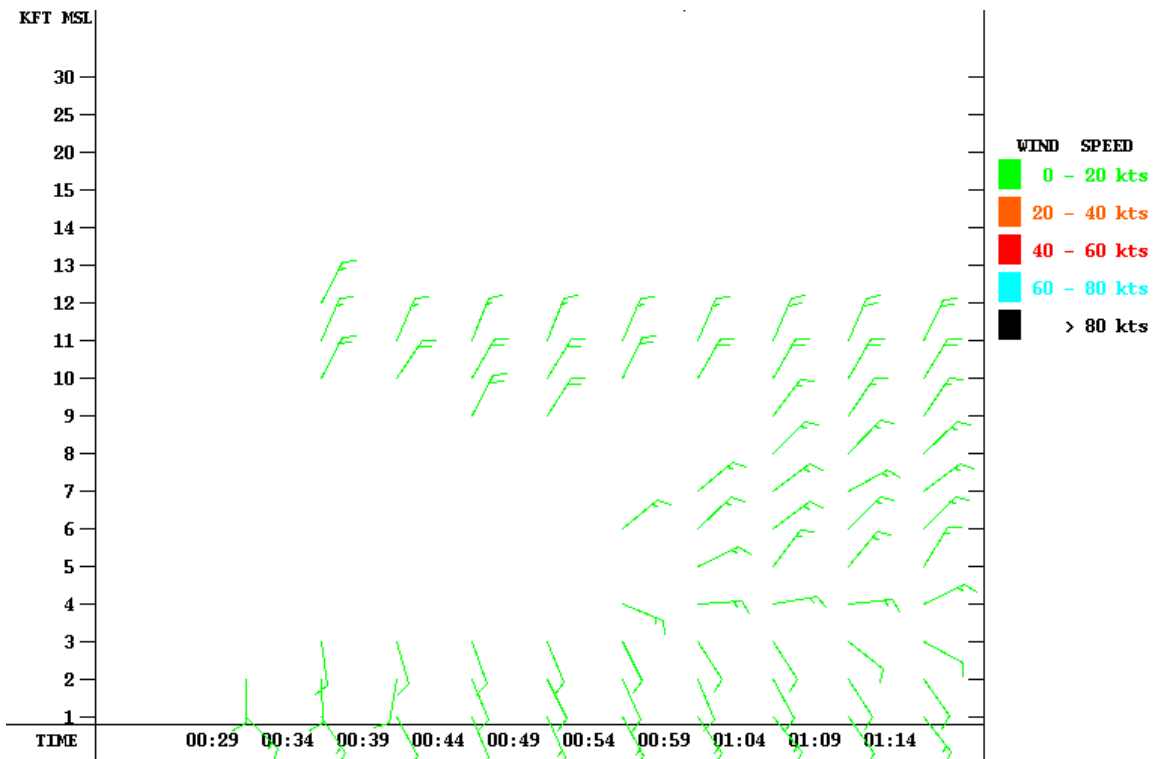
Fig. 16. WATADS VWP for KHGX on September 17, 1997 between 0:29Z and 1:14Z. Format is identical to Fig. 6.
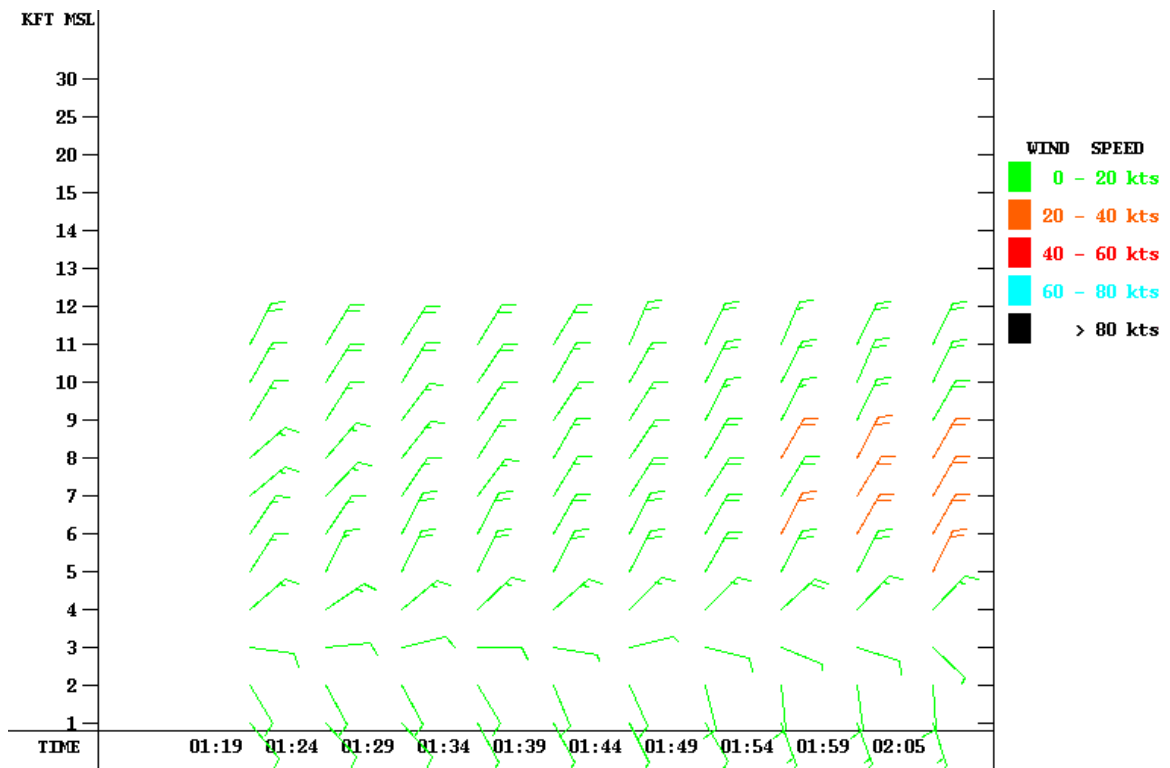
Fig. 17. WATADS VWP for KHGX on September 17, 1997 between 1:19Z and 2:05Z. Format is identical to Fig. 6.
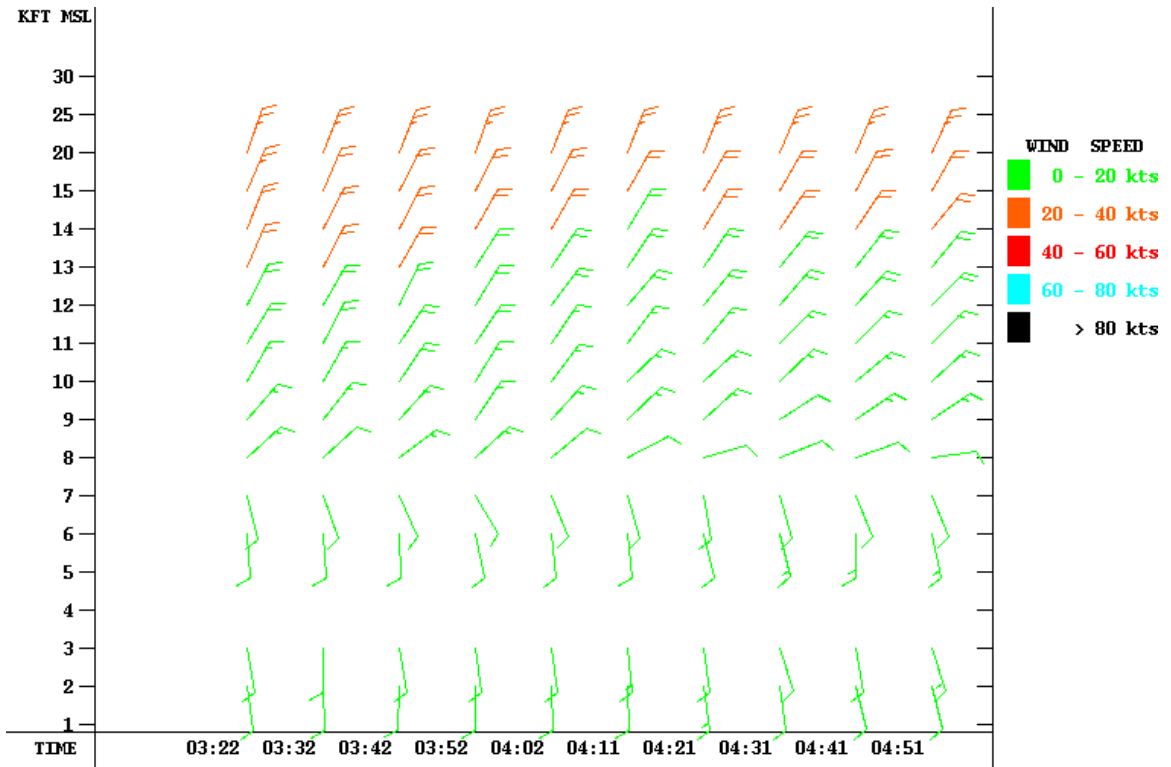
Fig. 18. WATADS VWP for KHGX on September 17, 1997 between 3:22Z and 4:51Z. Format is identical to Fig. 6.
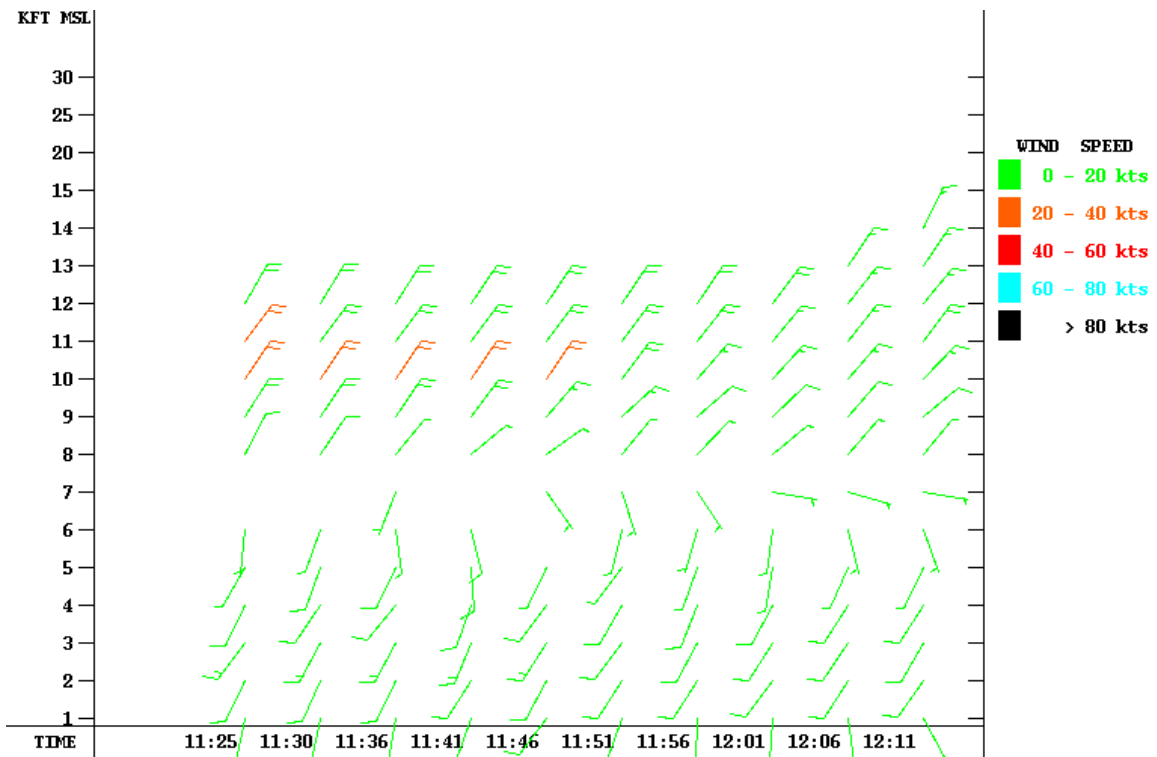
Fig. 19. WATADS VWP for KHGX on September 17, 1997 between 11:25Z and 12:11Z. Format is identical to Fig. 6.

Fig. 20. Surface weather chart from 3Z on September 17, 1997. Data are depicted as in Fig. 4.

(a)

(b)
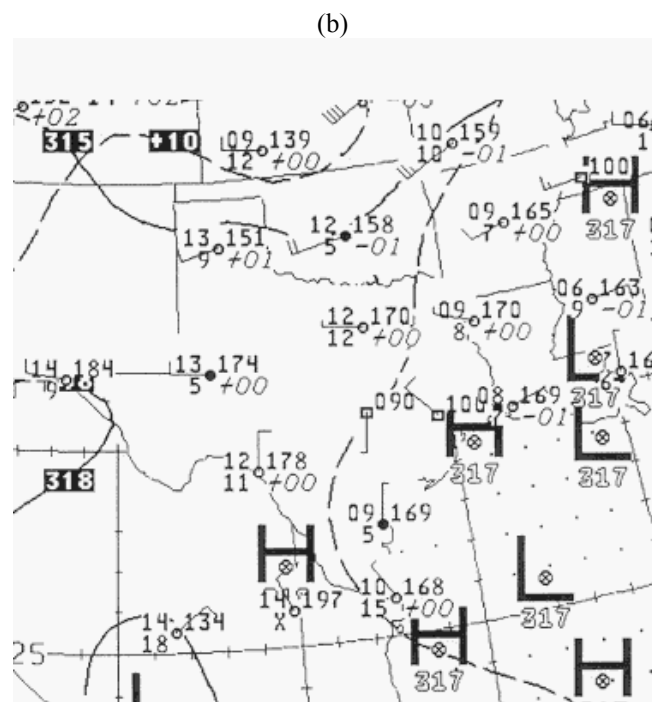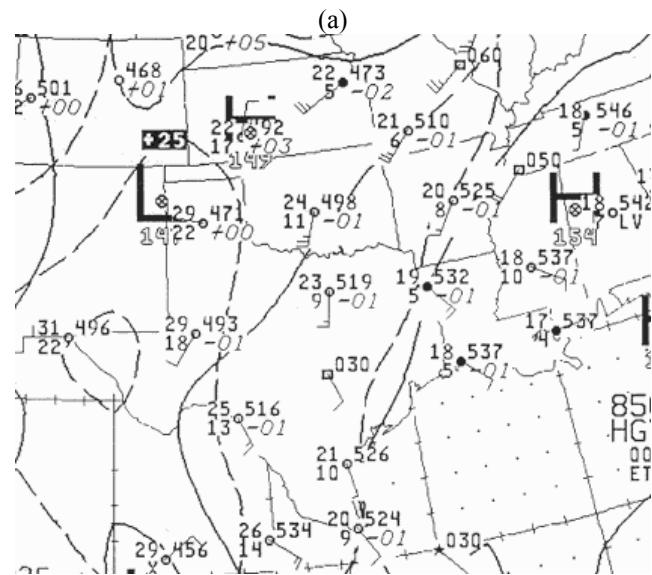
Fig. 21. Upper-air weather charts from 0Z on September 17, 1997 for the (a) 850-mb surface; (b) 700-mb surface. Data are depicted in the same manner as Fig. 5.

Turning our attention to how well the VWP verifies with the actual observed conditions, Fig. 20 is the surface chart nearest the time of moon-watching activities. Winds in southeast Texas were from the southeast at 5 to 10 knots, with a stronger 15 knots reported at Galveston. Looking at Lake Charles, Louisiana (nearest radiosonde site to Houston), Fig. 21a shows that the 850-mb winds in the Houston area were approximately from the southeast at 10 knots. Fig. 21b shows that the 700-mb winds should be light and variable, with perhaps a slight tendency towards a component from the north.

Fig. 22 shows the surface weather conditions at 12Z on September, 17. Fig. 23a shows the 850-mb weather conditions and Fig. 23b shows the 700-mb conditions at the same time. Comparisons between the 0Z and 12Z weather charts do not show drastic differences with regard to the surface or 850-mb. There is a rather significant difference at 700-mb; developing low pressure off the coast of south Texas has resulted in the winds at that level to be from the northeast at 20 knots over Del Rio. An aircraft report near San Antonio supports the increasing winds from the northeast over southern Texas.

Comparing the actual observations with the VWP output, the VWP is again overzealous with the wind speeds. The Lake Charles observation has only 10 knots at 700-mb and that is half of the VWP reported wind of 20 knots overnight at Houston. The VWP is again reporting winds from the northeast at very high altitudes. Consultation with the 500-mb charts will again prove helpful. Fig. 24a is the 500-mb chart from 0Z on September 17, and Fig. 24b is from 12Z on the same day. The 500 charts show the same development and strengthening of the winds from the northeast
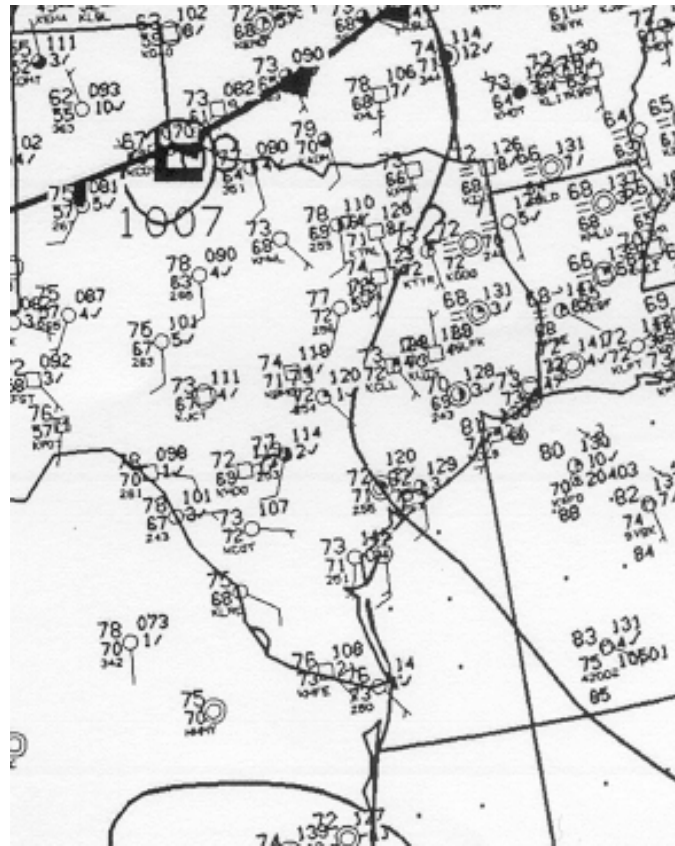
Fig. 22. Surface weather chart from 12Z on September 17, 1997. Data are depicted as in Fig. 4.

(a)

(b)

Fig. 23. Upper-air weather charts from 12:00Z on September 17, 1997 for the (a) 850-mb surface; (b) 700-mb surface. Data are depicted in the same manner as Fig. 5.

(a)

(b)
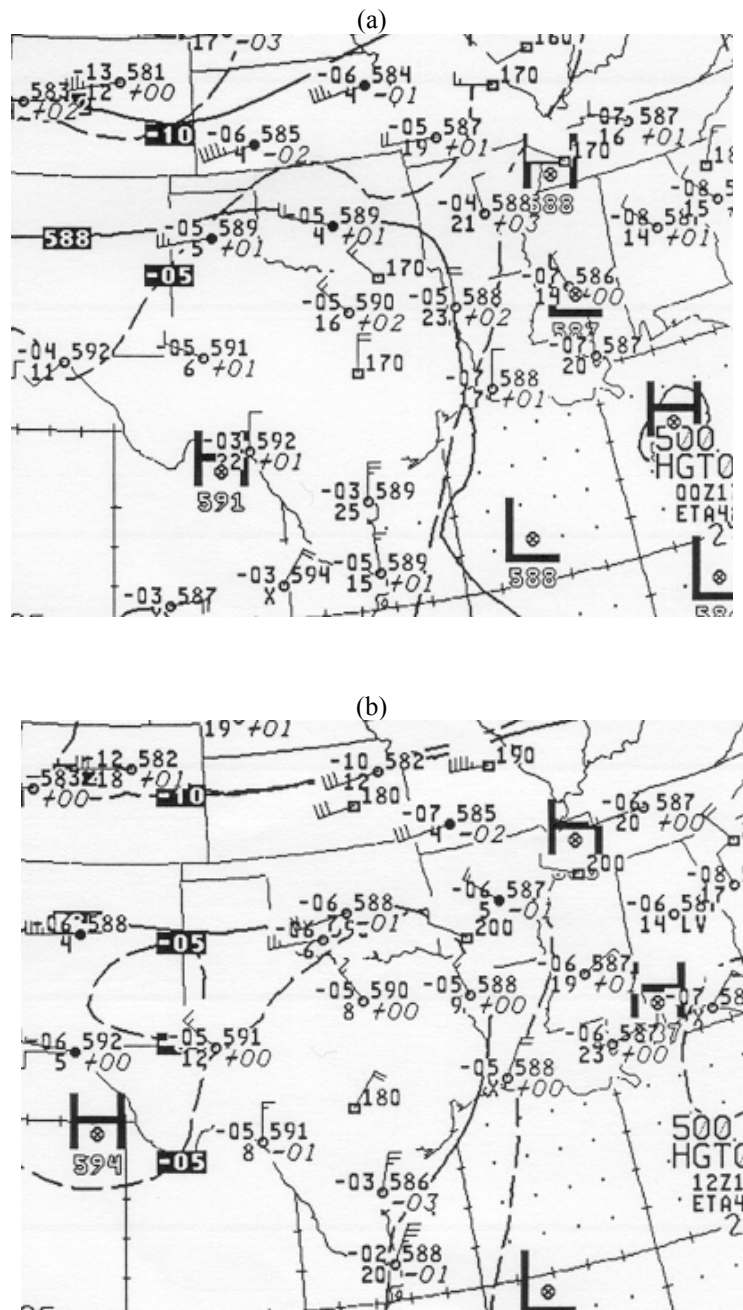
Fig. 24. 500-mb pressure surface charts for September 17, 1997 at (a) 0Z and (b) 12Z. Data are depicted in the same manner as Fig. 12.

over southeast Texas. Were birds actually contaminating the VWP product on this day at all?   To answer this question conclusively, one should examine the reflectivity, radial velocity, and spectrum width images to see if they offer the same characteristics as the previous case study.

Fig. 25a through Fig. 25d is a series of reflectivity images from KHGX on September 17, 1997, with the same relationship between sunset and sunrise as the images from the prior case study. Fig. 25a is the reflectivity product 24 minutes after sunset, and resembles Fig. 13a in that it has very few targets. Fig. 25b, taken an hour after Fig. 25a, shows an increase in targets. However, the increase in this case is not as remarkable as the increase shown in Fig. 13b. Fig. 25c, an image from the middle of the night (9:50Z), shows a decrease in the number of targets from Fig. 25b, and continues to contain less targets than its counterpart in Fig. 13c. Finally, Fig. 25d is an image taken one hour after sunrise, and it shows an increase in the number of targets at a close range to the radar. Clearly, the comparison between reflectivity images from the two dates gives the impression that fewer birds were flying on this date.

Fig. 26a through Fig. 26d is a series of radial velocity images identical in time and place to Fig. 25a through Fig. 25d. Fig. 26a shows low-level flow from the southeast consistent with the surface weather charts. Fig. 27b begins to show winds from the northeast at farther ranges (higher altitudes). Fig. 27c shows continued winds from the south at low levels, and also shows that most distant targets in Fig. 26c are range folded. Finally, Fig. 26d shows continued low-level movement from the south.
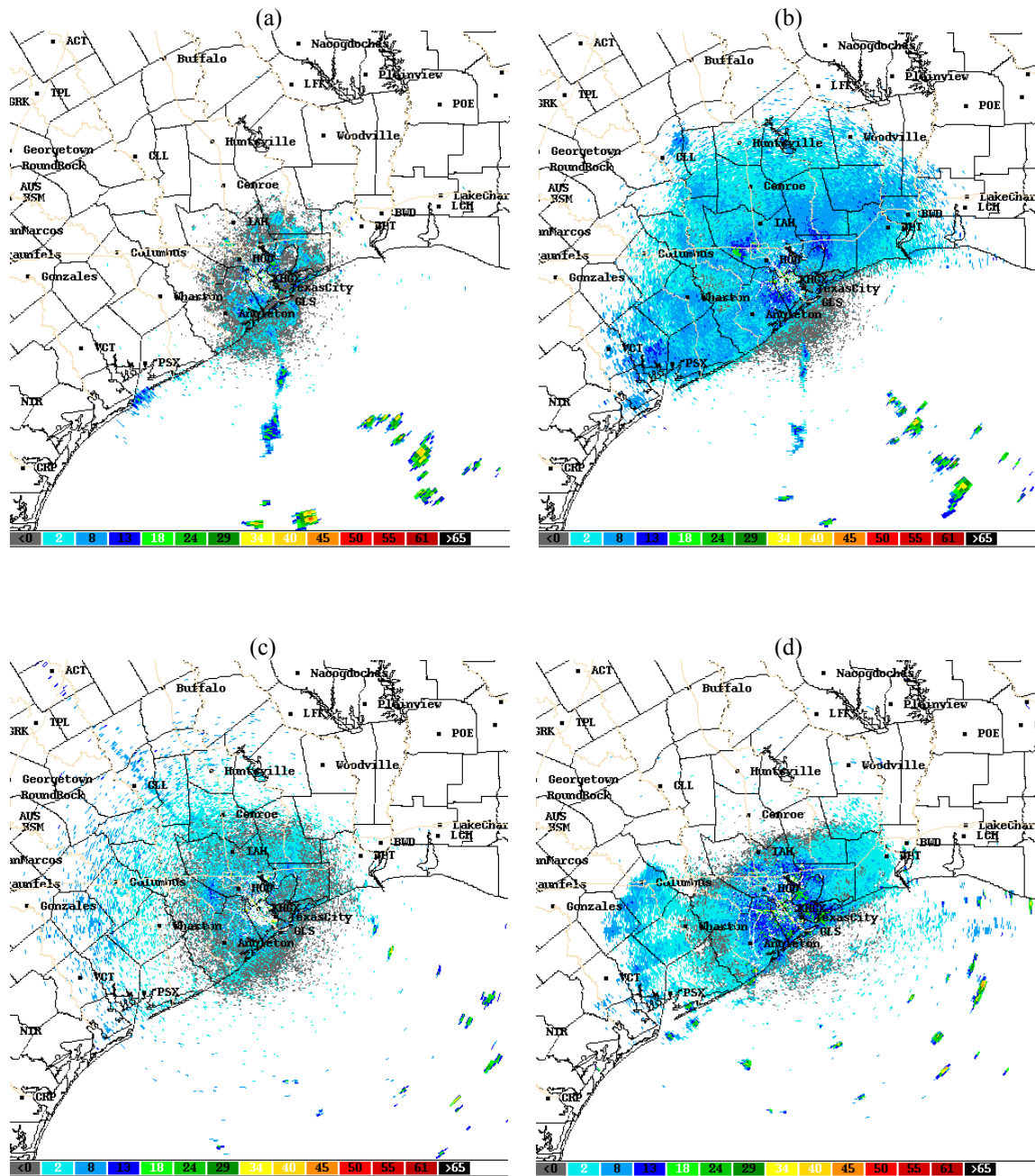
Fig. 25. 0.5 degree reflectivity images from KHGX on September 17, 1997 at (a) 0:49Z, (b) 1:50Z, (c) 9:50Z and (d) 13:07Z. Reflectivity values (dBZ) are according to the color code on the bottom of each image: from left to right, grey is < 0 dBZ, light blue is 2 dBZ, medium blue is 8 dBZ, dark blue is 13 dBZ, light green is 18 dBZ, medium green is 24 dBZ, dark green is 29 dBZ, light yellow is 34 dBZ, medium yellow is 40 dBZ, dark yellow/gold is 45 dBZ, light red is 50 dBZ, medium red is 55 dBZ, dark red is 61 dBZ, and black is >65 dBZ.
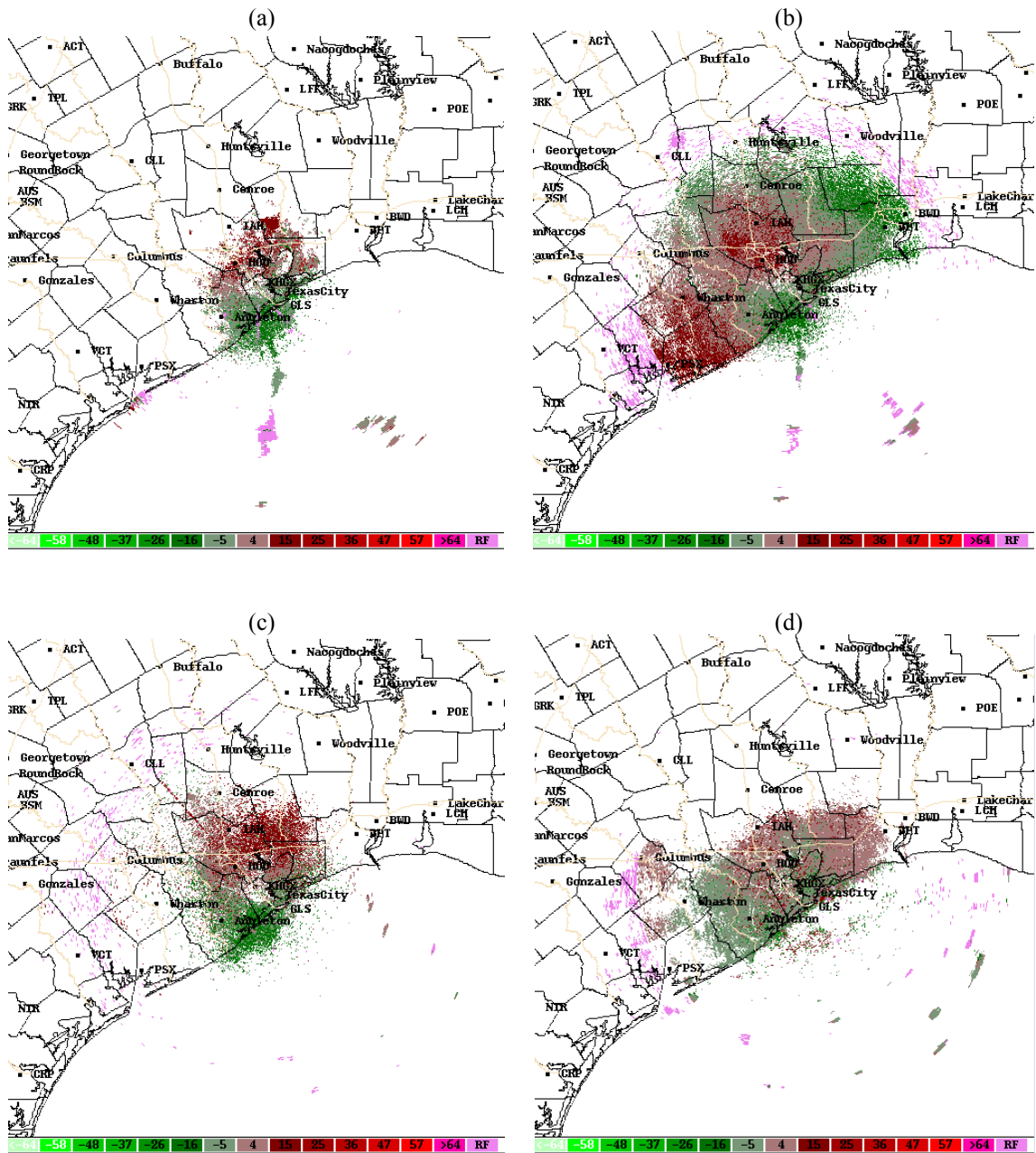
Fig. 26. 0.5 degree radial velocity images from KHGX on September 17, 1997 at (a) 0:49Z, (b) 1:50Z, (c) 9:50Z and (d) 13:07Z. Velocity values (knots) are according to the color code on the bottom of each image; negative values for inbound velocities and positive values for outbound velocities. Green values, from left to right on the scale at the bottom are: <-64, -58, -48, -37, -26, -16, and -5 knots. Red values, from left to right on the scale are: 4, 15, 25, 26, 36, 47, 57, >64 knots, and RF, which denotes range-folded velocity data.
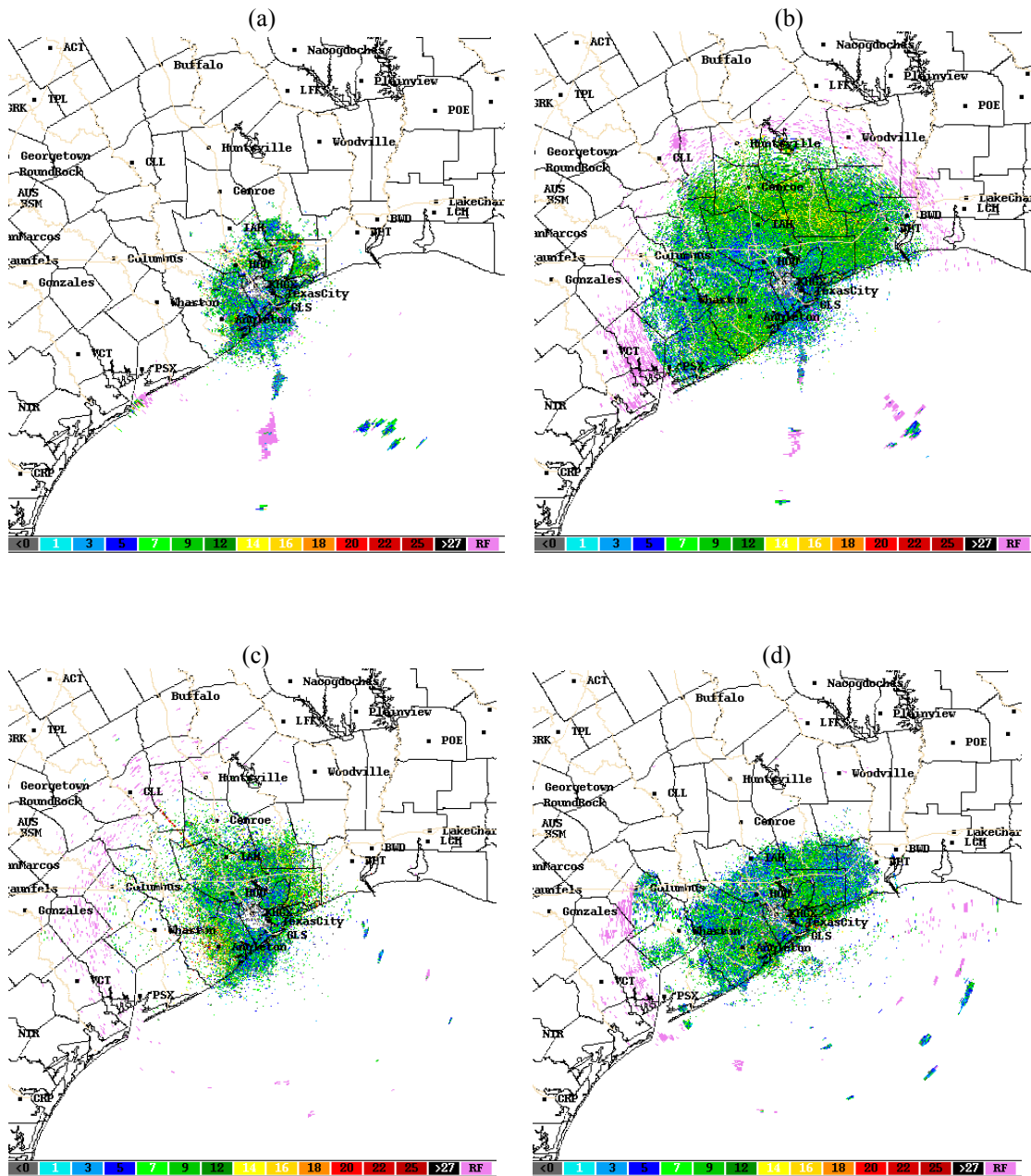
Fig. 27. 0.5 degree spectrum width images from KHGX on September 17, 1997 at (a) 0:49Z, (b) 1:50Z, (c) 9:50Z and (d) 13:07Z. Spectrum width values (knots) are according to the color code on the bottom of each image: grey is < 0, light blue is 1 knot, medium blue is 3 knots, dark blue is 5 knots, light green is 7 knots, medium green is 9 knots, dark green is 12 knots, light yellow is 14 knots, medium yellow is 16 knots, dark yellow/gold is 18 knots, light red is 20 knots, medium red is 22 knots, dark red is 25 knots, and black is >27 knots. Light purple (RF) denotes range-folded data.

Fig. 27a through Fig. 27d are the spectrum width products from the same corresponding times in Fig. 25 and Fig. 26. These images continue what was observed in Fig. 15a through Fig. 15d; spectrum width products tend to appear rather speckled, and there is a minimum in spectrum width values where the velocity values are smallest. The zero radial velocity area in Fig. 26b extends from the radar up towards College Station. There is a minimum area of spectrum width values in this area in Fig. 27b, but this conclusion is not as evident as it is in Fig. 15 due to the fewer number of targets. The reason why this case study fails to have such a pronounced bird contamination as the first case study must be sought after the literature review of bird migration in the next chapter.

In summary, the moon-watching technique allowed me to visually confirm that birds were flying on the evening of August 20, 1997 in which the VWP from New Braunfels was in error. The moon-watching reslults from September 17, 1997 also confirmed that birds were flying on that evening; however, the conclusion that birds contaminated the Houston VWP that night is inconclusive. If the Houston office had a radiosonde observation, this question could be answered more strongly. Despite potential errors with the quantitative results of my moon-watching observations, the qualitative evidence of birds flying allows one to reasonably suspect that birds are the targets responsible for erroneous VWP output. The veracity of this conclusion will be further tested through an ornithological literature review in the next chapter.

CHAPTER III

LITERATURE REVIEW

To better understand the phenomenon being observed on the WSR-88D, and to perhaps come up with potential solutions, a literature review covering many disciplines is now required. In the first section, I review bird migration and in particular, nocturnal migration. Questions regarding what birds migrate at night, and how and why they do so will be answered. The second section looks more closely at the links between migration and weather conditions that may precede the departure and affect the number of birds flying. The third section concerns radar ornithology and examines the principles on how birds are detected by radar. The fourth section covers the VAD algorithm and how the WSR-88D uses it to produce the VWP product. The fifth section is a literature review of articles written about bird contamination of the WSR-88D VWP product, including articles written since this research began that propose possible solutions to the problem. Finally, the sixth section concludes this chapter by applying what was learned during the review of the literature towards the questions raised in Chapter II.

1. Migration and Nocturnal Migration

Migration can be defined as any movement from one temporarily inhabited home area to another (Berthold 1996, 3-4), and roughly half of the bird species on the planet perform some type of migratory movement (Berthold 1996, p. 1). The prime motivator for migration is food availability, which depends on both the food supply and the

number of food competitors (Alerstam 1990, p. 168). Birds are primary and secondary consumers in the food chain, feeding on the plant kingdom (grass, seeds, buds and fruit) or on primary consumers such as insects and worms (Alerstam 1990, p. 24). The mid-latitudes of the United States and Canada provides an expansive area rich in food sources and nesting sites from late spring to early fall, and the birds choose to come to these locations to breed and add to their numbers. With the onset of winter, however, lakes freeze, insects disappear and plants cease to produce seeds and fruit, which results in a lack of food for many birds. Birds migrate southward, and do so well before the resources are exhausted, to ensure better quantities of food later on.

The length of daylight seems to be the most reliable cue for control of annual cycles, including bird migration (Berthold 1996, p. 80). Berthold (1996, p. 87) cites examples of juvenile birds (hatched late in the season) that had their development accelerated when the length of daylight decreased. In addition, fat deposition has been found to accelerate under the same decreasing daylight conditions. Therefore, the bird most likely uses day length to determine when migration should commence, and the bird departs as soon as it is physically ready to do so. Departure is also strongly dependent on weather conditions, and this will be addressed in the next section.

Migratory birds can be separated into three broad categories based on, in addition to other things, their migratory flight behavior: Passerines (songbirds), waterfowl (including shorebirds) and soaring birds. Most passerines prefer to migrate at night and do so alone; an exception to this are robins, which migrate in flocks during the day (Kaufman 1996, p.477). However, passerines are observed to migrate in flocks when

flying during the daylight hours (Gauthreaux 1971). While they overwhelmingly prefer

to migrate at night, passerines are forced to fly during the day when they cross the Gulf

of Mexico because the journey can't be completed until they finally reach land (which

occurs normally during the afternoon following their evening departure). Waterfowl and

shorebirds migrate exclusively in flocks and migrate during the day or at night. Finally,

soaring birds migrate only during the day when strong thermals are present, and many

birds can sometimes be seen sharing the same thermal.

Because the VWP contamination takes place at night, and assuming that birds

can be detected by radar (an issue to be addressed in a later section of this review), we

can exclude soaring birds from our list of suspects. Since waterfowl and shorebirds

migrate in flocks, they cause discrete and strong echoes on the radar screen, not the

broad area of featureless echoes usually seen during VWP contamination (Eastwood

1967, 242-243). Because the entire PPI usually becomes saturated with usually weak

echo, we can easily assume that passerines that are migrating alone are responsible for

much of the echo observed. Based on my own moon-watching data contained earlier in

Chapter II, the majority of the birds I observed were migrating alone, which confirms

passerine migrants. While flocks of waterfowl certainly can't be excluded from being

part of the population of targets responsible for VWP contamination, I will concentrate

on passerine migration throughout the remainder of this review and thesis.

In the spring, birds travel great distances in a hurry to stake their claim to the

prime nesting sites and to begin the search for a mate (Alerstam 1990, p. 317). In the

fall, the majority of passerines proceed slowly due to longer stopovers (Berthold 1996, p.

119). In between the spring arrival and fall departure, mating takes place, offspring are born and nurtured, and usually a molt (replacement of feathers) takes place (Kerlinger 1995, p. 128). Finally, the bird fattens up in preparation for its migratory journey southbound (Kerlinger 1995, p. 50).

The arrival of most passerines in the United States in the spring usually begins in the first or second week in March, peaks in late April or early May, and concludes by the third week in May (Gauthreaux and Belser 1998). Fall passerine migration can begin as early as July, peaks along with the appearance of cold frontal passages in August, and normally concludes by the end of November (O'Bannon 1985). It should be noted here that spring migration covers a shorter time period (approximately 2 months) than fall migration (5 months), and this agrees with Alerstam's statement that birds undergo spring migration in a hurry. The shorter period of migration during the spring might explain why Steve Allen didn't notice VWP contamination during the spring months.

It seems surprising that passerines, which engage in their life's routine activities solely during the daylight hours, would choose to migrate exclusively at night (Berthold 1996, p. 34). There have been many ideas suggested to explain this preference. Berthold (1996, 35-36) finds that four reasons seem to be the most plausible. First, is a bird that migrates at night can spend the daylight hours foraging for food. Second, a bird that feeds during the day will gain time by migrating at night. Migrating only during daylight would result in very short flights being possible with the remaining time after feeding, and this would lengthen the duration of the entire journey. Third, the atmospheric conditions for flight are typically much better at night than during the day.

The air is cooler, winds are usually slower and less variable, and vertical wind currents due to daytime convection are nonexistent. Finally, night flight in cooler temperatures prevents dehydration.

In regards to the hypothesis that nocturnal migration is due to avoidance of predators, Berthold (1996, p. 35) admits that, although the predator-prey relationship is not well understood during migration, there are certainly night predator species (such as owls) that can prey on nocturnal migrants. The existence of nocturnal predators calls into question the validity of the predator-avoidance hypothesis as being a primary explanation for nocturnal bird migration.

The temporal characteristics described to me by Steve Allen at the start of this chapter are consistent with the observations made during many radar and moon-watching studies of passerine nocturnal migration over the past several decades. A summary of such prior studies conducted prior to 1967 can be found in Eastwood (1967, 108-141). More recently, studies by Sidney Gauthreaux have further confirmed the temporal characteristics of passerine nocturnal migration as viewed on radar. Gauthreaux (1971) found that the beginning of passerine migration occurs between the end of civil twilight (when the sun is 6 degrees below the horizon and objects are still visible on the surface) and the end of nautical twilight (when the sun is 12 degrees below the horizon and the horizon is indistinct). The time between the start of civil twilight and the end of nautical twilight takes place approximately 30-45 minutes after sunset, and matches Steve Allen's observations exactly.

Gauthreaux (1971) noted that when passerine migration commenced, the PPI quickly became saturated with echo. This also supports Steve Allen's observations. In an earlier study, Gauthreaux (1969) found that the number of migrants aloft peaked one to two hours after dark, and steadily decreased until they entirely ceased their travels prior to sunrise. Studies such as Hassler et al. (1963), Jungbluth et al. (1995) and O'Bannon (1995) support Gauthreaux's temporal observations.

In conclusion, because of the temporal characteristics and the extent of targets observed on the PPI, we can conclude that passerines are primarily responsible for the contamination of the VWP. These birds regularly depart 30 to 45 minutes after sunset and migrate alone. The regularity of the departure time suggests that the WSR-88D can use the addition of sunset data to perhaps run any additional algorithm that can be used to determine if birds are flying that evening.

2. Migration and Meteorology

While studying bird migration using radar and visual methods, ornithologists have found that the number of birds flying can differ by a factor of 100 or 1000 from one day to the next, even during the peak of the migration season (Richardson 1978). Richardson also notes that during the migration season, at least a few birds are almost always observed aloft, regardless of weather. However, it is clear from the day-to-day variance in the number of migrants that birds prefer to migrate on specific days. Ornithologists have found that weather conditions prior to and during departure time have a great impact on whether birds decide to fly at all at that particular time.

Richardson provides an excellent review of past literature and combines their results in order to discuss how each weather variable appears to impact bird migration. Four weather factors seem to have the most importance, and each of them will be discussed now.

a. Wind and Wind Direction

One of the most important weather variables that impacts migration is wind speed and direction. Birds have been found to prefer tailwinds, and they choose a flight altitude that offers the most favorable winds for their preferred direction of travel (Gauthreaux 1991). The preference of birds to fly with tailwinds has also been noted by Blokpoel and Burton (1975) and Hassler et al. (1963). Mechanics of bird flight have suggested that a certain air speed exists which results in a minimum consumption of energy per distance traveled, and this speed of maximum range decreases as tailwinds increase (Bruderer 1997b). As tailwinds increase, the bird is able to fly at a slower airspeed, thereby saving energy. Flying with a headwind or crosswind results in increased energy expenditure (Richardson 1978).

Because of the strong urge to fly with tailwinds, reverse migration (migration in a seasonally inappropriate direction) can be observed when winds blow in the wrong direction for the intended migratory journey. In simple terms, spring-like wind conditions (winds from the south) bring about a spring-like response in the birds, and vice versa. Under these conditions, the number of birds flying are usually of a lower

magnitude, indicating that some birds may realize the unfavorable conditions and refuse to fly that night (Gauthreaux and Able 1970).

The relationship between fall bird migration activity and synoptic weather patterns is shown in Fig. 28a. Since the birds wish to travel south, they will often choose to follow cold fronts, which are located in the wake of a midlatitude cyclone and downstream of high pressure. The relationship between bird migration activities for spring is shown in Fig. 28b. Because the intended flight direction is towards the north, birds will seek out the winds from the south that are located in the warm sector of mid-latitude cyclones and to the west of high pressure.

Despite the desire for passerines to fly with tailwinds, they don't exactly fly in the same direction as the winds at all times. Birds flying along the Texas coast in the spring have been observed to follow the coastline (towards the northeast) regardless of the direction of the wind (Forsyth and James 1971). Eastwood (1967, p. 146) also notes that some studies have observed certain birds (like the chaffinch) correcting for wind drift in order to maintain a certain heading. Therefore, some species have shown a desire to maintain a certain heading, whether to reach a specific target or simply to follow topographic features such as coasts.

b. Precipitation

Another weather variable which has a large impact on the number of birds flying is precipitation. Forsyth and James (1971) found that rain will stop migrations in progress. Gauthreaux (1972) observed that upon encountering rain, birds plummeted

(a)

(b)
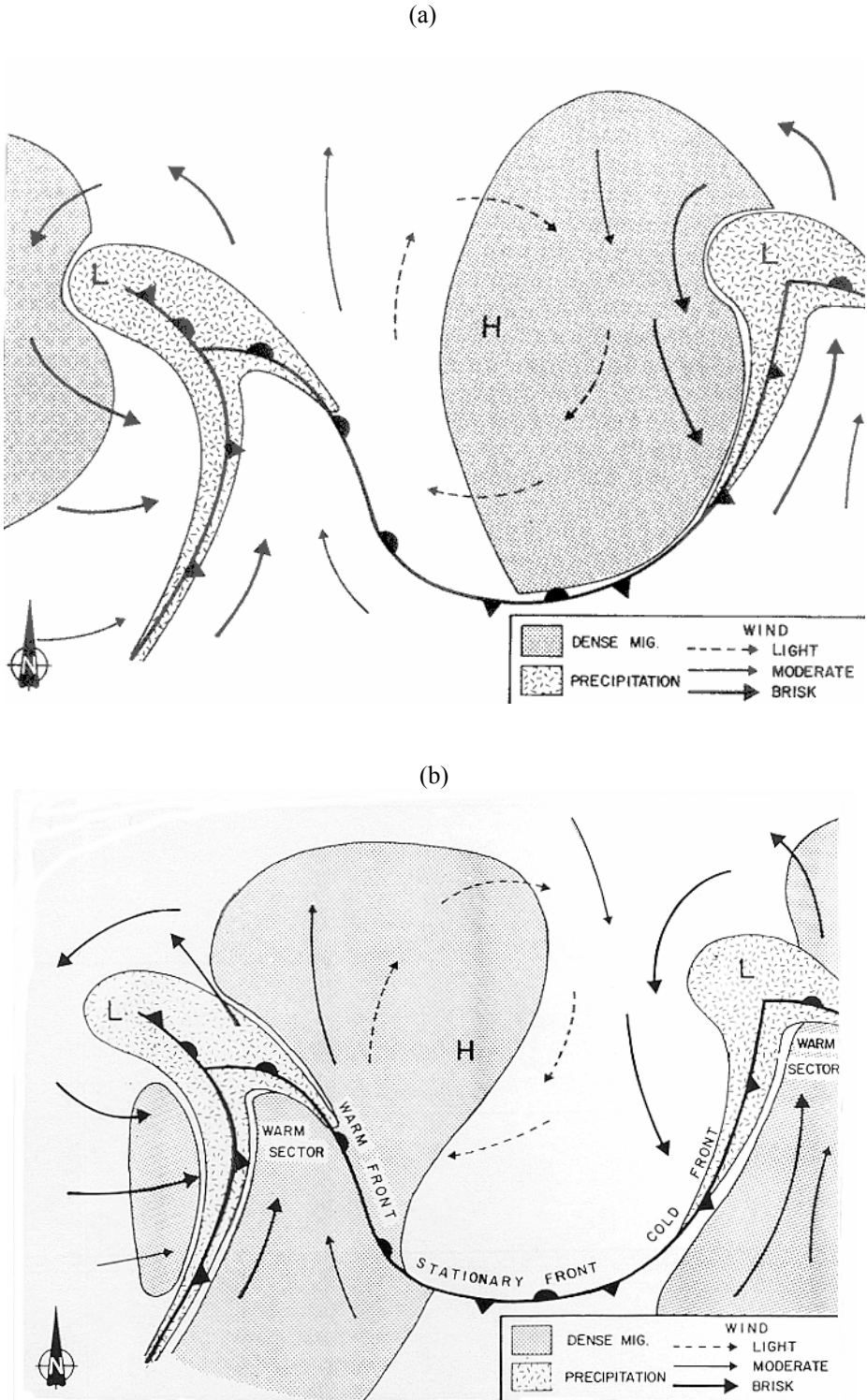
Fig. 28. Relationship between synoptic weather features and dense bird migration (a) in the fall; (b) in the spring. From Richardson (1978).

down to the ground to such an extent that they resembled dark hail. Rain and snow

cause a loss of body heat (which amounts to a loss of valuable energy), add extra weight

and increase energy consumption required for flight (Richardson 1978). Hail is simply

lethal and an obvious hazard.

Fig. 29 is a series of radar reflectivity images from the Del Rio, Texas WSR-88D

(KDFX) of nocturnal spring bird migration that took place on April 29, 1999. A strong

thunderstorm is located in southwest of the radar in Mexico. There appears to be a lack

of reflectivity that develops on the northwestern flank of the thunderstorm as time

progresses from Fig. 29a to Fig. 29d. Fig. 30 is a series of radial velocity images taken

at the same time as the corresponding lettered image in Fig. 29. One should note that the

targets were generally flying towards the northwest.

An explanation for the lack of reflectivity on the northwest flank of the

thunderstorm is simply that birds migrating towards the northwest flew around the

thunderstorm as they encountered it. After they successfully circumnavigated the

thunderstorm, the birds continued to fly on their current heading, which resulted in a

lack of birds aloft to the immediate northwest of the thunderstorm.

c. Clouds

The presence of clouds without precipitation has a more subtle effect on the

number of migrants flying. Gauthreaux (1971) states that solid overcast will not delay
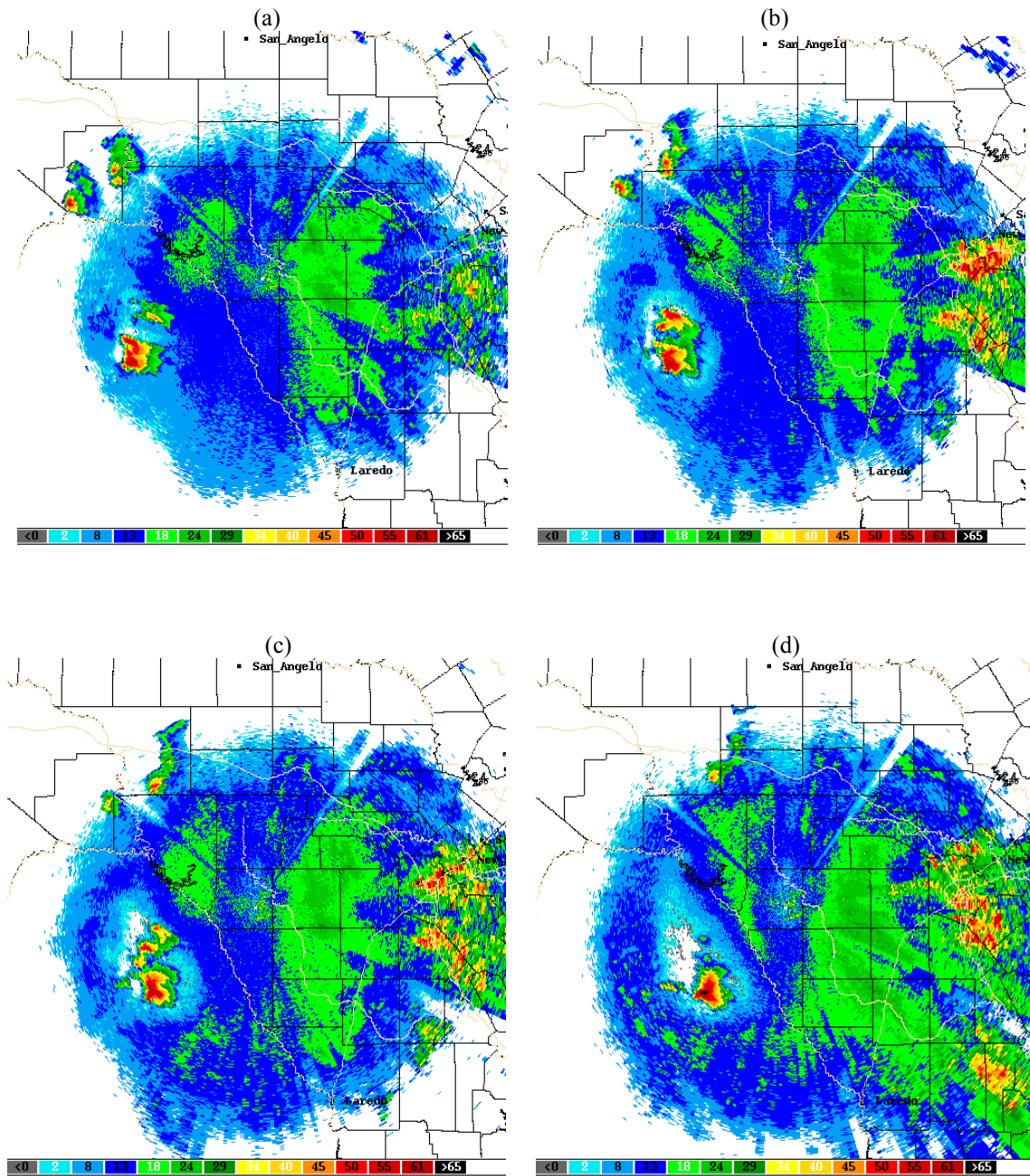
Fig. 29. 0.5 degree reflectivity images from KDFX on April 29, 1999 at (a) 3:41Z, (b) 4:16Z, (c) 4:34Z and (d) 5:10Z. Reflectivity values (dBZ) are according to the color code on the bottom of each image: from left to right, grey is < 0 dBZ, light blue is 2 dBZ, medium blue is 8 dBZ, dark blue is 13 dBZ, light green is 18 dBZ, medium green is 24 dBZ, dark green is 29 dBZ, light yellow is 34 dBZ, medium yellow is 40 dBZ, dark yellow/gold is 45 dBZ, light red is 50 dBZ, medium red is 55 dBZ, dark red is 61 dBZ, and black is >65 dBZ.
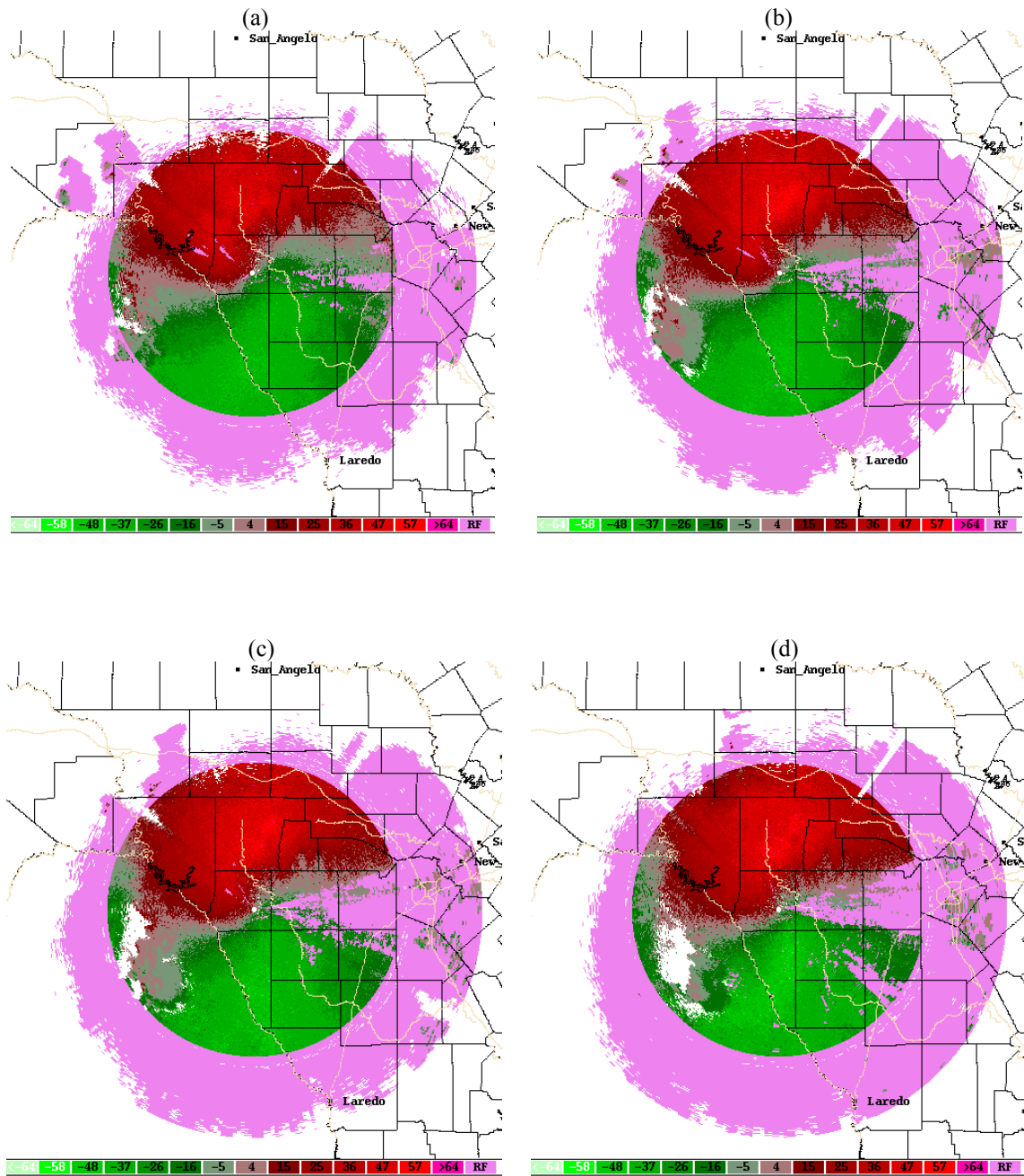
Fig. 30. 0.5 degree radial velocity images from KDFX on April 29, 1999 at (a) 3:41Z, (b) 4:16Z, (c) 4:34Z and (d) 5:10Z. Velocity values (knots) are according to the color code on the bottom of each image; negative values for inbound velocities and positive values for outbound velocities. Green values, from left to right on the scale at the bottom are: <-64, -58, -48, -37, -26, -16, and -5 knots. Red values, from left to right on the scale are: 4, 15, 25, 26, 36, 47, 57, >64 knots, and RF, which denotes range-folded velocity data.

departure. Gauthreaux (1972) found that birds will fly above an overcast layer if the cloud base is below 7000 feet. Blokpoel and Burton (1975) agreed and determined that birds will fly above low clouds and below medium or high clouds. However, Hassler et al. (1963) and Forsyth and James (1971) found that not all birds will depart under cloudy conditions. In Richardson's examination of many more migration studies, he concludes that clouds can suppress bird migration, but not completely.

d. Stability

Gauthreaux (1972) found that arriving springtime passerine migrants flying during the day fly at a higher altitude than they would at night. The difference between flight altitude during the day and night was approximately 3000 feet. He surmised that the passerines arriving from a trans-Gulf migration during the day were flying at a higher altitude to stay above the cumulus clouds and turbulence that was present at the time. Richardson mentions that while turbulence would seem to increase the energy requirements for flight (because of the constant need to correct the flight orientation), there wasn't a sufficient number of studies which made a note of stability to reach a conclusion.

e. Other Factors

Richardson (1978) found insufficient correlation between atmospheric variables such as temperature, pressure, visibility and humidity (by themselves) and the number of migrants aloft. While temperature can severely impact the availability of food at a

particular location, Hassler et al. (1963) concluded that temperature alone was an improbable trigger for departure.

3. Radar Ornithology

The fact that birds can be detected using radar was discovered soon after the deployment of military radars in England during World War II. Since that discovery, radar has been one of the few tools ornithologists have available to directly observe bird migrations. A good history of the development and use of radar by ornithologists can be found in Eastwood (1967) and Bruderer (1997a, 1997b). Ornithologists have especially used meteorological radars due to their dense network (especially in the United States), availability of the radar data which are stored on tapes, and due to various technical issues (such as the wavelength of the radar energy used) which allow birds to be more easily detected with weather radars than to other types of radars available (Gauthreaux, 1970).

The power returned (P_r) to the radar from a point target (such as a bird) out in space is governed by the radar equation:

$$P_r = \frac{P_t\, g^2\, \lambda^2\, \sigma}{64\, \pi^3\, r^4} \qquad (4)$$

where P_t is the power transmitted by the radar, g is the antenna gain of the radar, λ is the wavelength of the radar wave, σ is the backscattering cross-sectional area of the target, and r is the radius to the target. All of the above terms are constants in regards to a particular radar system except σ and r. From equation 4, we note the power received is

inversely proportional to the fourth power of the radius to the target, so doubling the distance yields a weaker return of 16-times that of a target at the original distance.

The backscattering cross-sectional area for a particular target depends on five parameters, as listed by Bruderer (1997a): the dielectric constant of the target, its size, shape, aspect, and the polarization of the radar waves. When a radar wave encounters an object or portion of the atmosphere where the refractive index differs, then a secondary wave is produced, a portion of which is sent back to the radar. Eastwood (1967, 46-48) discloses that the water contained in the bird's body is responsible for scattering the radar energy back to the target; the amount of energy returned by a bird is approximately equal to the amount of energy sent back by a water sphere of the same mass as the bird. Water has a high dielectric constant, which is a fact already known by meteorologists. Because they have low water content, wing movements have a negligible effect.

The size of the bird is important for a couple of reasons. First of all, larger birds have a larger physical size and more water mass (resulting in a better ability to send radar energy back). Size also matters because the scattering of radar waves by a target has been shown to be size-dependent (see Fig. 31). If the object is large compared to the radar wavelength (ratio of the target's circumference to the wavelength being greater than 10), the reflected energy is approximately proportional to the target's shadowing area (Bruderer 1997a). If the target is small compared to the radar wavelength (ratio of circumference to wavelength less than 1), Rayleigh scattering takes place in which the energy returned increases with the 6th power of the target diameter. However, if the target is of the same order of magnitude to the radar wavelength, a secondary or creeping

wave is also returned which interferes with the surface scattering to produce a fluctuating region, called the Mie region (Bruderer 1997a). Meteorologists select the wavelength of weather radars so that the power returned from hydrometeors safely falls in the stable Rayleigh region in order to accurately equate power returned to the size and numbers of hydrometeors present.

The aspect of the target with regards to the radar wave is also important in regards to how much radar energy is intercepted by the target. One study regarding this is Edwards and Houghton (1959), and the results are shown in Fig. 32. A bird's body was suspended by a nylon cord a short distance away from a 3-cm wavelength radar. The bird's orientation with respect to the radar wave was changed in order to see how the backscattering cross-sectional area changed with respect to the bird's position to the wave. Three different birds were used in this study: a domestic pigeon, a European starling, and a house sparrow. The largest cross-sectional area for each bird occurred when the radar beam struck the bird broadside. The smallest cross-sectional areas occurred when the radar beam was struck the bird head-on or tail-on.

This phenomenon is often recognizable on the WSR-88D during bird migration. A maximum value of reflectivity on the PPI occurs when the radar wave is orthogonal to the direction of migration. Fig. 33a is a reflectivity image from Del Rio from later in the night than Fig. 29 and Fig. 30. Higher reflectivity values can be seen in Fig. 33a to the east and southeast as well as to the west and northwest of the radar compared to other areas. O'Bannon (1995) coined this pattern as the butterfly pattern (due to appearance only), and this pattern is a visual clue to the operational meteorologist (beyond
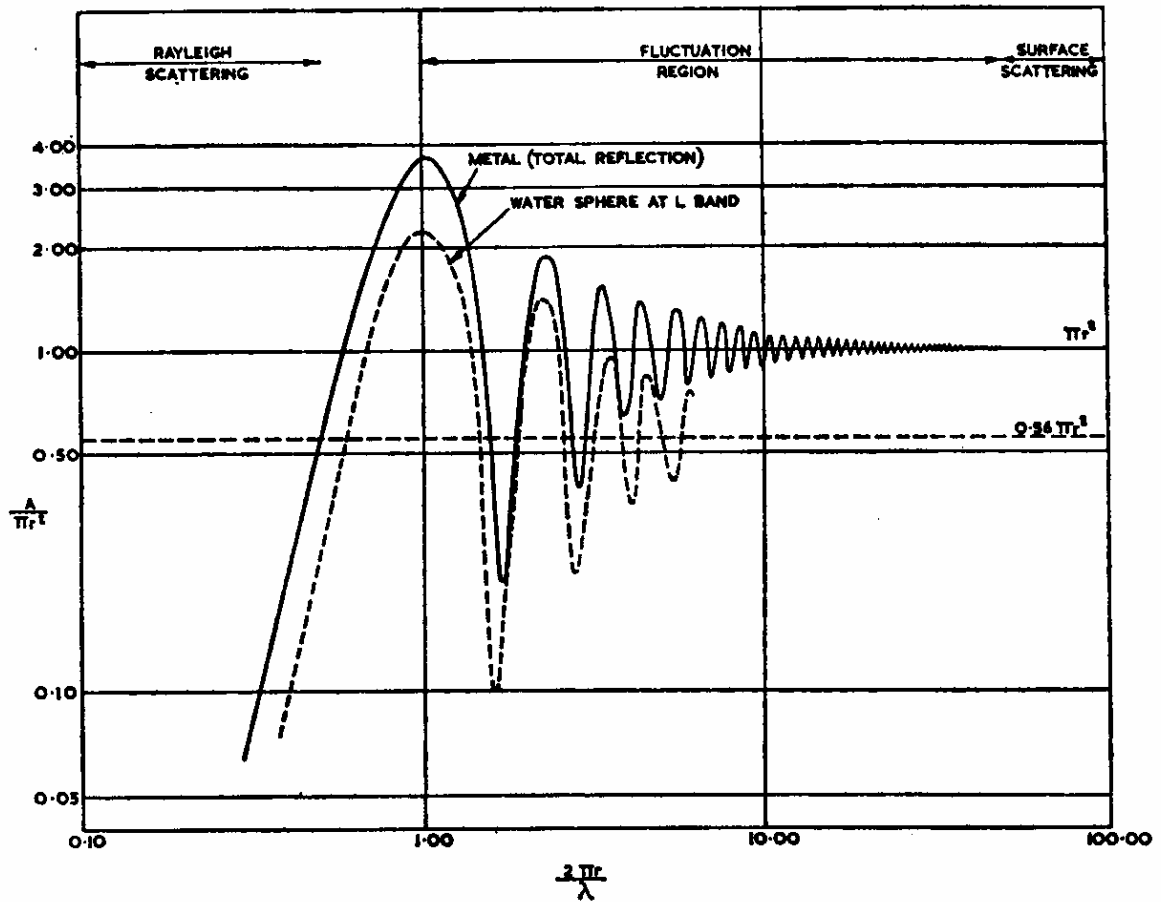
Fig. 31. Variation in backscattering cross-sectional area with respect to the ratio of target circumference and radar wavelength (from Eastwood 1967). Solid curve denotes the results for a metal sphere (perfect scatterer) and the dashed curve is a water sphere.
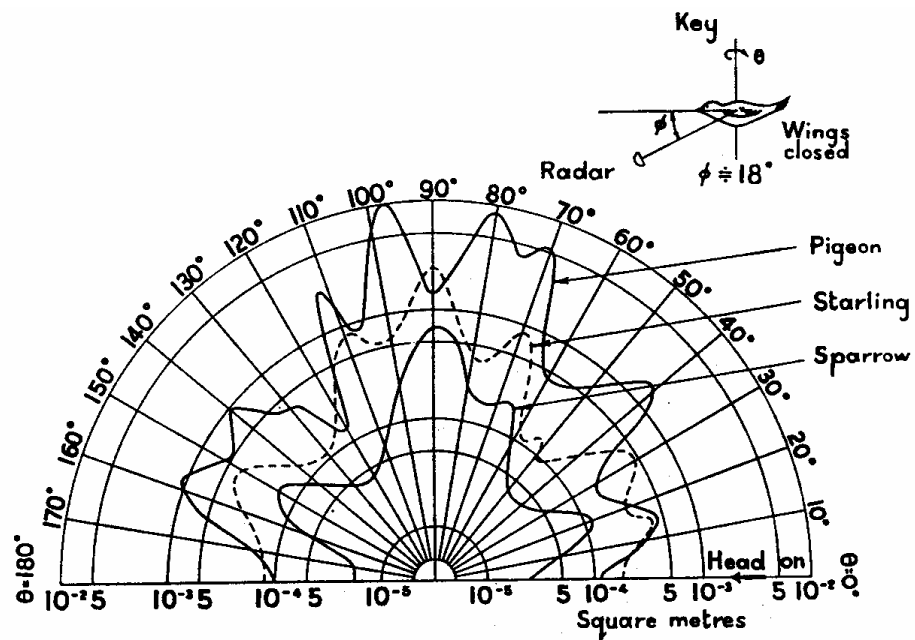
Fig. 32. Polar diagram showing the difference in a bird's backscattering cross-sectional area as the bird's aspect to the radar wave changes (from Edwards and Houghton 1957). 90 degrees corresponds to the radar wave striking the bird broadside. 0 degrees is the wave striking head-on and 180 degrees is tail-on.
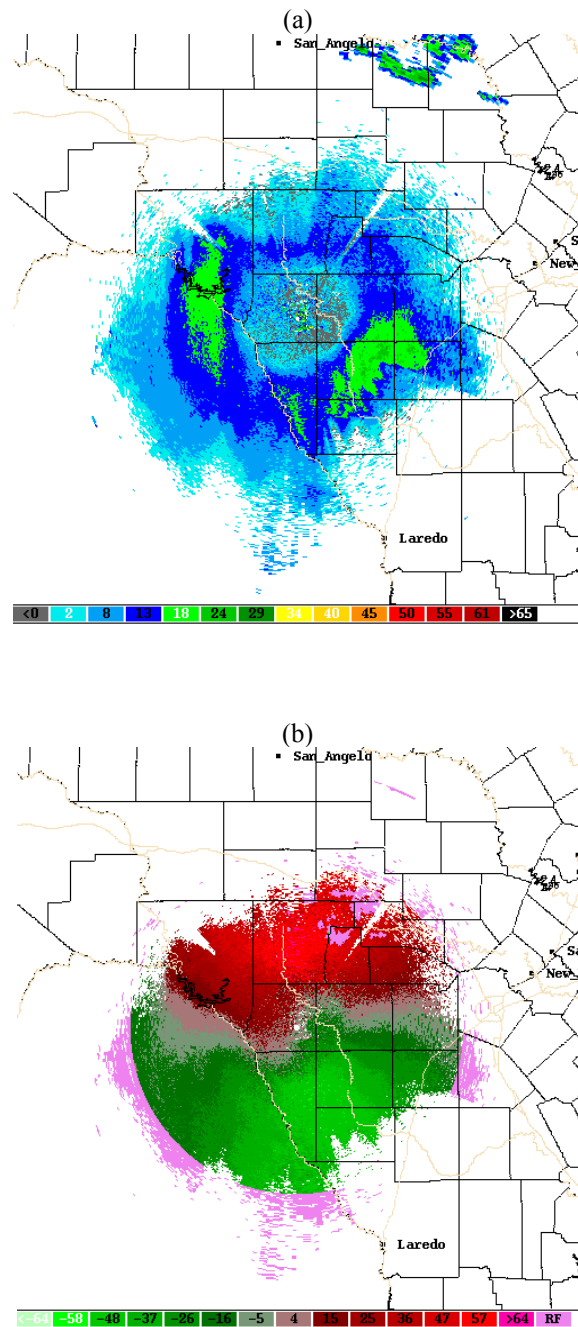
Fig. 33. 0.5 degree KDFX images from April 29, 1999 at 11:24Z of (a) reflectivity and (b) radial velocity. Reflectivity values (dBZ) for (a) are according to the color code on the bottom of the image: from left to right, grey is < 0 dBZ, light blue is 2 dBZ, medium blue is 8 dBZ, dark blue is 13 dBZ, light green is 18 dBZ, medium green is 24 dBZ, dark green is 29 dBZ, light yellow is 34 dBZ, medium yellow is 40 dBZ, dark yellow/gold is 45 dBZ, light red is 50 dBZ, medium red is 55 dBZ, dark red is 61 dBZ, and black is >65 dBZ. Velocity values (knots) for (b) are according to the color code on the bottom of each image; negative values for inbound velocities and positive values for outbound velocities. Green values, from left to right on the scale at the bottom are: <-64, -58, -48, -37, -26, -16, and -5 knots. Red values, from left to right on the scale are: 4, 15, 25, 26, 36, 47, 57, >64 knots, and RF, which denotes range-folded data.

witnessing the temporal onset of migration) that bird migration and velocity contamination is taking place. Fig. 33b is the velocity image from the same time as Fig. 33a. The velocity image confirms the flight direction was from south to north and verifies that the radar wave was intercepting the birds broadside where the reflectivity values are indeed greatest.

Finally, the shape of the target and the polarization of the radar wave also affect the backscattering cross-sectional area of the target. In the case of the WSR-88D, the radar wave is horizontally polarized because raindrops are slightly flattened as they fall; the resulting horizontal radar wave intercepts a greater area of the raindrop than a vertical wave would. A target that is taller than it is wide would not appear as strongly on the WSR-88D as a target of the same area that has opposite dimensions. One should note that equation 4 is valid for a single point target only. When you have more than one target in a pulse volume, the different scattered waves from each target can interfere with each other, depending on the positions of the targets with respect to each other. For instance, if two targets are separated by a distance of $\lambda/2$ wavelengths (or any interval thereof), the two scattered waves will exactly cancel each other out and produce no net wave (no echo)! Inserting more targets into the pulse volume will tend to cause the fluctuations to average out, thereby producing a less variable signal.

4. VAD and VWP

The only velocity that Doppler radar can detect is radial velocity, or the extent to which a target is moving towards or away from the radar along the radar beam. A

technique to determine the horizontal wind using radial velocity was first developed by Lhermitte and Atlas (1961). As the radar antenna revolves about a complete circle at a constant elevation angle, the radar beam will intercept a particular height at a given range from the radar (see Fig. 34).

If sufficient radar targets are present, one can plot the radial velocity measured by the radar as a function of azimuth, as shown in Fig. 35. This is how the VAD algorithm gets its name (Velocity-Azimuth Display). The wind speed is determined by the magnitude of the sine curve (using the scale at left). The wind direction is determined from the absolute minimum of the sine curve, because the Doppler frequency shift of the radar wave is the shortest when looking directly upwind.

Fig. 34 shows some trigonometric expressions as it relates to the VAD technique. In this figure, the horizontal wind is blowing from left to right at a magnitude V_h. The dashed line sloped up and to the left represents the radar beam, which is at an elevation angle α measured from the ground up. The angle β is the angular difference between the beam and the direction of the wind ($\beta = 0$ when the beam is pointed directly upwind). V_t represents the terminal fall speed of the particle. Therefore, the equation that gives the total radial velocity (V_d) measured by the radar is:

$$V_d = V_t \sin \alpha - V_h \cos \alpha \cos \beta \tag{5}$$

The VAD algorithm uses a Fourier transform on the data to compute the wind for a given height. Using Fourier transforms allows the use of non-continuous data about the circle (Allen 1996). The minimum amount of data points that is allowable for the wind to be computed with this method is a user-supplied parameter for the WSR-88D
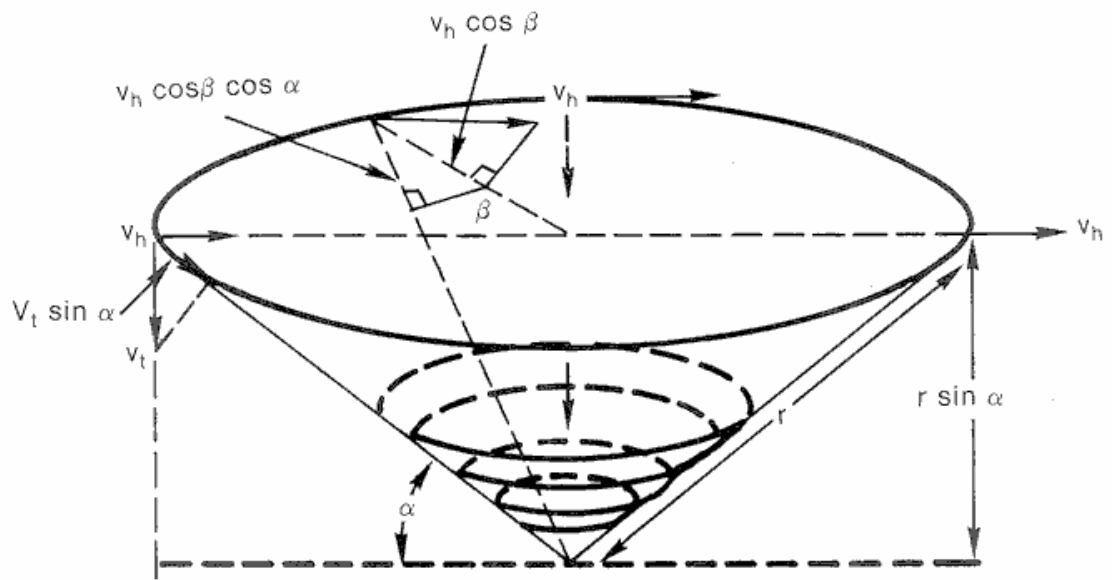
Fig. 34. Geometry of a radar scan to determine the horizontal wind (from NOAA 1991a).
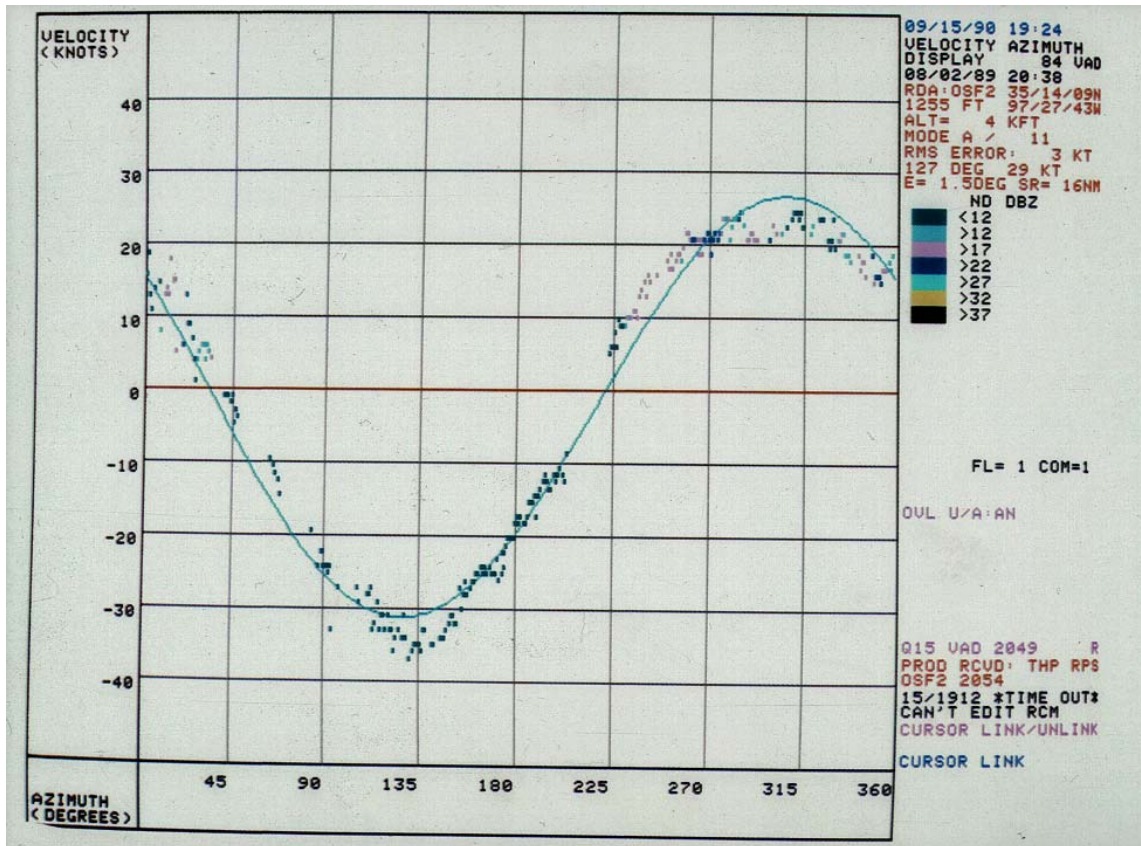
Fig. 35. Example of VAD display from the WSR-88D (From NOAA 1991b). This image is from a photograph (black and white reversed) taken of the WSR-88D Operational Support Facility radar at Norman, Oklahoma on September 15, 1990 at 19:24Z, and shows the VAD curve for the 4,000 foot altitude. The dots represent each target detected with the different colors representing their reflectivity value (in dBZ). The blue sine curve is the best-fit curve to the data computed by algorithm. In this case, the wind is from 127 degrees at 29 knots.

(ranging from 1 to 360), but the default value is 25 (NOAA 1991c, p. B-22). If the number of data points is less than this number, no wind will be reported for that altitude. In addition to requiring a certain number of samples, the algorithm also applies symmetry and fit tests to the data in order to accept the VAD wind estimate.

5. Bird Contamination of the VWP Product

Larkin (1991) was perhaps the first to discuss the potential of biological targets contaminating WSR-88D algorithms. He mentioned that large flocks of birds (geese) could occupy more than one gate and therefore pass through a clutter algorithm designed to reject such returns. Larkin also mentions that the departure of roosting birds in the morning could trip the microburst detection algorithm, if it weren't for the fact that the algorithm searches for echo aloft as well. Finally, citing an example from New England, he mentions that migrating birds could contaminate the VAD algorithm, leading to erroneous winds in the VWP product.

Davis et al. (1995) compared VWP output from twelve sites with winds measured via weather balloon near those sites. The authors found that the root mean square vector difference between winds measured by radiosonde and winds calculated on the VWP (863 data pairs) was higher during the fall and winter period than during the summer. They theorized that inversions, which allow anomalous propagation of the radar beam, could cause the VWP winds to differ from those measured by balloon. However, they did mention that fall bird migration could not be discounted as a cause.

Jungbluth et al. (1995) did a similar study at a wind profiler site in Iowa. They launched hourly pibals and compared those results to the 404-MHz wind profiler during the night when bird migrations were suspected. The authors found that the vector difference between the profiler and the pibal wind measurements was roughly from the North at 15 knots. They named this vector difference the bird vector, although they didn't personally observe birds flying at the time. They also noted that the Johnston, IA WSR-88D had anomalous VWP-derived winds at the times when the profiler was in error.

O'Bannon (1995) highlighted several cases of VWP contamination from across the country. He does a very good job of discussing the evolution of the events leading to the nightly VWP errors, which is similar to what Steve Allen relayed to me in personal communications. This paper does not offer any solutions, but does recommend some mitigation techniques (such as awareness of the problem by WSR-88D operators and comparing the VWP output with radiosondes nearby).

Zrnic and Ryzhkov (1997) present a possible solution using polarimetric radars. Since the WSR-88D can be upgraded to become polarimetric, the possibility of identifying birds using polarimetric radars could solve the VWP contamination problem in the future. The authors found that the cross-correlation coefficient of birds is significantly lower than those caused by meteorological targets, so it could be possible for a computer algorithm to distinguish between the two. Not having polarimetric radar at my disposal, I cannot use the results of this paper for my research. Besides, a solution needs to be found in order to eliminate the migratory bird contamination from VWP

output from stored radar data, and from future VWP calculations, until the WSR-88D is upgraded to be polarimetric nationwide.

Haro and Gauthreaux (1997) along with Gauthreaux et al. (1998) dealt with WSR-88D VWP contamination by migrating birds, but did not attempt to solve the problem. Both papers are excellent supporting documentation to augment what has been written in this chapter and in Chapter II. The authors noted that the VWP errors are usually to the velocity value itself, and not to the wind direction (supporting the hypothesis that birds fly with tailwinds).

Gauthreaux and Belser (1998) not only discussed the qualitative and temporal qualities of WSR-88D contamination by migrating birds, but they also calculated the number of birds flying past a mile (1.6 kilometer) front per hour as a function of reflectivity value seen on the WSR-88D. The counting of the birds was done visually using the moon-watching technique, and from using an image intensifier (night vision technology) on evenings without a full moon. Their quantification results are shown in Fig. 36.

Finally, a recent paper since my research began proposes a technique to eliminate bird contamination using existing WSR-88D technology (Zhang et al. 2002). The authors' method involves calculating the 7-point running mean along a radial and subtracting this mean from the original velocity data. They found that birds had a higher standard deviation of Doppler velocity than did a region of thunderstorms. They combined this standard deviation with the reflectivity value of the echoes to obtain a score, the exact computation of which is not disclosed. Additional comments regarding
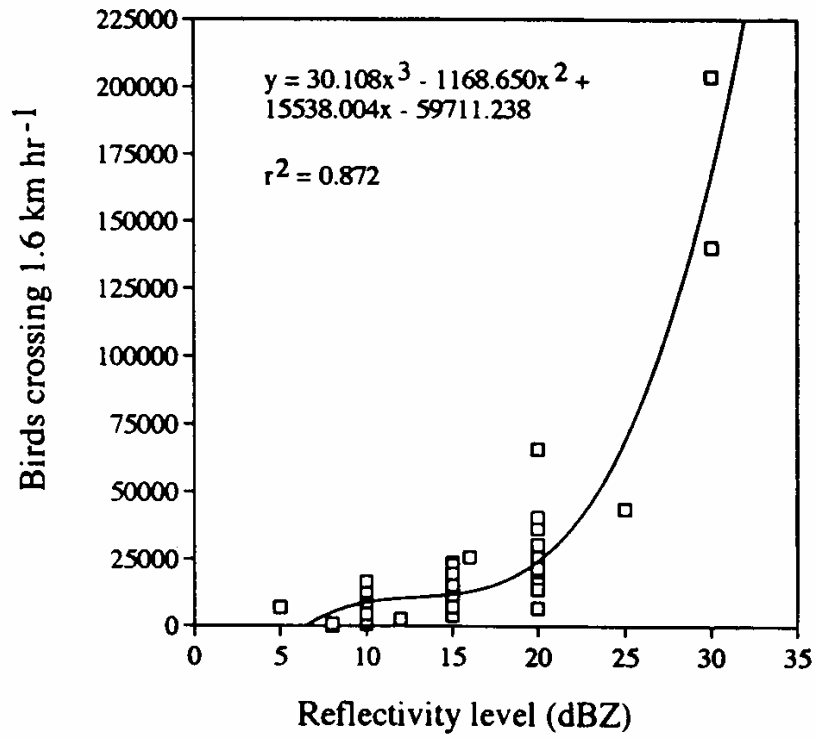
Fig. 36. Migration traffic rate past a mile (1.6 km) front per hour as a function of reflectivity (from Gauthreaux and Belser 1998). A reflectivity of 20 dBZ translates to approximately 25,000 birds per mile front per hour.

this technique will be made in the next chapter when I discuss solutions to the bird contamination issue.

6. Application to Observations Made in Chapter II

The moon-watching observations reported in Chapter II, compared with the WSR-88D data from New Braunfels and Houston, raised some questions that I deferred to this chapter. I will now make use of the knowledge gained from the literature review in an attempt to answer them satisfactorily.

The first question regarded the seemingly random bird directions computed from my observations on August 20, 1997 and summarized in Table 1. We know that birds prefer to fly with tailwinds, and seem to take their cue to migrate on a particular night when the winds are favorable to their intended direction of flight. The winds at the surface (see Fig. 4) and aloft (see Fig. 5a and Fig. 5b) began very light and from the south, and increased with height. Because some birds can be caught migrating in seasonally inappropriate directions when strong environmental factors such as winds are present, it is possible that some birds rely on a nudge from the winds to get them flying in any particular direction. With very light winds at the surface, there was not much of an environmental nudge to encourage them to fly in any particular direction at low altitudes. As the bird climbed in altitude, it would encounter stronger winds from the south and suggest to them to fly northward (reverse migration). The smaller silhouettes (flying higher) were the ones flying in a reverse manner, so this perhaps explains the results that are contained in Table 1.

The other question raised in Chapter II was why the radar data from September 17, 1997 fails to show without question bird contamination. Clearly, I observed birds flying on this night, and the radar reflectivity images contained in Fig. 25 suggest birds, yet the VWP output fails to show an obvious bird contribution. As I mentioned in that chapter, the first problem is a lack of upper-air data in the Houston area. Looking at Fig. 23b, the 700-mb winds at Lake Charles were from the northeast at 10 knots. The VWP was showing winds at 20-25 knots, although at a higher altitude than 700-mb. The winds at 500-mb over Lake Charles had more of a component from the north than is depicted on the Houston VWP. One explanation is that the birds are flying in a slightly different direction, and the VWP output is showing the vector sum of the wind velocity and the bird velocity. The vector component of the bird velocity to the VWP velocity could simply be to alter the direction and not impact the speed as much.

A more probable explanation lies with anomalous propagation of the radar beam. The WSR-88D assumes a standard atmospheric temperature and humidity profile when it figures the path of the radar beam through the atmosphere. A strong inversion aloft will cause the beam to bend more towards earth, yet the radar still assumes propagation of the beam under standard atmospheric conditions. The winds being attributed to the 500-mb level could, in fact, be winds from lower in the atmosphere due to anomalous propagation.

Fortunately, radiosonde data collected during TexAQS will help fill in the hole of upper-air observations over the Houston area in Chapter IV. This will help to verify the

VWP output with a nearby observation, and verify any presence of anomalous

propagation in the data as well.

CHAPTER IV

SOLUTION

While Zhang et al. (2002) appear to have arrived at a solution to discriminate radar sample volumes containing biological targets (such as birds) from those radar sample volumes containing only those targets of interest to meteorologists (such as precipitation), their method is not an ideal solution to the problem of VWP contamination. An ideal solution would not only identify and remove the birds from the data, but it would also allow for the computation of the true wind by the VWP algorithm using whatever remaining legitimate meteorological data may exist.

Because nocturnal passerine migration involves birds flying independently of each other, a velocity difference may exist between one radar sample volume containing a bird and adjacent radar sample volumes containing birds. This velocity difference is due to a variance in flight heading and/or flight speed of each bird (which can differ due to age, species, and health of the bird), as well as a difference in the total number of birds contained in each radar sample volume.

As mentioned in the last chapter, the method by Zhang et al. (2002) incorporates a seven-point running mean of Doppler velocities along a radial, and calculating for each radar sample volume the variance of its velocity from this seven-point running mean. A score for each radar sample volume is computed that includes this variance. Radar sample volumes with scores that meet or exceed the threshold found for birds will be removed from the data entirely.

The fundamental problem with this method is that, if there exists one or two valid meteorological data within the seven points being averaged, this valid data could be thrown out along with the birds. That scenario is likely to happen if there are more birds within the seven bins being averaged than meteorological data, because the velocity of the meteorological data would be at greater odds from the neighboring birds' higher velocities. A better method for discriminating birds from valid meteorological data would allow for the occurrence of valid meteorological data embedded amongst birds, and allow for that valid data to be included in the VAD algorithm calculations.

A good beginning approach to solving the VWP contamination problem is to examine the raw data being used in the VAD algorithm. If the raw data show a unique attribute that would differentiate normal meteorological conditions from those conditions with migrating birds, perhaps the data could provide a way to exclude the birds from any algorithm calculations.

1. Double VAD Curve Hypothesis

When birds are not flying, all the radar targets will be wind-borne (with the negligible exception of insects). A VAD plot for each level will show points clustered about a single curve, similar to the one shown in Fig. 35 on page 67. The absolute minimum point in the VAD curve corresponds to where the radial velocity is most negative. Negative velocity in radar is defined to be where the radar wave's frequency is shifted higher, or the radar wave's wavelength is shortened, due to the Doppler effect. Assuming horizontal flow, the most negative radial velocity will be found where the

radar beam is pointed at targets moving directly towards the location of the radar. At this point, the azimuth of the radar beam will indicate the direction from which the targets are coming, which is how wind direction in meteorology is defined. The amplitude of the curve varies according to the speed (a higher speed results in higher amplitude).

Assume that, at a time when birds are migrating, each individual radar sample volume at a given height contains either birds or a sufficient number of wind-borne targets only (dust, slow-flying insects, chaff, etc.) to return a detectable signal. Because the birds are partaking in powered flight, there will be a difference in the radial velocity between radar sample volumes containing birds and those nearby radar sample volumes that do not. The only exception to this is where the radar beam is orthogonal to the orientation of the birds in flight.

Further assume that, at a particular height, there are a comparable number of radar sample volumes containing birds and radar sample volumes that do not. When one looks at the VAD display for that height, there should be two clusters of points present and not one. One cluster will be due to the birds (the vector sum of the bird velocity and the wind velocity), and the other will be due to the wind-borne targets (wind velocity only). If two clusters are observed, the real wind could possibly be differentiated from the birds' velocity and be reported.

Prior to a migration event, there should be only one VAD cluster present and that cluster would represent the actual wind. When the birds start to migrate, the existence of two clusters should begin. From the review of bird migration in the last chapter, the

time when the maximum number of birds are flying is around two to three hours after

sunset. Therefore, the number of birds flying should be lower at the onset of migration

than later in the evening. Because wind-borne targets (other than hydrometeors) are

usually surface-based or generated by turbulence, the number of such targets will be a

maximum when the atmospheric boundary layer is active (which is during daylight). At

the onset of the migratory movement, the number of wind-borne targets are decreasing

while the number of birds are increasing. The implication is that the time immediately

following the onset of migration could be a critical time for detecting two VAD clusters

of points.

The wind-borne targets of interest typically have reflectivity values below 0 dBZ

(O'Bannon 1995). O'Bannon also notes that a single songbird at the default WSR-88D

VAD range of 30 km can yield a 10 dBZ return. While a radar sample volume can

contain a mixture of wind-borne targets and birds, the Doppler velocity value being

reported is heavily weighted towards the target creating the strongest return (O'Bannon

1995). Therefore, the radar sample volumes must be small enough so that many contain

wind-borne targets only.

The dimensions of the radar sample volume is critical in excluding birds from the

sample volume, because the odds of having a bird (randomly distributed in space)

contained in a radar sample volume increases as the size of the radar sample volume

itself increases. The WSR-88D has a horizontal and vertical beam width of

approximately one degree (NOAA 1991b, p. 2-3) and the depth of the radar sample

volume is 250 meters (NOAA 1991b, p. 2-4). Because of the angular beam width, the

width and height of the radar sample volume increases with range; at 57 kilometers, the radar sample volume will be 1 kilometer in diameter (Rinehart 1999, p. 81). Clearly, we must concentrate on the nearby radar sample volumes in order to attain a sufficient number of radar sample volumes with wind-borne targets only in our VAD. This maximum allowable range value will be determined later.

2. Data

In order to test the validity of the double-curve hypothesis, level-II radar data from the Houston WSR-88D (KHGX) collected during the period of TexAQS 2000 are used. Level-II data contain the azimuth angle (in degrees), elevation angle (in degrees), reflectivity (in dBZ), radial velocity (in m/s), spectrum width (in m/s), and range (in kilometers) to the center of the each radar volume returning a detectable signal to the WSR-88D. All data on the level-II tapes have passed through the WSR-88D clutter suppression algorithms, so the effect of clutter is minimized as much as possible. The clutter suppression is a band-reject filter with an adjustable notch around zero radial velocity. This can also remove valid meteorological data whose radial velocity falls within the zero isotach being rejected (NOAA 1991a, p. 3-11).

The data are read off the 8-mm tape by a computer program named WSR-88D Visualization Software, or WVS (NCDC, 2003). The source code has been modified to write the pertinent variables for drawing a VAD curve (azimuth angle, elevation angle, radial velocity, and range) for each volume scan to a separate data file. A second

program has been written in the IDL computer language to take the pertinent radar variables from the data file and construct the VAD output.

The VAD is a plot of the radial wind and azimuth for a constant height. The height (H) above ground of each radar target can be calculated with the following equation from Rinehart (1999, p. 62):

$$H = (r^2 + R^{*2} + 2\,r\,R^* \sin \varphi)^{1/2} - R^* + H_0 \qquad (6)$$

where r is the range to the center of the radar volume, R^* is the effective Earth radius which has a value of 4/3 of the Earth's actual radius (R^* allows us to treat the radar beam as traveling in a straight path, despite the fact that refraction in a standard atmosphere bends the beam down towards Earth), φ is the elevation angle of the beam, and H_0 is the height of the radar dish.

The IDL program will be written to calculate the height for each radar target. If the height of the target falls within a specified range of the altitude being sought (to be determined later), the program would calculate the horizontal velocity of the target and plot it on the VAD graph. Assuming zero vertical velocity, the horizontal velocity (V_H) of the target can be determined from the radial velocity (V_R) using a simplification of Eq. (5), using only the horizontal term and neglecting the wind direction angle (β):

$$V_H = V_R / \cos \varphi \qquad (7)$$

where φ again represents the elevation angle of the radar beam.

Winds are calculated by the WSR-88D VWP algorithm for whole values of thousands of feet, and this selection will be kept here. However, the IDL program will not mimic the production of the VAD graphs by the WSR-88D entirely. The WSR-88D

VAD algorithm does not use every single elevation angle where it intersects every single reporting altitude to obtain data; it only makes use of radar sample volumes at a single, specific range for a single, specific elevation angle. The radar operator can change the radar sample volume used by changing the slant range parameter (Allen 1996). Nevertheless, data from only one of the 9-14 elevation angles, at a single range, are used by the VWP algorithm to compute winds at a given level.

In a personal communication with Tim O'Bannon, the primary contact person at the National Weather Service's NEXRAD Support Facility for the VAD and VWP, this method was created to reduce the workload on the early Radar Product Generator (RPG). All algorithms were designed to operate as efficiently as possible, and this meant settling for only a subset of the total data available for the VWP algorithm. With today's more advanced computer processors, along with larger and cheaper computer memory, I will instead look at all the data available rather than using the specific slant range technique. In other words, every elevation angle will be used where it intersects the height of interest, as long as it is within the specified range limit designed to limit the size of the radar sample volume.

3. Results

a. August 15-16, 2000

The first complete day of level-II radar data (starting one hour before sunset to allow for comparison with later times) available during the TexAQS 2000 project was the evening of August 15, 2000. Sunset on this date in League City, Texas (location of

the Houston NWS office) was 1:00Z (on August 16) and sunrise the following morning was at 11:49Z. The accuracy of the WATADS VWP output for this night will be judged by looking at weather balloon launches from Wharton Power Plant (29.95N Lat., 95.54W Long.) for the TexAQS 2000 project (hereafter referred to as Wharton). Calculation of the winds was made by the use of a GPS unit attached to the balloon. For this first night, the only balloon launch was at 11:15Z, or approximately a half-hour before sunrise.

Fig. 37 is a series of reflectivity images from one hour before sunset (Fig. 37a), sunset (Fig. 37b), one hour after sunset (Fig. 37c), and three hours after sunset (Fig. 37d). In Fig. 37a, there are scattered thunderstorms occurring in southeast Texas. In Fig. 37b, most of the thunderstorm activity has died off by sunset. The spike of reflectivity going from the Houston radar towards the west-northwest is due to the setting sun (sun spike). Fig. 37c shows that low-reflectivity echoes have begun to appear one hour after sunset, which is consistent temporally and qualitatively with the onset of nocturnal bird migration. Fig. 37d continues to show the low-reflectivity echoes and the fact that they have grown in aerial extent in the two hours between Fig. 37c and Fig. 37d.

Fig. 38 is WATADS VWP output from the time near sunset. The default value for the VAD range (30 km) was used to construct the WATADS VWP figures. The VWP in Fig. 38 is only reporting winds for the lowest several thousand feet because of the lack of echoes within the radar sample volumes (see Fig. 37b).
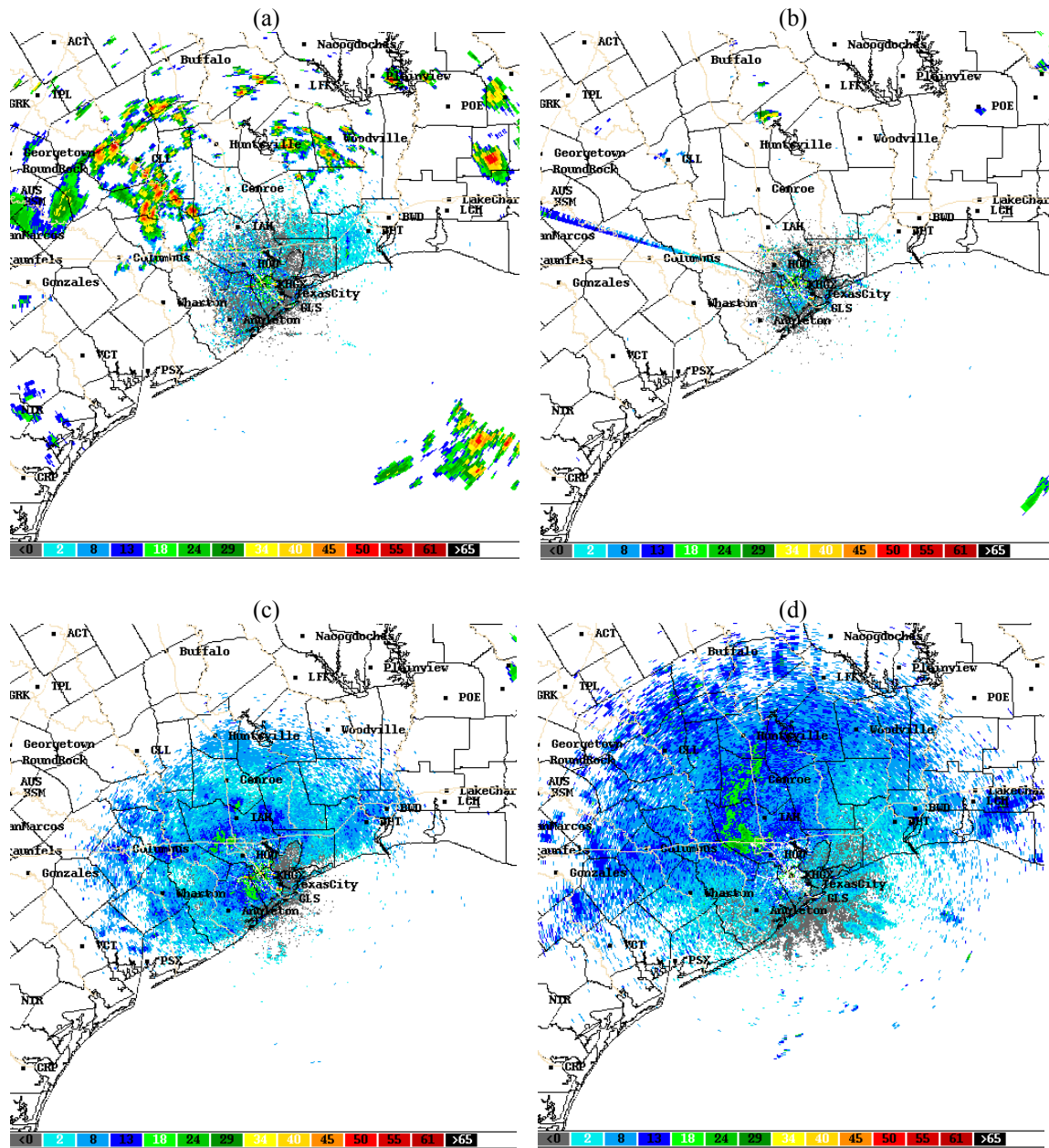
Fig. 37. 0.5 degree reflectivity images from KHGX for (a) August 15, 2000 at 21:58Z, (b) August 16, 2000 at 0:59Z, (c) August 16, 2000 at 1:59Z and (d) August 16, 2000 at 3:59Z. Reflectivity values (dBZ) are according to the color code on the bottom of each image: from left to right, grey is < 0 dBZ, light blue is 2 dBZ, medium blue is 8 dBZ, dark blue is 13 dBZ, light green is 18 dBZ, medium green is 24 dBZ, dark green is 29 dBZ, light yellow is 34 dBZ, medium yellow is 40 dBZ, dark yellow/gold is 45 dBZ, light red is 50 dBZ, medium red is 55 dBZ, dark red is 61 dBZ, and black is >65 dBZ.
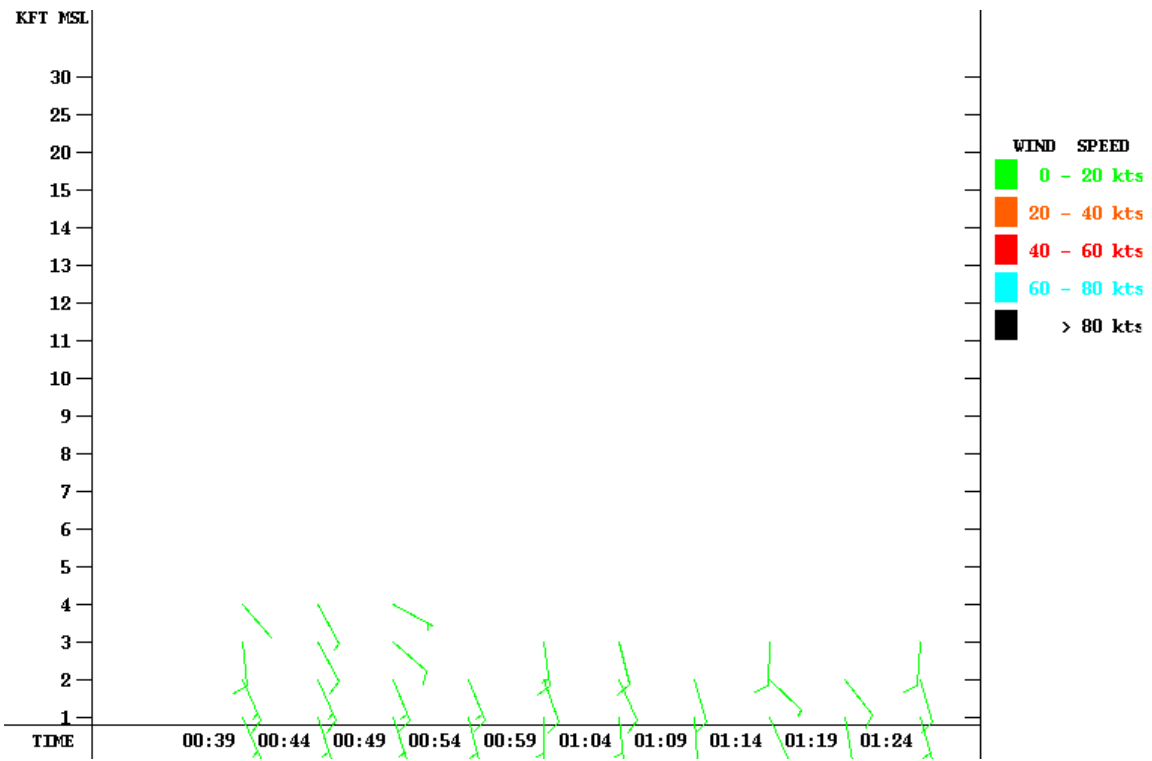
Fig. 38. WATADS VWP for KHGX on August 16, 2000 between 00:39Z and 1:24Z.
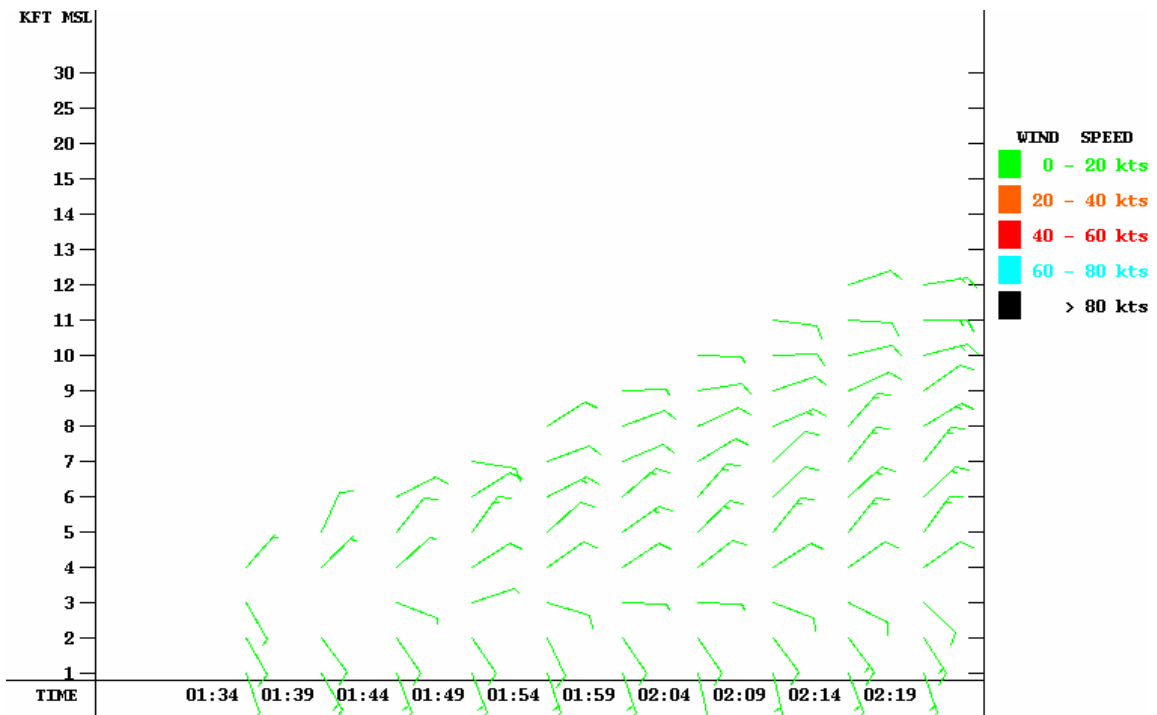
Fig. 39. WATADS VWP for KHGX on August 16, 2000 between 01:34Z and 2:19Z.
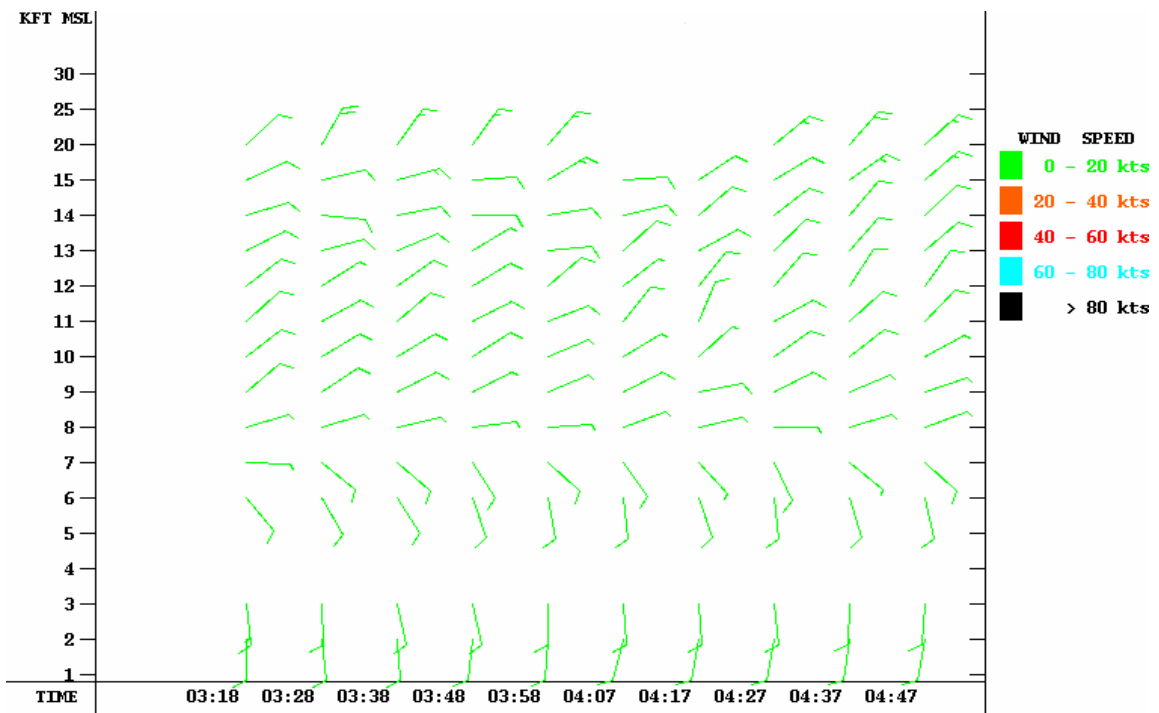
Fig. 40. WATADS VWP for KHGX on August 16, 2000 between 3:18Z and 4:47Z.

Fig. 39 is WATADS VWP output from around one hour after sunset. One can note that winds from the east to northeast are beginning to be reported, and these winds are being reported for higher and higher altitudes as time progresses. Fig. 40 is WATADS VWP output from around 3 hours after sunset and continues the trend from Fig. 39.

A curious difference in the VWP can be seen between Fig. 39 and Fig. 40. In particular, the winds at 6,000 feet can be seen to switch from the northeast at 15 knots at 2:19Z in Fig. 39 to blowing from the southeast at 10 knots at 3:18Z in Fig. 40. Could the velocity difference be due to migrating birds?

Fig. 41 is the WATADS VWP between 2:39Z and 3:38Z. Clearly, a striking change in the winds reported occurs between the 3:04Z volume scan and 3:08 volume scan. Between these two volume scans, the change in the wind at 6,000 feet takes place. Further investigation into these two volume scans found that the Volume Coverage Pattern (VCP) was switched from VCP 11 at 3:04Z to VCP 32 at 3:08Z. Because of this change, another reason for the wind difference besides migrating birds is suspected.

Fig. 42 is an illustration of VCP 11 and Fig. 43 is an illustration of VCP 32. VCP 11 is regarded as a precipitation scanning strategy and employs a greater number of elevation angles than VCP 32, which is a clear-air scanning strategy. Because the VAD algorithm uses a single elevation angle to compute the wind at a particular height, the implication in regards to the VWP is that the elevation angle used by the VAD algorithm could change from one VCP to another.
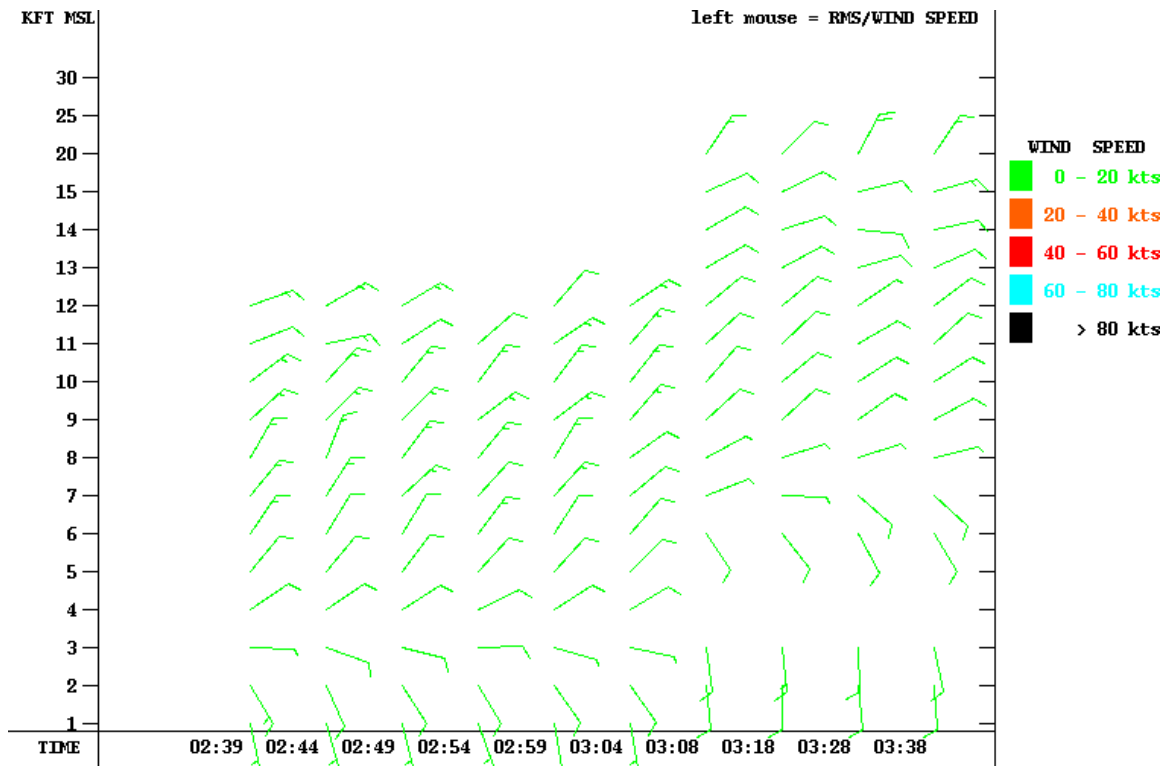
Fig. 41. WATADS VWP for KHGX on August 16, 2000 between 2:39Z and 3:38Z.
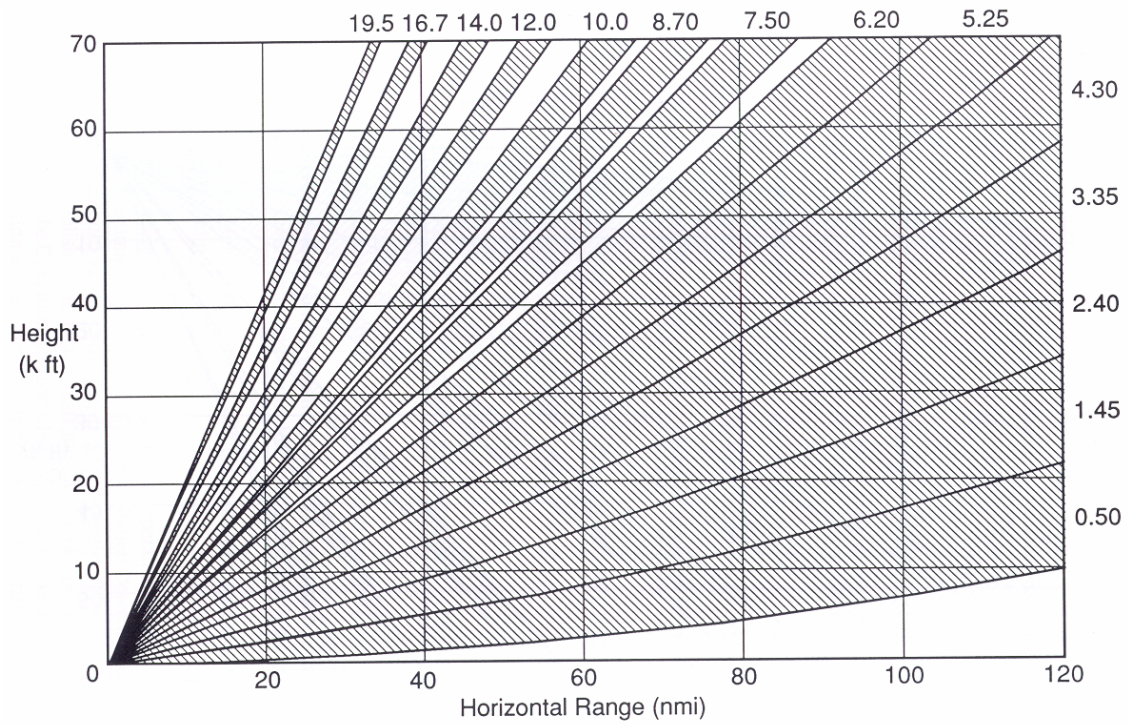
Fig. 42. WSR-88D radar volume coverage pattern for VCP 11. Shaded areas denote space where a radar beam is capable of making a measurement. The numbers at the right and top of the figure denote the elevation angle of the beam responsible. From NOAA (1991b).
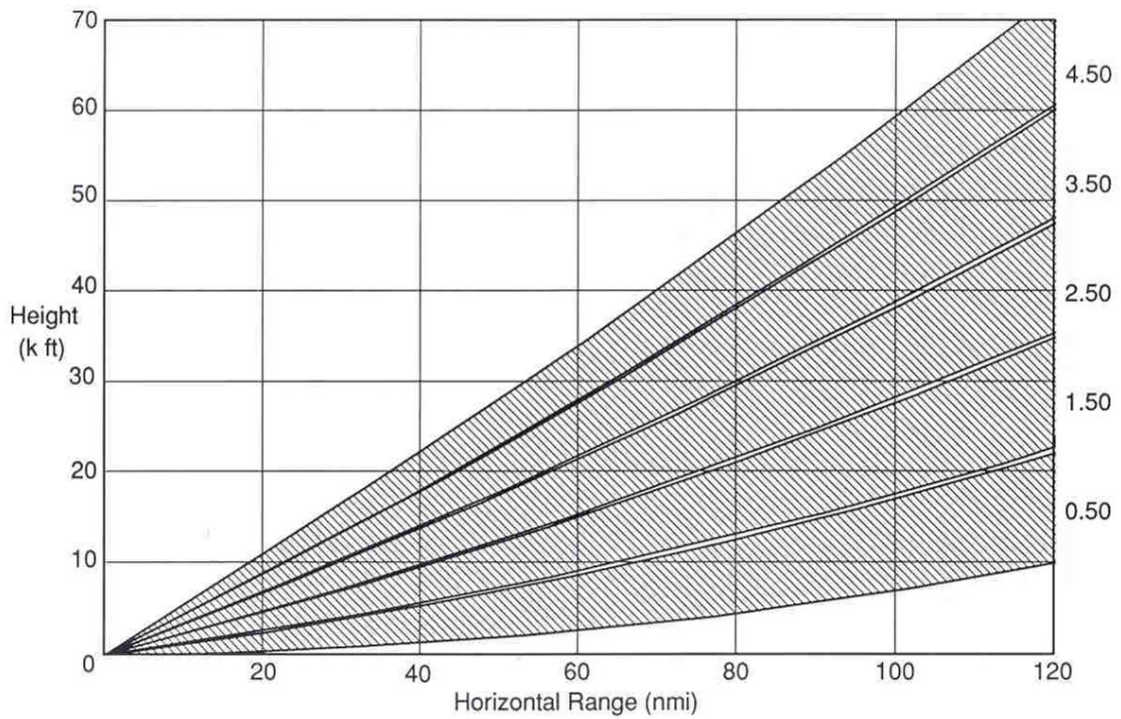
Fig. 43. WSR-88D radar volume coverage pattern for VCP 31. Shaded areas denote space where a radar beam is capable of making a measurement. The numbers at the right of the figure denote the elevation angle of the beam responsible. From NOAA (1991b).

For the WATADS VWP output shown, a default setting of 30 kilometers is used for the slant range parameter. This setting means that the elevation angle that intersects a particular reporting altitude closest to the 30 kilometer slant range is chosen. 30 kilometers is approximately 16.2 nautical miles. Consultation with Fig. 42 suggests that the 3.35 degree elevation angle could be used for the 6,000 foot level, whereas Fig. 43 suggests that the 2.5 degree elevation angle could be used for the same 6,000 level instead.

The use of different elevation angles could result in velocity differences if anomalous propagation of the radar beam is taking place. If the beam with a 2.5 degree elevation angle is bent more towards the earth than the 3.35 elevation angle, the beam with a 2.5 degree elevation angle will be sampling the atmosphere lower than the beam with a 3.35 degree elevation angle. If the winds are different at the two different locations in the atmosphere, a different wind will be reported by the VWP when changing the VCP.

To test this hypothesis, a VAD plot was constructed for the 6,000 foot level using only the data on the 3.35 degree elevation angle at 3:04Z. In order to better mimic the amount of data used in the VWP, only the data within 15 feet of the 6,000 foot level are included in the VAD plot. The result of this method is shown in Fig. 44. The data plotted support the VWP calculation of a wind from the northeast at 10 knots depicted in Fig. 41.
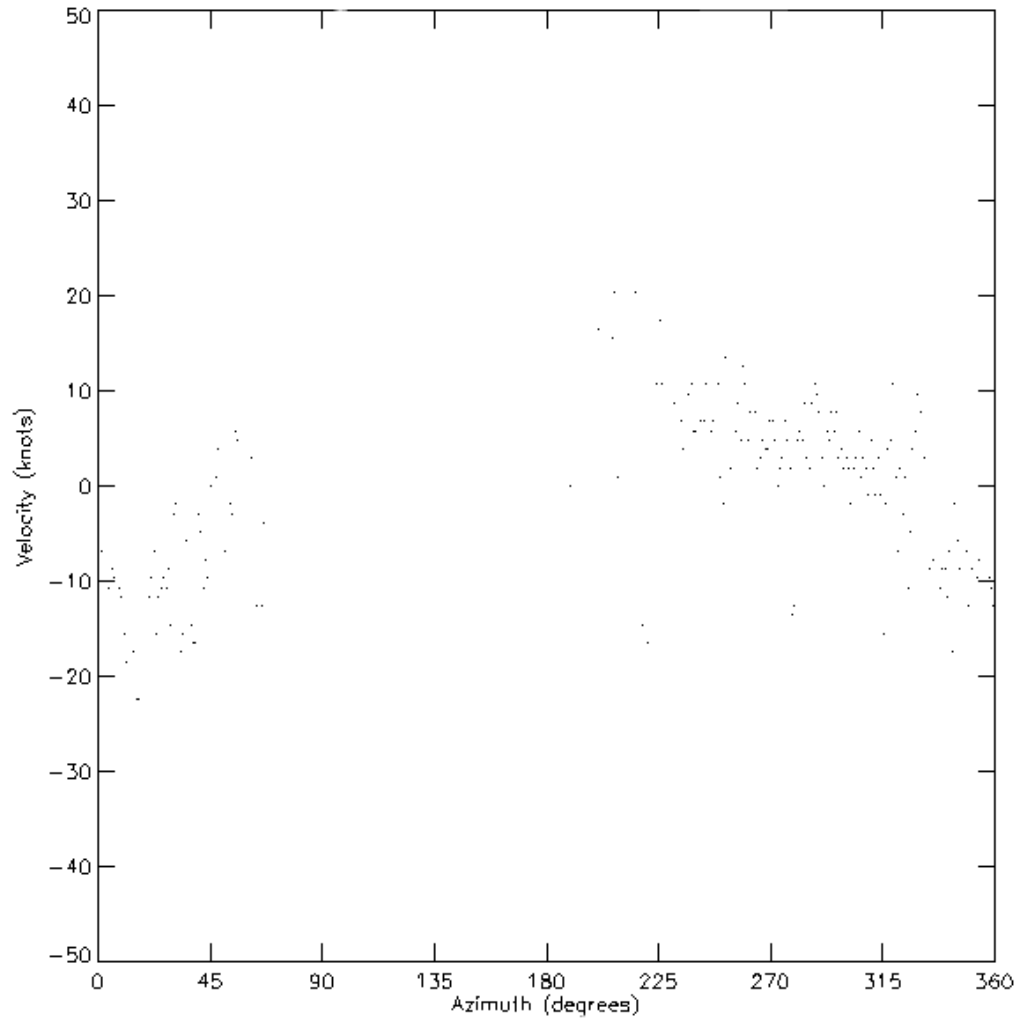
Fig. 44. VAD plot for 6,000 feet on August 16, 2000 at 3:04Z using only the 3.35 degree elevation angle. The azimuth angle (in degrees) is depicted on the abscissa from 0 degrees at left to 360 degrees at right, with tick marks every 45 degrees. Velocity (in knots) is depicted on the ordinate from -50 knots at the bottom to 50 knots at the top, with tick marks every 10 knots.
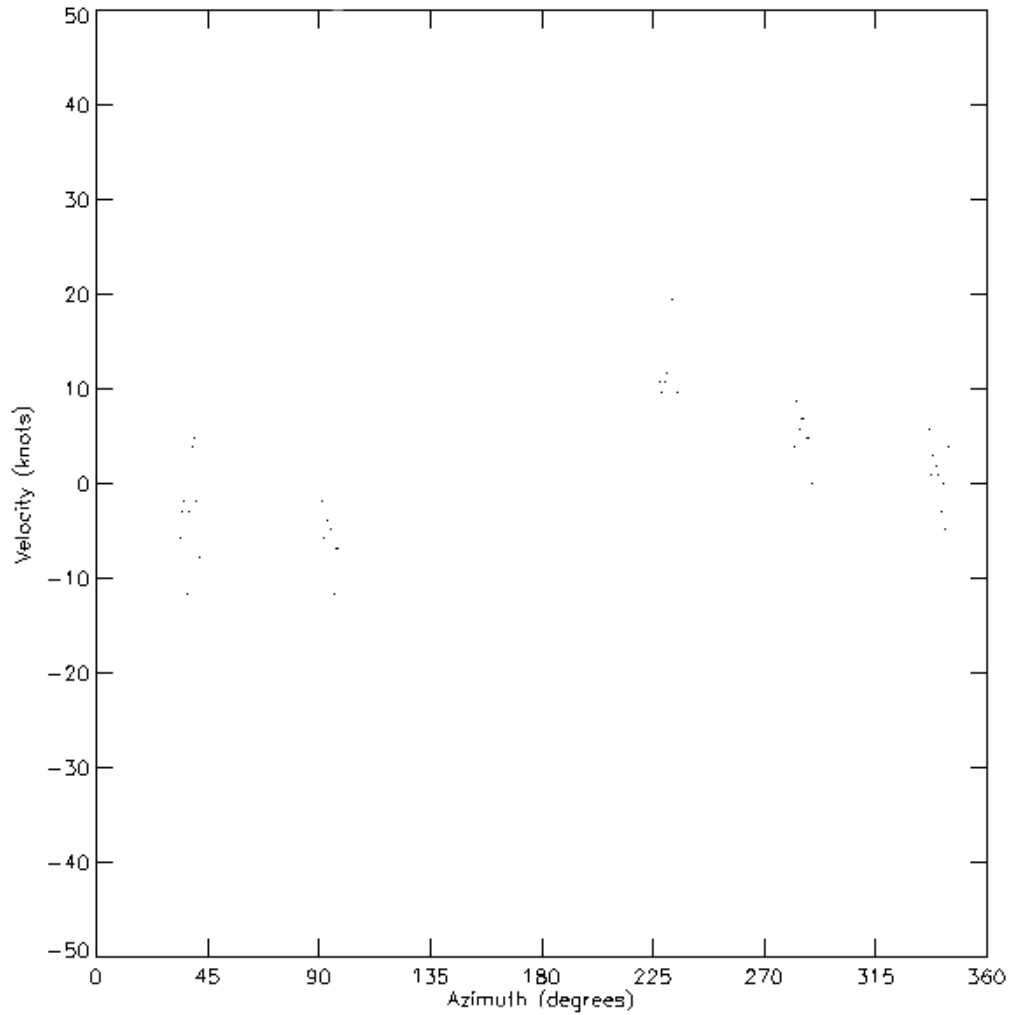
Fig. 45. VAD plot for 6,000 feet on August 16, 2000 at 3:08Z using only the 2.5 degree elevation angle. Axes and data are plotted in the same manner as Fig. 44 (page 98).

Fig. 45 is a VAD plot for 6,000 feet at 3:08Z using only the data from the 2.5 degree elevation angle. Again, the VAD plot in Fig. 45 supports the VWP result shown for this time in Fig. 41.

To test whether the use of a lower elevation angle results in a different wind estimate, a VAD plot for 3:04Z was drawn using the next lowest elevation angle in that VCP (2.4 degrees). Fig. 46 is the result of using the 2.4 degree elevation angle for computing the wind at 6,000 feet. Because Fig. 46 more closely agrees with Fig. 45 than Fig. 44, this suggests that anomalous propagation was the cause for the radical change in the VWP output. Clearly, the elevation angle of approximately 2.5 degrees is not sampling the same level in the atmosphere as the elevation angle of 3.35 degrees due to anomalous bending of the radar beam.

Based on the time of year, the temporal onset of the echoes, the fact that the echoes in Fig. 37c and Fig. 37d are mostly contained over land, and the fact that the reported winds aloft on the VWP are consistent with the argument that birds are flying along the coast towards Mexico, nocturnal bird migration is a possibility for this night.

Fig. 47 is a series of VAD plots for the 1,000 foot level. The graphs are constructed using all radar data with the center of the radar sample volume between the heights of 990 feet and 1010 feet, and within a maximum range of 60,000 feet. Fig. 47a shows the VAD plot for August 16, 2000 at 0:59Z, or sunset. There are a large number of targets cluttered around the zero velocity line, indicating that ground clutter was a problem this evening.
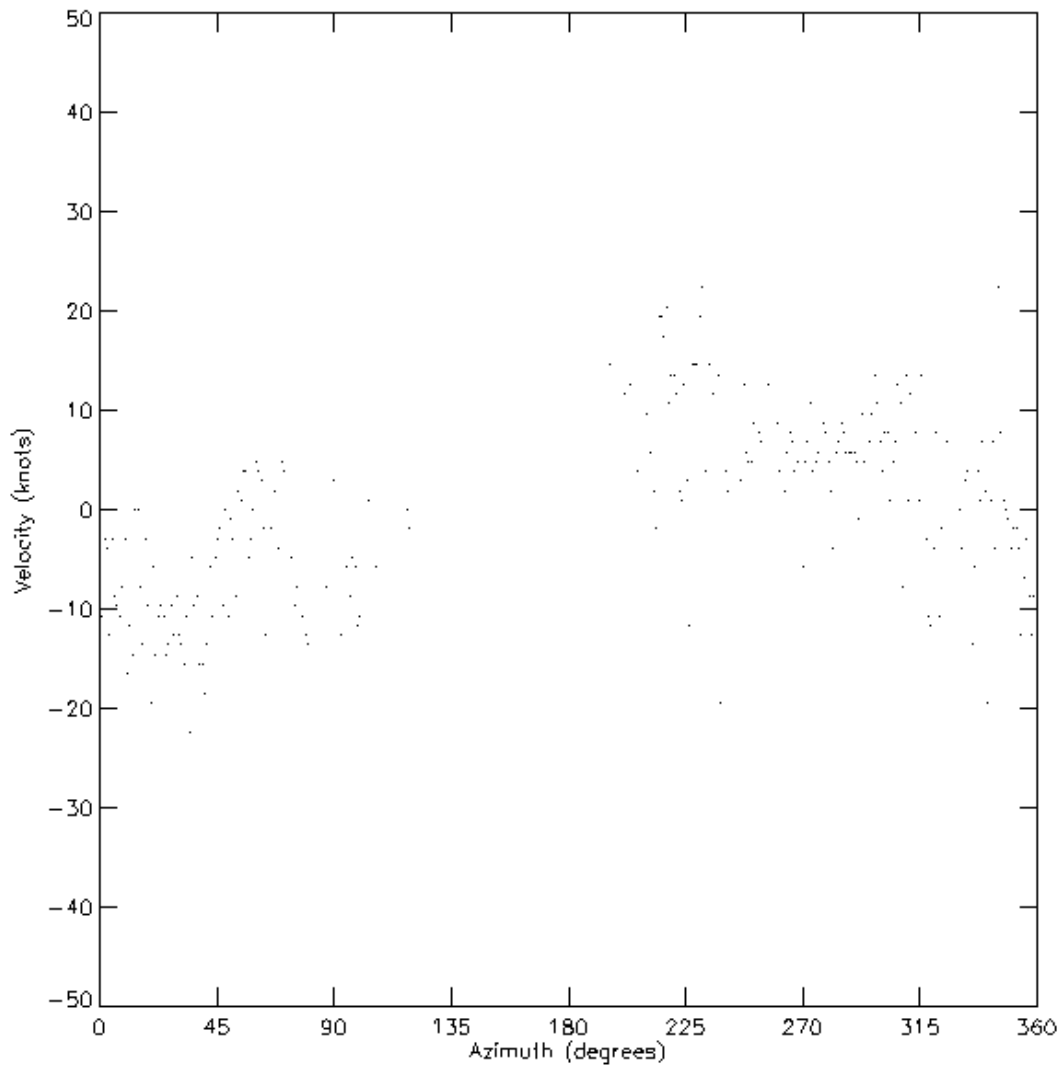
Fig. 46. VAD plot for 6,000 feet on August 16, 2000 at 3:04Z using only the 2.4 degree elevation angle. Axes and data are plotted in the same manner as Fig. 44 (page 98).

(a)

(b)
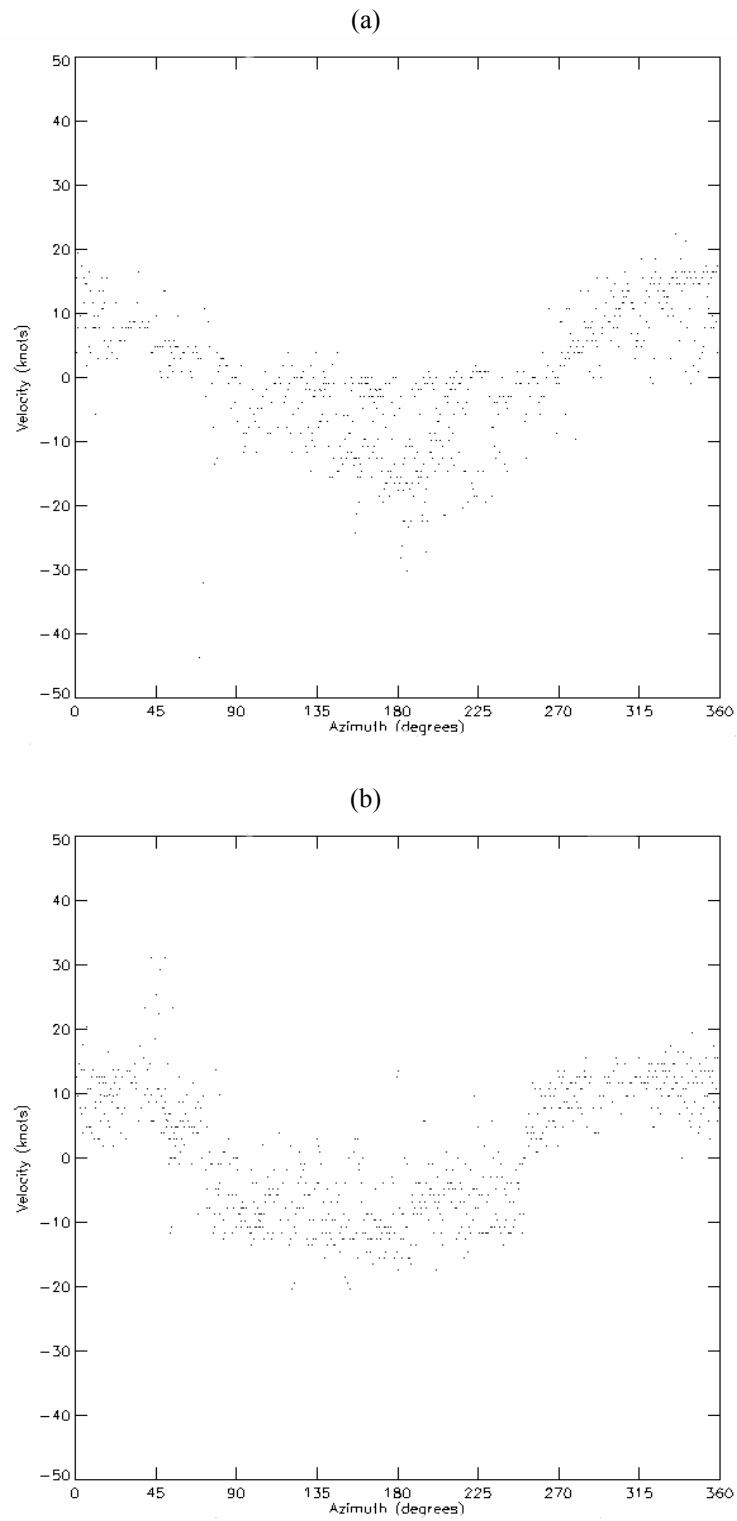
Fig. 47. VAD plots for 1,000 feet on August 16, 2000 at (a) 0:59Z and (b) 1:59Z. Axes and data are plotted in the same manner as Fig. 44 (page 98).

Fig. 47b is the VAD plot for 1,000 feet on August 16, 2000 at 1:59Z, or one hour after sunset. According to Fig. 37c, targets believed to be birds have already started flying, but Fig. 47b fails to show a second cluster. Comparing Fig. 47b with the VWP output in Fig. 39 for this time, the direction is in general agreement but the velocity is slower (perhaps due to clutter). The single cluster of points in Fig. 47b, coupled with the fact that the computed wind at this level is not consistent with birds migrating south, establishes that birds were not flying at the 1,000 foot level. Because two clusters of points were not visible at 1,000 feet, other levels should now be consulted to see if two clusters exist elsewhere.

Fig. 39 suggests that the 4,000 and 5,000 foot levels would be good to look at, since they are the first levels to show winds from the northeast (the direction birds would fly from if they were following the coastline). Fig. 48a and Fig. 48b are for the 4,000 foot level, and Fig. 49a and Fig. 49b are for the 5,000 foot level, for the same times as the corresponding images in Fig. 47a and Fig. 47b. Fig. 48a and Fig. 48b are constructed using all data between 3,950 feet and 4,050 feet due to insufficient data using the 20-foot interval that was used to construct Fig. 47a and Fig. 47b. Fig. 49a and Fig. 49b also use the greater 100-foot interval. Both Fig. 48b and Fig. 49b fail to show a second cluster of points, despite the fact that the reflectivity display in Fig. 37c showed the trademarks of the commencement of nocturnal bird migration.

In addition, the differences in the VAD plots between sunset and an hour after sunset, at both 4,000 feet and 5,000 feet, are not significant enough to suspect birds. Fig. 48a and Fig. 49a show data clustered around zero velocity (no identifiable maximum or

(a)

(b)
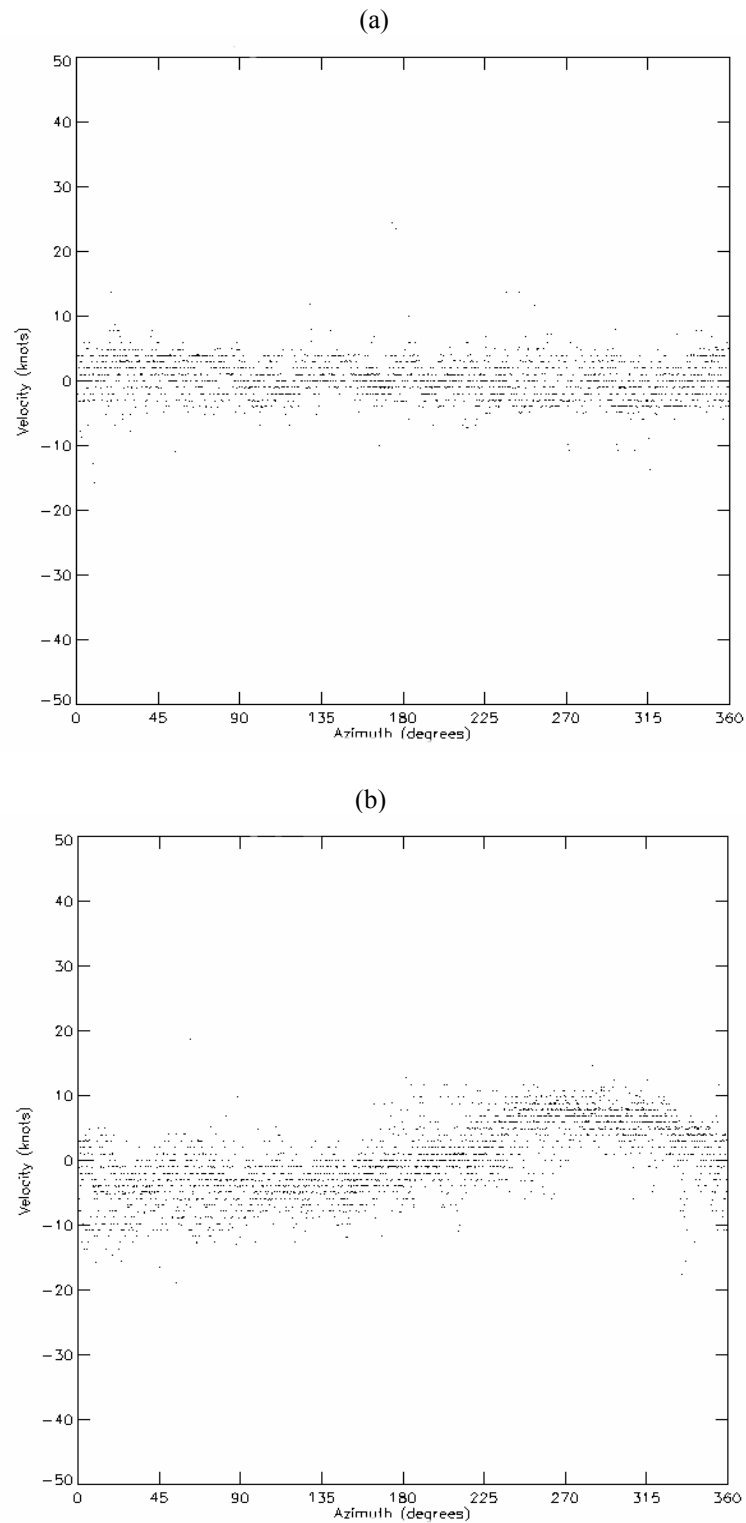
Fig. 48. VAD plots for 4,000 feet on August 16, 2000 at (a) 0:59Z and (b) 1:59Z. Axes and data are plotted in the same manner as Fig. 44 (page 98).

(a)

(b)
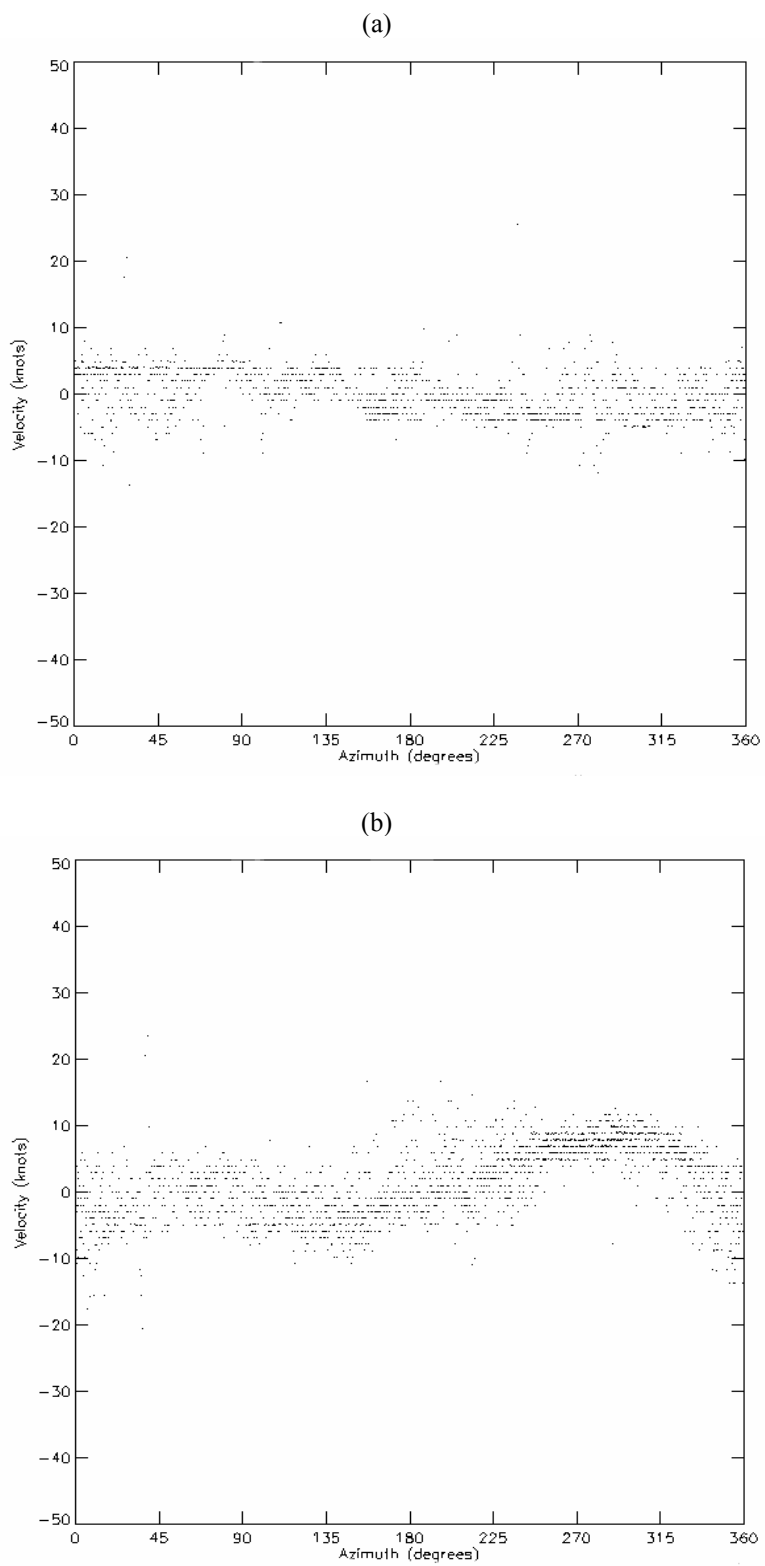
Fig. 49. VAD plots for 5,000 feet on August 16, 2000 at (a) 0:59Z and (b) 1:59Z. Axes and data are plotted in the same manner as Fig. 44 (page 98).

minimum points to the cluster exist, consistent with wind speeds near zero). Fig. 48b

and Fig. 49b show more of a cluster resembling a sine curve, but the corresponding wind

speed is only 10 knots for both. Small songbirds typically fly between 10 and 30 miles

per hour (Kerlinger 1995, p. 132), which is approximately 9 to 26 knots. Therefore, bird

migration is not likely for this night. In order to reasonably conclude that birds were not

migrating in great numbers on this particular evening, consultation with the weather

balloon data should be made and compared with the VWP output. The only balloon

launch for this night was at the very end of what would be considered the time for

nocturnal bird migration (half hour before sunrise).

Fig. 50 is WATADS VWP output from the time around the balloon launch

(11:15Z). The radar volume scan at 11:12Z is the time nearest to the launch time, and

the vertical column of wind barbs for that time is the third column from the right. Fig.

50 shows that the algorithm computed winds from the southwest at 10 knots at 2,000

feet and 3,000 feet. Winds could not be computed at 4,000 feet and 5,000 feet. At 6,000

and 7,000 feet, winds were calculated from the south-southwest at 10 knots, weakening

to 5 knots at 8,000 feet. Winds returned to be from the southwest at 10 knots at 9,000

feet, and from the southwest at 5 knots at 10,000 feet. Beginning at 11,000 feet, winds

were determined to be from the northeast, varying from 5 knots at 12,000 feet to 20
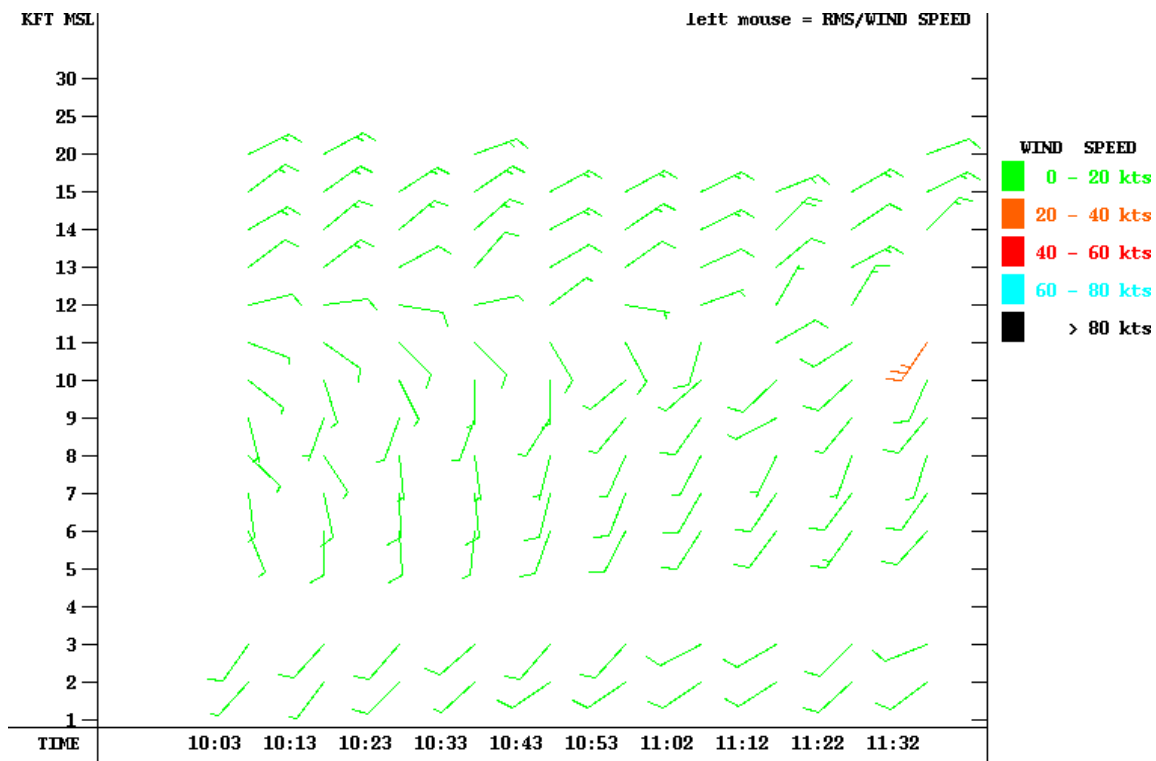
Fig. 50. WATADS VWP for KHGX on August 16, 2000 between 10:03Z and 11:32Z.

knots at 14,000 feet. While the wind direction and speed are slightly different for various heights in Fig. 50, the profile is generally consistent with Fig. 39 and Fig. 40: winds from the south at low levels turning to the northeast aloft, and wind speeds less than 20 knots.

Table 3 are data from the balloon launch at 11:15 from Wharton. The raw data from the balloon came with the wind speeds expressed in meters per second, which I converted and rounded to the nearest knot (1 knot equals approximately 0.51 meters per second). Wind direction was recorded in compass directions to the nearest degree. Heights in the raw data were reported in geopotential meters, which is approximately equal to actual meters for the low heights above the Earth's surface that we are concentrating on here. Heights were converted from meters to feet (1 meter equals approximately 3.28 feet). Only the raw data nearest to each thousand foot interval are included in Table 3.

Comparing Fig. 50 with the data in Table 3, there is good agreement. Both show winds to be from the south up to 10,000 feet, a weakness in the winds at 11,000 feet, and a shift in the wind direction above that level. The VWP output shows a more pronounced layer of winds from the northeast above 13,000 feet, whereas the balloon data show very light and variable winds. The VWP is showing stronger wind speeds above this level as well (up to 15 knots), but the balloon data show winds to be 5 knots or less.

To best compare the VWP output with the balloon data, I expressed the wind direction and speed from both the VWP and balloon into vector components: east-west

Table 3. Winds for 11:15Z on August 16, 2000 measured by weather balloon from Wharton.

Height (feet)	Wind Direction From (degrees)	Wind Speed (knots)
1,000	224	15
2,000	218	13
3,000	198	11
4,000	184	7
5,000	200	7
6,000	164	4
7,000	196	4
8,000	147	5
9,000	178	5
10,000	182	4
11,000	184	4
12,000	0	0
13,000	32	4
14,000	330	3
15,000	1	3
20,000	157	4
25,000	73	19
30,000	75	27

and north-south.   The direction of the VWP data were estimated by looking at the barbs. Because the velocity of any biological target will be the vector sum of the wind and their velocity through the air, we can determine their velocity alone by subtracting the wind velocity (balloon data) from the vector sum (VWP data). Table 4 is the result of subtracting the balloon data from the VWP data for each level. The resultant velocity would be the direction and speed of whatever targets are partaking in powered flight, if any. Of course, this assumes that any differences between the VWP and balloon data are due to biological targets alone, and not due to mechanical or other errors.

All differences below 10,000 feet are less than 10 knots, which is too slow to be caused by migrating birds. The large velocity differences above 10,000 feet are most likely not due to migrating birds as well, because nocturnal passerine migration is known to take place within a few thousand feet of the surface (Kerlinger 1998, p. 161).

Superrefraction of the radar beam will cause migrating birds, flying at a much lower level, to be reported higher in the VWP because the radar assumes a standard atmosphere and less refraction of the beam. However, because the comparison between VWP and balloon data is quite good, particularly with both having the same height where winds change direction and begin to blow from the northeast, we can discount superrefraction of the radar beam as a cause for the greater velocity differences above 11,000 feet.

For the above reasons, I can reasonably declare that birds were not migrating in great numbers on this particular night, despite the reflectivity display showing the temporal and qualitative characteristics of the onset of nocturnal bird migration, and the

Table 4. Vector difference between VWP output and weather balloon data on August 16, 2000 at 11:15Z. N/A denotes the difference could not be computed because the VWP or balloon had no result for that level.

Height (feet)	Direction (from) in Degrees	Speed (knots)
1,000	N/A	N/A
2,000	353	5.3
3,000	318	7.8
4,000	N/A	N/A
5,000	N/A	N/A
6,000	234	7.7
7,000	221	5.8
8,000	264	4.5
9,000	280	9.7
10,000	242	7.1
11,000	36	13.5
12,000	30	5
13,000	60	6.6
14,000	49	19.2
15,000	86	14.1
20,000	N/A	N/A
25,000	180	27.2

VWP showing northeasterly winds. Because some insects (such as moths, grasshoppers, and locusts) also migrate following sunset (Drake and Farrow 1988), nocturnal insect migration could explain the temporal and qualitative similarities for this evening with nocturnal bird migration. Nocturnal insect migration, as observed by radar, has been confused for bird migrations in the past (Larkin 1990). Therefore, we must not rely solely on reflectivity images to determine whether or not birds are migrating. Only the velocity data could provide us with the answer.

As indicated in Table 3, the winds on this particular date were not from a direction favorable for bird migration along the Texas coast towards Mexico. In order to find migrating birds and to test the double VAD curve hypothesis, it would be best to move forward in time to find weather conditions more suitable for nocturnal bird migration.

b. September 4-5, 2000

The next evening I decided to investigate was the night of September 4-5, 2000. High pressure was located near the panhandle of Texas. The resulting clockwise flow around the center of high pressure resulted in favorable northeasterly winds aloft for migration. Fig. 51a is the 850-mb weather chart for 0Z on September 5, and Fig. 51b is the 700-mb chart for the same time. Both Fig. 51a and Fig. 51b show an ideal flow for migration that parallels the Texas coast and offers tailwinds for birds flying to the southwest towards Mexico.

(a)

(b)

Fig. 51. 0Z upper air weather charts on September 5, 2000 for (a) 850-mb and (b) 700-mb.

As was learned in the previous section, the most ideal way to determine if migrating birds are contaminating the VWP output is to compare the VWP data with the balloon launches for this particular evening. At 4:59Z on September 5, a weather balloon was launched. This corresponds to midnight, local daylight savings time, and is ideally suited temporally for the purpose of deciding birds were contaminating the VWP.

Table 5 is the data from the weather balloon launch at 4:59Z on September 5, 2000. The raw data were again converted so that heights were in feet and velocity was in knots, and only that data closest to each thousand-foot interval are included in the table. Comparison between Table 5 and Table 3 verifies that the wind was much stronger and much more favorable for migratory flight on September 4-5 than it was on August 15-16.

Fig. 52 is WATADS VWP output for the time around the balloon launch. The closest radar volume scan to the balloon launch was 4:57Z. Upon brief inspection and comparing Fig. 52 with Table 5, the VWP winds at 3,000 feet and 4,000 feet were light and southwesterly, whereas Table 5 has easterly winds at those levels at around 10 knots. No estimation of the winds was possible by the VWP for 1,000 feet and 2,000 feet, and again between 5,000 feet and 6,000 feet. Despite the weather balloon data showing northeast to easterly winds beginning at 3,000 feet, the VWP fails to show these winds until the 7,000 foot level. While the wind speed calculation by the VWP is in good agreement with the speeds observed by weather balloon, the direction of the winds are more from the east in the VWP than the winds by weather balloon. Determination

Table 5. Weather balloon data from Wharton at 4:59Z on September 5, 2000.

Height (feet)	Wind Direction From (degrees)	Wind Speed (knots)
1,000	176	12
2,000	151	9
3,000	82	8
4,000	82	12
5,000	74	17
6,000	56	19
7,000	54	19
8,000	42	20
9,000	33	24
10,000	25	23
11,000	21	26
12,000	25	29
13,000	22	28
14,000	26	29
15,000	33	31
20,000	45	35
25,000	43	27
30,000	19	32
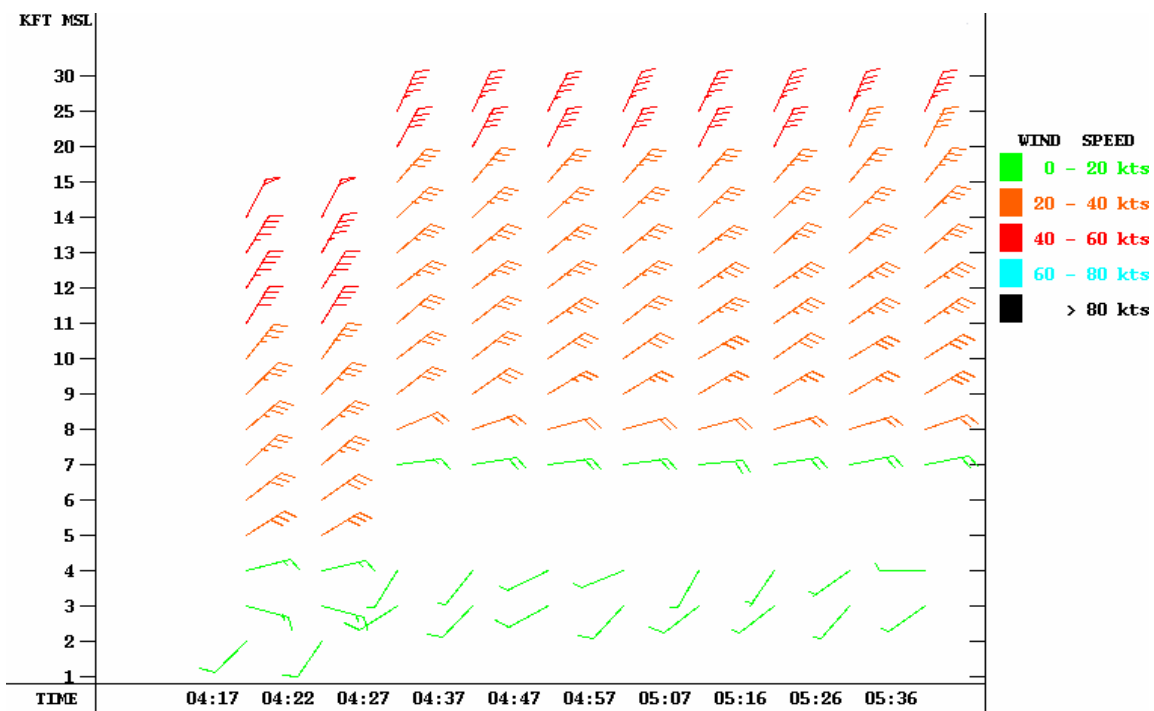
Fig. 52. WATADS VWP for KHGX on September 5, 2000 between 4:17Z and 5:36Z.

whether these differences could be the result of migrating birds must again be made by calculating the vector difference between VWP and weather balloon.

Table 6 shows the result of this vector difference, computed in the same manner as Table 4, for the evening of September 4, 2000. The results show that the VWP is not in good agreement with the weather balloon data. The direction and speed of the difference vector at 3,000 feet and 4,000 feet does not suggest contamination by migrating birds at those particular levels. Because the Wharton balloon location is further inland than the location of the KHGX WSR-88D, the diurnal sea/land breeze circulation that sets up near Galveston Bay can also result in differences between the VWP and the weather balloon data. The vector difference result of a west wind at 3,000 to 4,000 feet can be explained by the commonly observed veering of the sea breeze wind direction with time; at sunset, the sea breeze should be paralleling the coast (Simpson 1994, p. 12). The balloon was launched at approximately midnight local daylight time, so the sea breeze should have veered even more. For League City, the VWP winds support the conclusion that it was observing a sea breeze that the balloon did not.

Because the sea breeze is a local wind (Wharton balloon site was not affected), migrating birds that depart from locations away from the coast would not have been affected by the sea breeze. The winds away from the coast were favorable (tailwinds) for migration towards Mexico. Examination of the VAD plots drawn by my IDL program will hopefully provide the two clusters of points that I suggest should exist, if birds are indeed migrating and a sufficient number of wind-borne targets are present.

Table 6. Vector difference between VWP output and weather balloon data from Wharton on September 5, 2000 at 4:59Z. N/A indicates that the difference could not be computed due to missing VWP data.

Height (feet)	Direction (from) in Degrees	Speed (knots)
1,000	N/A	N/A
2,000	N/A	N/A
3,000	239	17.1
4,000	259	17.1
5,000	N/A	N/A
6,000	N/A	N/A
7,000	148	8.8
8,000	151	13.0
9,000	131	11.5
10,000	110	17.3
11,000	120	19.1
12,000	117	20.0
13,000	112	21.5
14,000	117	19.6
15,000	79	5.9
20,000	334	10.9
25,000	12	19.8
30,000	N/A	N/A

Investigation of the 3,000 and 4,000 feet levels will be done first, since those are

the first levels depicted in the VWP. Fig. 53a is the VAD plot for 3,000 feet on

September 5, 2000 at 00:36Z, or near sunset. All data between 2,950 feet and 3,050 feet

have been included in the plot, up to a slant range of 80,000 feet. Fig. 53a allows one to

observe what the winds were at this level prior to the onset of bird migration. Fig. 53b is

the VAD plot for 3,000 feet on September 5, 2000 at 04:57Z, or the time nearest to the

balloon launch, using the same data restrictions as Fig. 53b.

Fig. 53b shows what could be two separate clusters of points. There appears to

be some separation in the data points between 0 degrees and 110 degrees azimuth, and

again from around 180 to 290 degrees azimuth. The apparent cluster with the lower

amplitude matches very well with the data plotted in Fig. 53a, therefore it is assumed to

be due to wind-borne targets. The separation in the two clusters is most noticeable

where the maximum and minimum points of cluster due to wind-borne targets are

located.

The wind direction for this evening allowed perfect tailwinds for bird flight along

the coast, therefore birds will be flying in the same direction as the wind. Certainly, if

birds are migrating with the tailwinds, their velocity will be at greater odds with the

radial velocity when the radar beam is pointed parallel to their direction of flight. At this

point, radar volumes containing birds will have the sum total of the bird's velocity

through the air and the air velocity, whereas radar volumes not containing birds will just

have the air velocity (resulting in a greater difference between the radar volumes with

(a)

(b)

Fig. 53. VAD plot for 3,000 feet on September 5, 2000 for (a) 0:36Z and (b) 4:57Z.   Axes and data are plotted in the same manner as Fig. 44 (page 98).

birds in them versus clear air). When the beam is orthogonal to the flight path and wind direction, the radial velocity for radar volumes with and without birds will both be zero (resulting in no discernable difference between the cluster due to birds and the cluster due to wind-borne targets in the VAD plot).

Examination of VAD plots, changing the maximum allowable range and the thickness of the layer used, should now be performed to see what combination of maximum thickness and maximum range allows for the best detection of the clear air targets while minimizing the saturation of the VAD plot by the birds. While we want to have enough birds in the plot for two clusters to be observed (especially after the cluster due to wind-borne targets are removed), we don't want to include so many that the cluster due to wind-borne targets is hidden from view.

Fig. 54 is a series of VAD plots for the 3,000 foot level on September 5, 2000 at 4:47Z. Keeping the thickness interval constant at 50 feet, the effect of increasing the maximum allowable range will be examined. A maximum range of 20,000 feet resulted in no data. The result for 40,000 feet is shown in Fig. 54a, 60,000 feet in Fig. 54b, 100,000 feet in Fig. 54c, and 125,000 feet in Fig. 54d. For the result using a maximum range of 80,000 feet, consult Fig. 53b.

Fig. 54a shows that a maximum allowable range of 40,000 is too short to yield much data. It appears the best choice of maximum allowable range is either 80,000 feet (Fig. 53b) or 100,000 feet (Fig. 54d). It will perhaps be better use the shorter of the range values (80,000 feet) to protect the valuable clear air data from being contaminated by too many birds due to the inclusion of data from farther ranges (larger radar sample
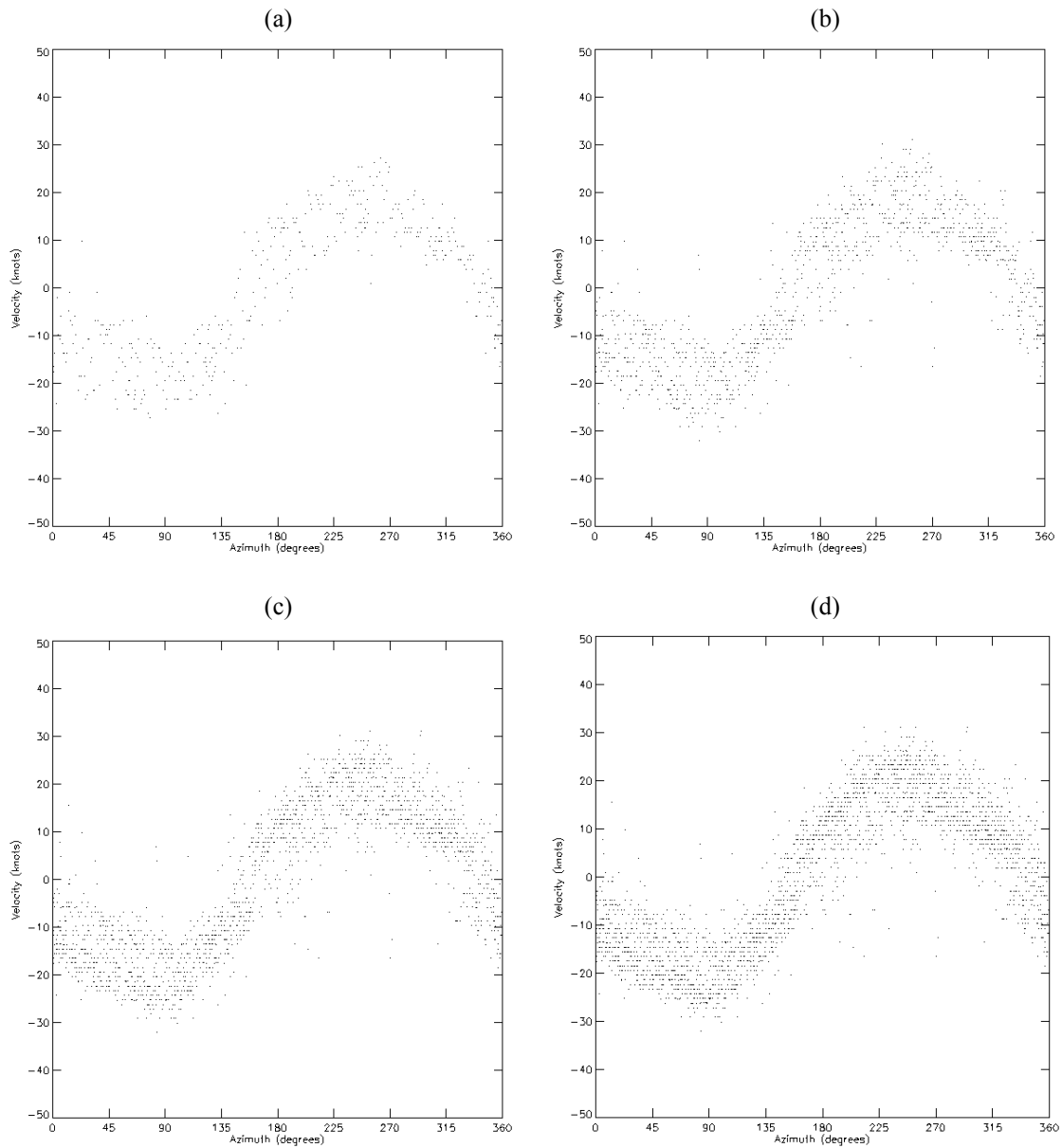
Fig. 54. VAD Plots for 4:57Z on September 5, 2000 for 3,000 feet, with a height interval of 50 feet and a maximum allowable range of (a) 40,000 feet, (b) 60,000 feet, (c) 100,000 feet, and (d) 125,000 feet. Axes and data are plotted in the same manner as Fig. 44 (page 98).
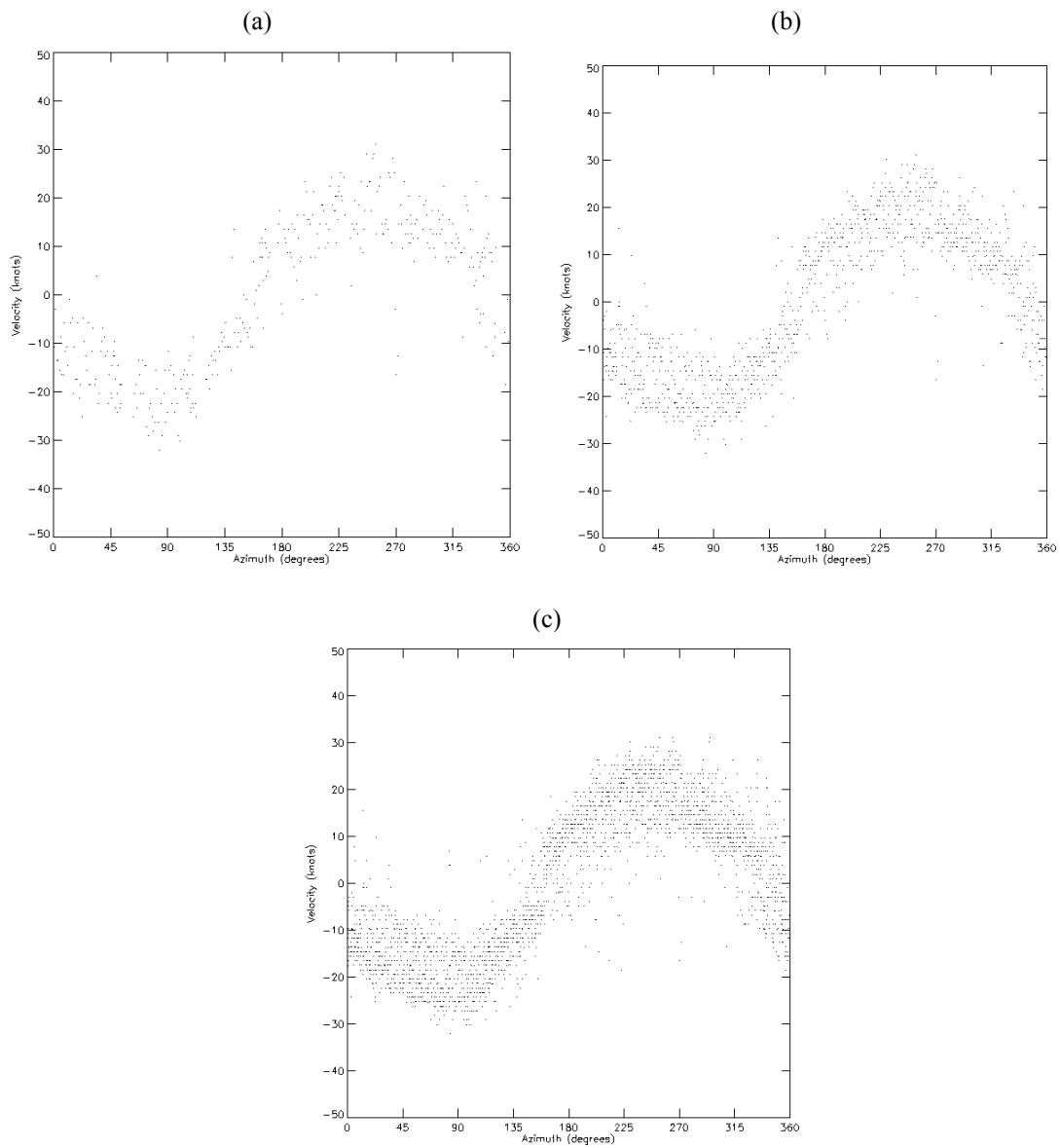
Fig. 55. VAD plots for 4:57Z on September 5, 2000 for 3,000 feet, with a maximum allowable range of 80,000 feet and a height interval of (a) 10 feet, (b) 32.8 feet, and (c) 100 feet. Axes and data are plotted in the same manner as Fig. 44 (page 98).

volumes). Because the maximum range setting could be situational dependent

(migratory density and quantity of clear air targets could vary considerably from night to

night), comparison using various range settings should be performed on other evenings

to verify these results.

Fig. 55 is a series of VAD plots for the 3,000 foot level on September 5, 2000 at

4:47Z. Now, keeping the maximum allowable range constant at 80,000 feet, we will

examine what the effect of increasing the thickness level will be. Fig. 55a is the VAD

plot using a maximum height thickness of 10 feet, Fig. 55b using a thickness of 32.8 feet

(approximately 0.1 km), and Fig. 55c using a thickness of 100 feet. Consultation with

Fig. 53b will allow one to see the results using a thickness of 50 feet. The most

pronounced plot showing two clusters is Fig. 55c (100 feet). As with the maximum

allowable range, this setting will need to be tested in future plots to see if this is the best

choice for all occasions.

Investigation regarding other levels for this evening shall now be performed to

see if two clusters are more easily seen at those particular levels. Fig. 56a is the VAD

plot for 4,000 feet on September 5, 2000 at 00:36Z, or near sunset. All data between

3,900 feet and 4,100 feet are included in the plot, up to a range of 80,000 feet (the

optimum values found for 3,000 feet). Fig. 56b is the VAD plot for 4,000 feet on

September 5, 2000 at 04:57Z, or the time nearest to the balloon launch. Looking at Fig.

56b, two clusters are as apparent in the data as there was at 3,000 feet.

While there is a noticeable difference between Fig. 56a and Fig. 56b in terms of

the amplitude of the curve (higher speed), there isn't sufficient clear air data to see a
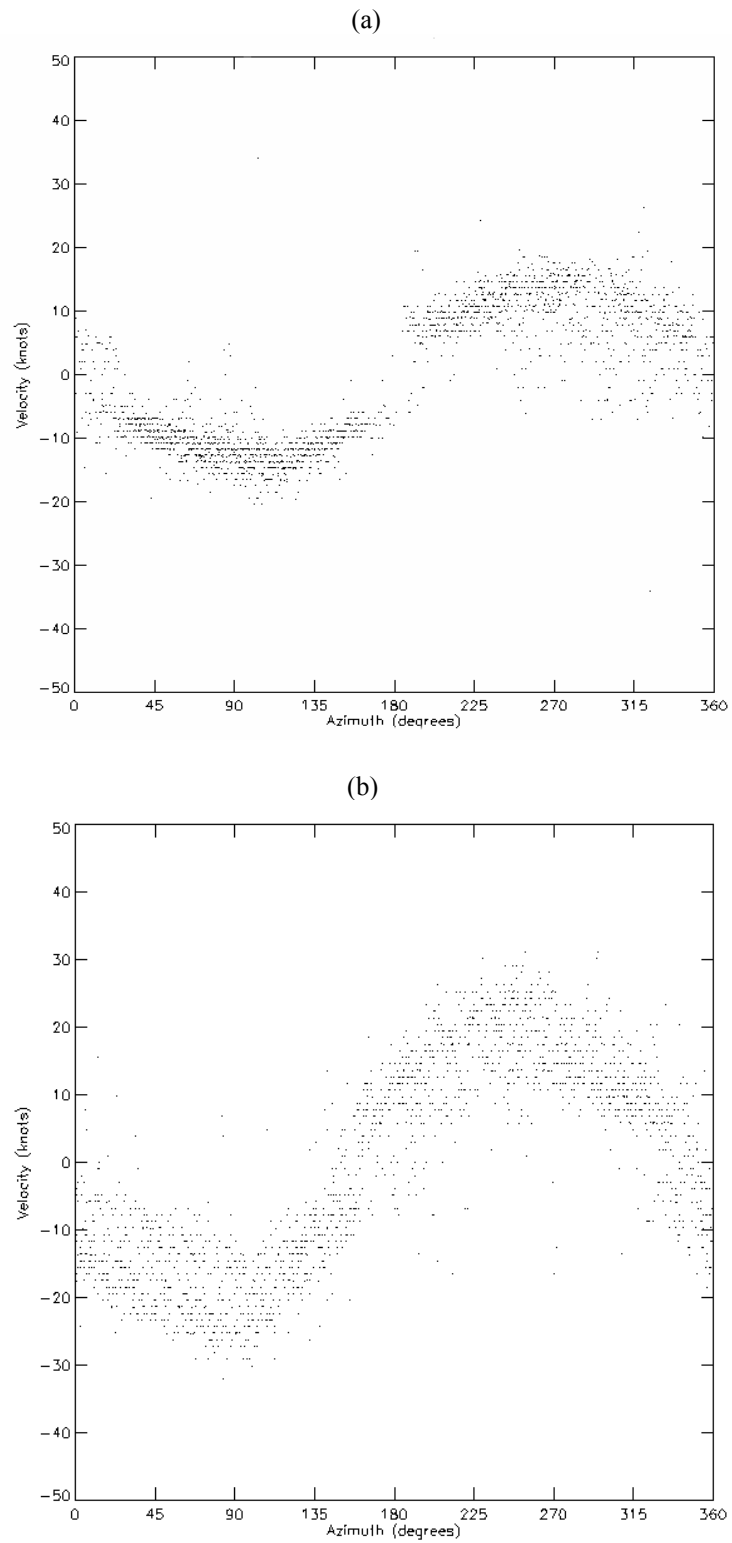
(a)

(b)

Fig. 56. VAD plot for 4,000 feet on September 5, 2000 for (a) 0:36Z and (b) 4:57Z. Axes and data are plotted in the same manner as Fig. 44 (page 98).

(a)

(b)

Fig. 57. VAD plot for 4,000 feet on September 5, 2000 for (a) 1:36Z and (b) 3:36Z. Axes and data are plotted in the same manner as Fig. 44 (page 98).

cluster similar to Fig. 56a in Fig. 56b. Looking at output for various maximum allowable ranges and thickness, no two clusters are visible at 4:57Z for the 4,000 foot level.

To see if there ever were two clusters present at 4,000 feet, we should look at a VAD display shortly after sunset. As mentioned at the beginning of this chapter, two VAD clusters should be more visible closer to sunset when the number of clear air targets is still significant and the number of birds flying is less. Fig. 57a is a VAD plot for 4,000 feet at 1:36Z, or one hour after sunset and Fig. 57b is a VAD plot for 4,000feet at 3:36Z, or three hours after sunset. Two VAD clusters are clearly visible in both graphs. The conclusion one can reach is that, from 3:36Z to 4:57Z, the two VAD clusters disappeared and only the cluster due to birds remained. This might mean that any double VAD curve detection algorithm developed may have a time limit on its effectiveness.

The VAD display for 5,000 feet at 4:57Z (Fig. 58) also failed to conclusively show two VAD clusters. Fig. 59a is the VAD plot for 5,000 feet at 1:36Z (one hour after sunset) and Fig. 59b is the VAD plot for 3:36Z (three hours after sunset). A change in the maximum allowable range parameter from 80,000 feet to 100,000 feet was necessary to construct more apparent double VAD clusters for this level. As one goes higher and higher, the maximum allowable range parameter must also increase in order obtain the same quantity of data points as the lower elevations. Two VAD clusters are apparent in Fig. 59a and Fig. 59b, but not as apparent in Fig. 56a and Fig. 56b.
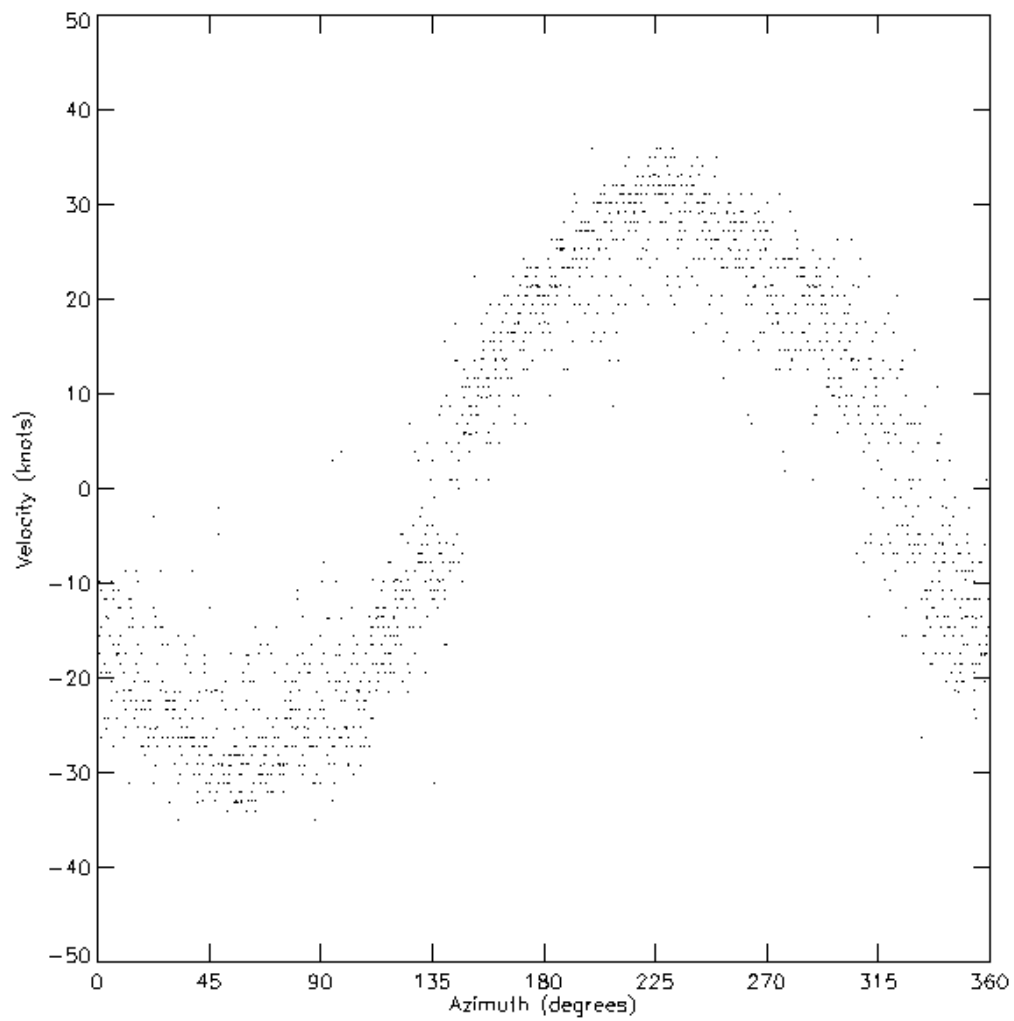
Fig. 58. VAD plot for 5,000 feet on September 5, 2000 for 4:57Z. Axes and data are plotted in the same manner as Fig. 44 (page 98).
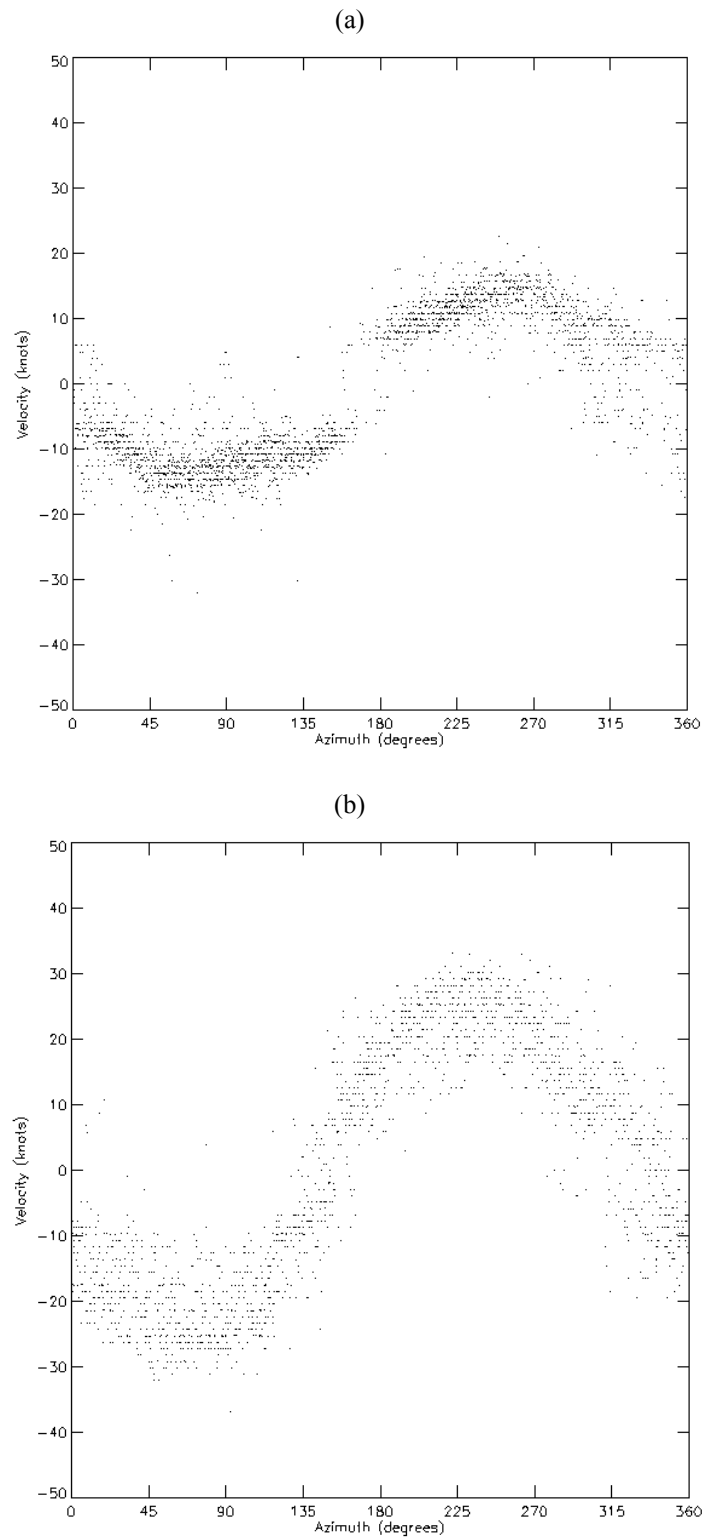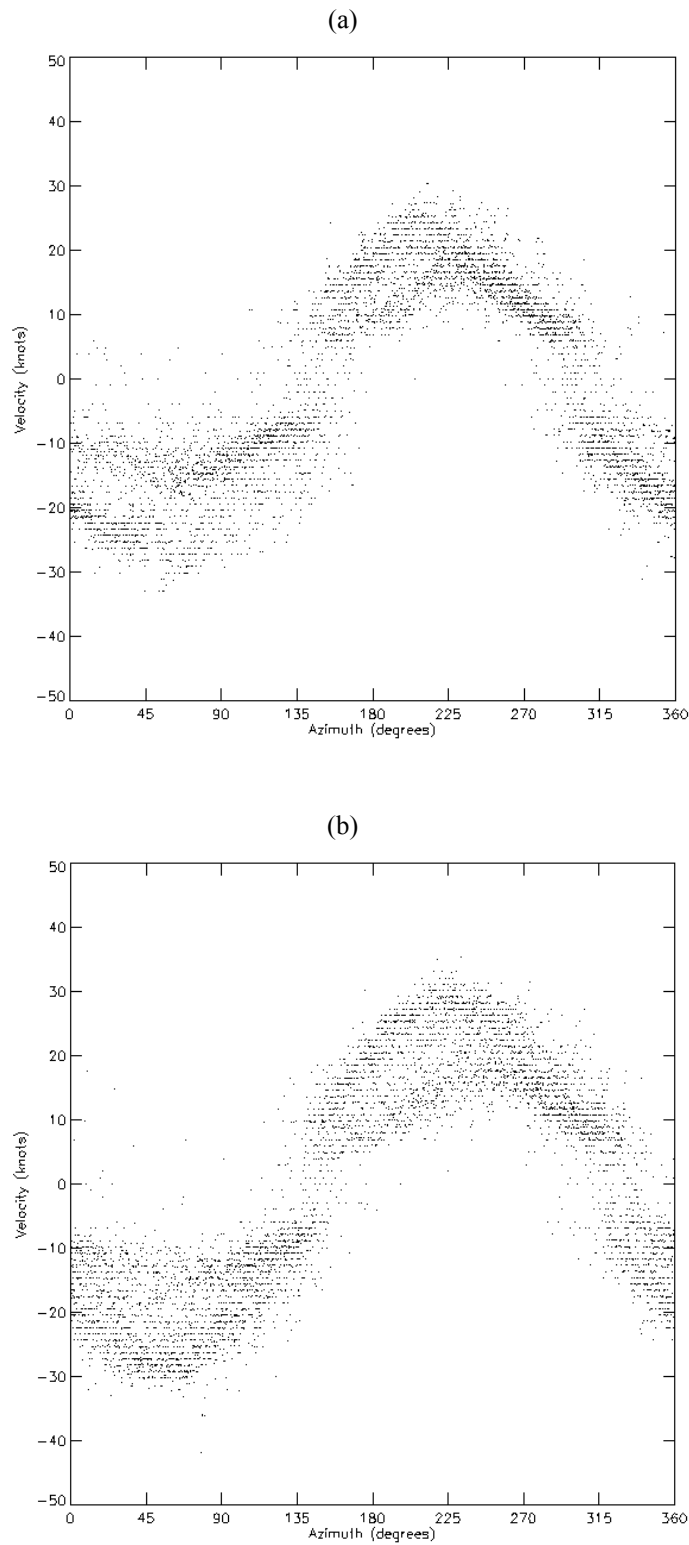
(a)

(b)
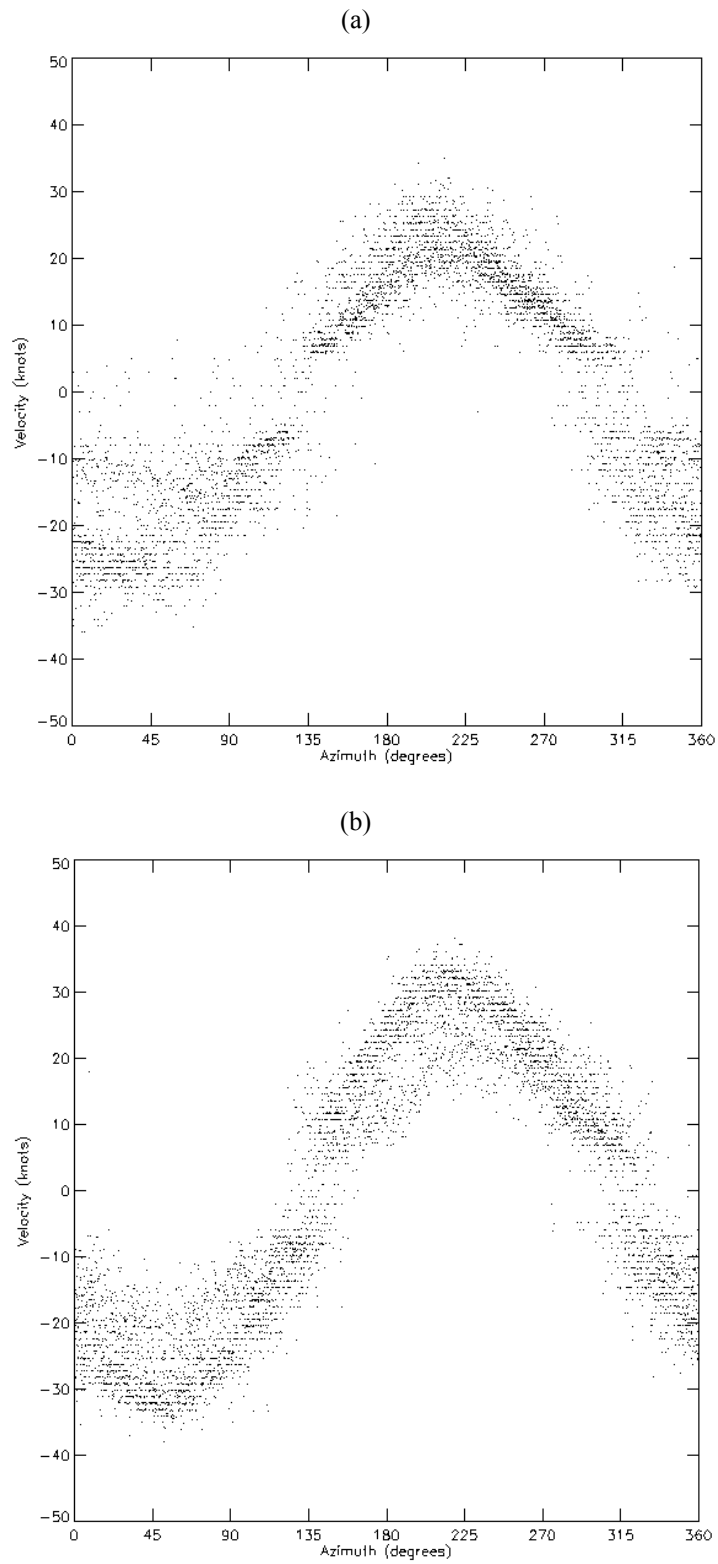
Fig. 59. VAD plot for 5,000 feet on September 5, 2000 at (a) 1:36Z and (b) 3:36Z. Axes and data are plotted in the same manner as Fig. 44 (page 98).

For 6,000 feet and above, two VAD clusters are not apparent at any time for this evening. This is primarily due to several reasons: the lower number of clear-air targets present at these levels, the decreasing probability that a radar sample volume doesn't have a bird at this height, and the fact that we are limiting the maximum range used to construct the VAD plots. Fig. 60 shows the radar coverage pattern for the WSR-88D in a typical operating mode (volume coverage pattern 21, or VCP 21). This range-height plot shows that measurements for heights greater than 10,000 feet rely on data from long ranges. Because we want to observe small radar volumes, we need to rely on shorter ranges, and that results in less radar coverage (fewer data in the VAD plot) for heights above 10,000 feet. Operation in a clear air mode will limit even further the coverage of higher altitudes since the last elevation angle for this volume scan is 4.5 degrees. Only operation in a precipitation mode, such as VCP 11 (Fig. 42), will allow enough coverage of the higher altitudes to include enough data to allow two VAD clusters to be seen.

Because all the radar elevation angles will satisfy reporting for the altitudes of 1,000 feet and 2,000 feet within the maximum slant range parameter, data were plentiful. However, the abundance of data (including clutter) make the detection of two distinct clusters more difficult due to all the data on the VAD plot for these altitudes. Limiting the amount of data plotted can be achieved by reducing the thickness of height values allowed. For the levels previously examined in this section, a thickness of 100 feet was found to be ideal. For the lower altitudes of 1,000 and 2,000 feet, this thickness yields too much data. Examining VAD plots using a variety of range and thickness values, I found that a thickness of 25 feet and a maximum slant range of 40,000 feet resulted in
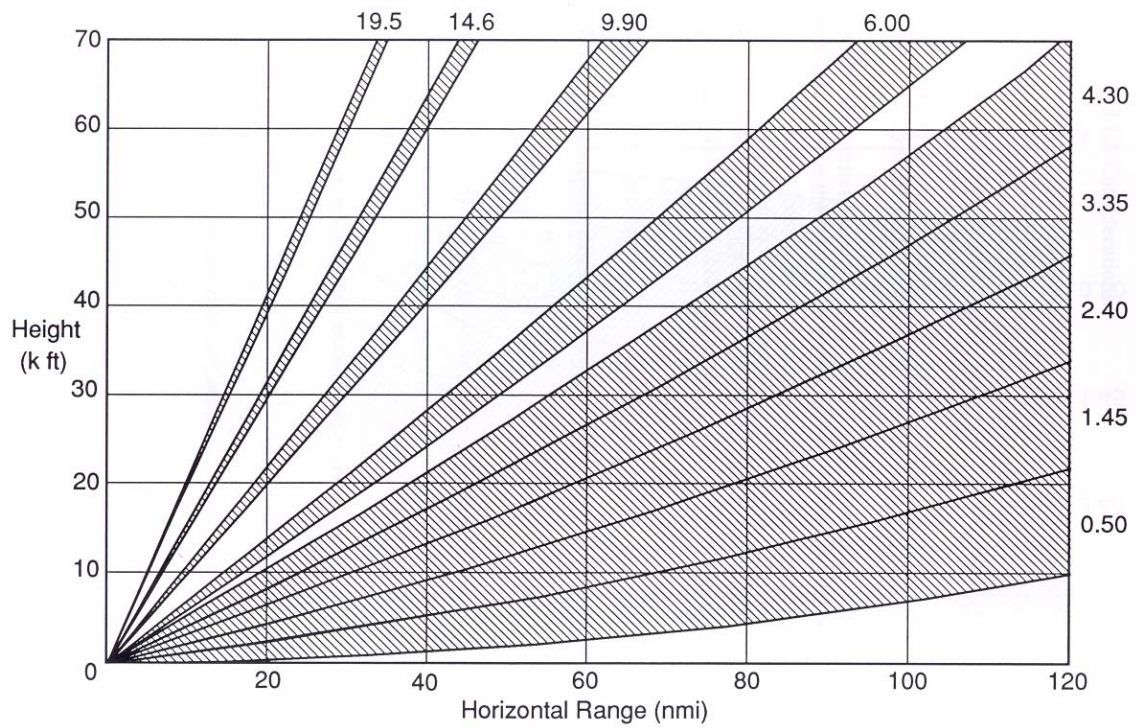
Fig. 60. WSR-88D radar volume coverage pattern for VCP 21. Shaded areas denote space where a radar beam is capable of making a measurement. The numbers at the right and top of the figure denote the elevation angle of the beam responsible. From NOAA (1991b).

the cleanest-looking VAD plot. Despite the smaller radar sample volumes at such a

short range, two VAD clusters can't be seen at 1,000 feet (Fig. 61a) or 2,000 feet (Fig.

61b).

While the onset of migration yielded two VAD clusters, the conclusion of a

night's migration does not offer the same result. Fig. 62a is a VAD plot for 3,000 feet

one hour before sunrise, and Fig. 62b is a VAD plot at sunrise. While the migratory

activity has not ceased in Fig. 62a, two clusters are not apparent. It is possible that the

amount of wind-borne targets, dependent upon an active atmospheric boundary layer to

appear in sufficient quantity, aren't in sufficient quantity to appear on the VAD plot.

Similar elevations had the same result for this day in that no two clusters were apparent.

The results from this evening are satisfying in that two VAD clusters are present.

However, the two clusters are only apparent from 3,000 to 5,000 feet from a period after

sunset until 4:57Z (approximately 4 hours and 20 minutes after sunset). The two clusters

become less apparent with time, eventually disappearing from view at all levels.

Examination of more nights is needed to see if the results from this particular evening

are common with other evenings.

c. September 5-6, 2000

The next night I want to examine is the very next evening. The ideal winds for

migratory flight were still in place, so bird migration is highly possible for this evening

as well. Unfortunately, the weather balloon launches at 5:40Z and 10:49Z on September

6 failed to record wind velocity data. Comparison of this evening's VWP output will

(a)

(b)
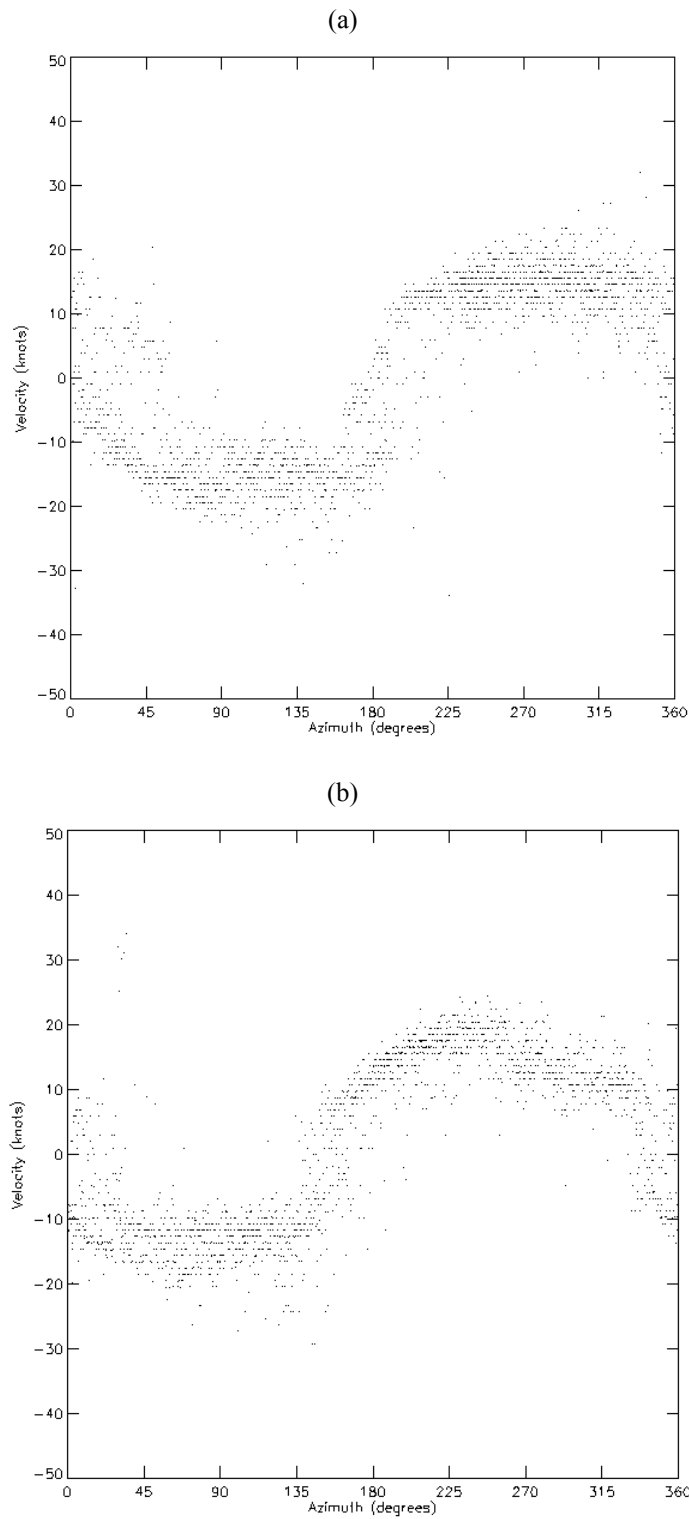
Fig. 61. VAD for September 5, 2000 at 1:36Z for (a) 1,000 feet and (b) 2,000 feet. Axes and data are plotted in the same manner as Fig. 44 (page 98).

(a)

(b)
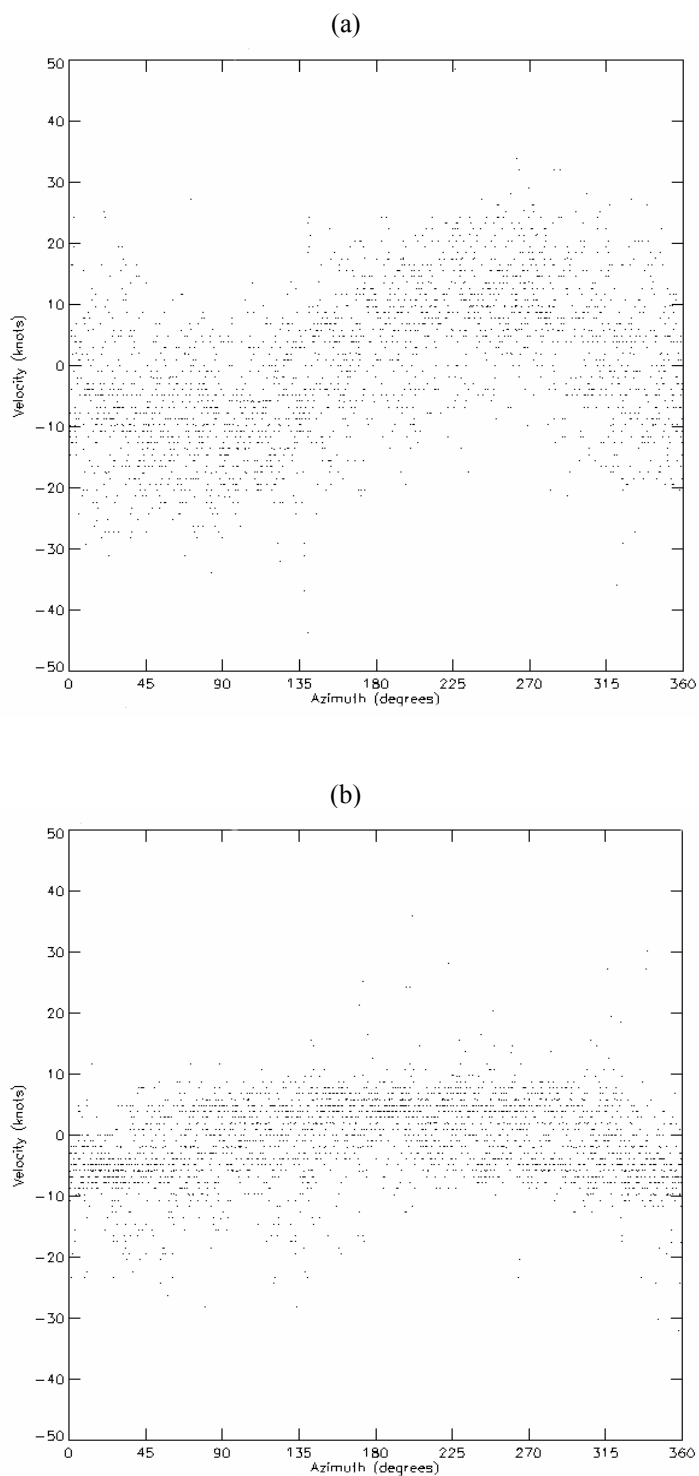
Fig. 62. VAD plots for 3,000 feet on September 5, 2000 at (a) one hour before sunrise and (b) sunrise. Axes and data are plotted in the same manner as Fig. 44 (page 98).

have to be made with the weather balloon launch from 22:59Z on September 5, and that data are shown in Table 7. Table 7 shows that the winds through the entire depth of the lower atmosphere were from the north to northeast.

Fig. 63 is WATADS VWP output for around 1:38Z on September 6, 2000, which is approximately 90 minutes after the balloon launch. Comparison between Table 7 and Fig. 63 reveals that the VWP was calculating winds from more of a northeasterly direction, and the wind speeds are higher than the balloon measurement. Table 8 is the vector difference between the VWP and balloon data for this particular evening. Table 8 verifies that the difference from 4,000 to 7,000 feet would support the argument that birds were migrating along the Texas coast towards Mexico at those levels.

Fig. 64a is the VAD for 4,000 feet on September 5, 2000 at 23:39Z (sunset), and Fig. 64b is the VAD for 4,000 on September 6, 2000 at 1:39Z. Two clusters can be seen in Fig. 64b; one being similar to the cluster shown in Fig. 64a, and the other having a greater magnitude than the first. The single cluster in Fig. 64a, and the similar cluster to it in Fig. 64b, corresponds to a wind direction and speed consistent with the weather balloon data for this altitude shown in Table 7 (from approximately 35 degrees at 20 knots). Therefore, it is reasonable to conclude that the similar clusters in Fig. 64a and Fig. 64b are due to wind-borne targets and the cluster with greater amplitude (having a faster speed than the wind) in Fig. 64b must be due to birds. While two clusters can be seen, there is a significant amount of overlap and not as much separation between the two clusters as there was on the previous night.

Table 7. Weather balloon data for 22:59Z on September 5, 2000 from Wharton.

Height (feet)	Wind Direction From (degrees)	Wind Speed (knots)
1,000	18	12
2,000	37	14
3,000	36	21
4,000	35	19
5,000	37	18
6,000	19	18
7,000	19	17
8,000	14	18
9,000	12	19
10,000	12	24
11,000	18	27
12,000	23	26
13,000	23	30
14,000	20	35
15,000	14	36
20,000	10	36
25,000	8	36
30,000	21	34
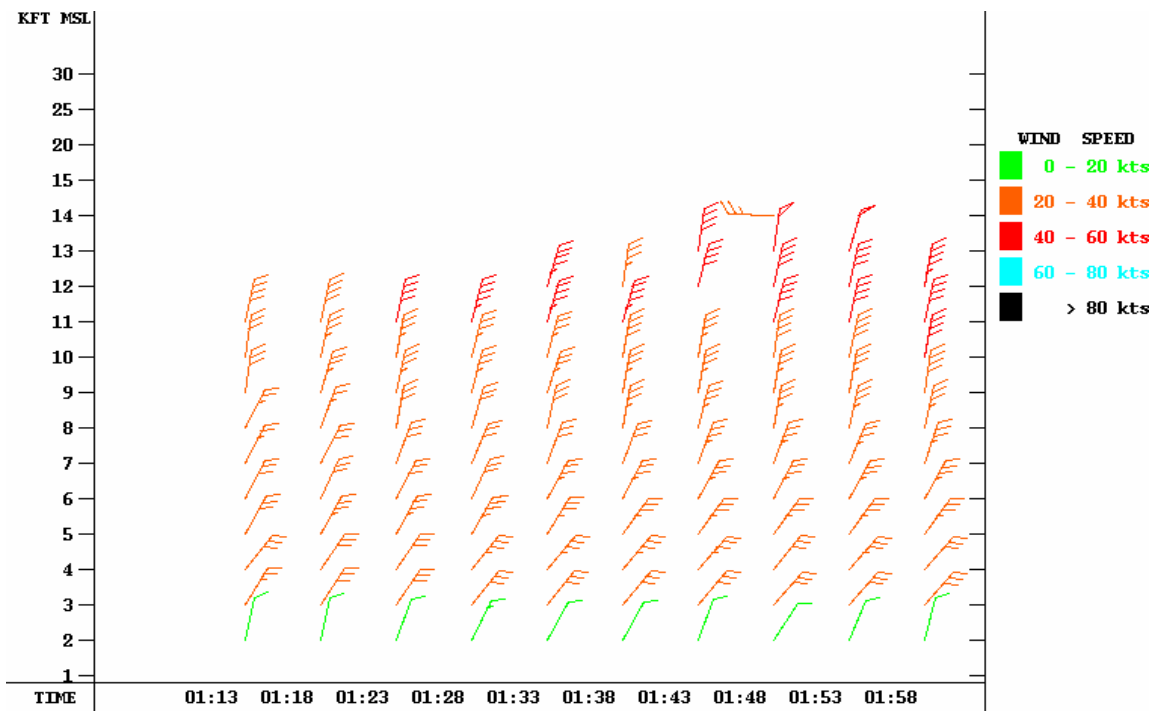
Fig. 63. WATADS VWP output for KHGX on September 6, 2000 between 1:13Z and 1:58Z.

Table 8. Vector difference between VWP output on September 6, 2000 at 1:38Z and weather balloon data from Wharton on September 5, 2000 at 22:59Z. N/A indicates that the difference could not be computed due to missing VWP data.

Height (feet)	Direction (from) Degrees	Speed (knots)
1,000	N/A	N/A
2,000	232	4.6
3,000	49	9.2
4,000	46	16.5
5,000	23	17.2
6,000	21	17.3
7,000	21	12.9
8,000	6	16.6
9,000	8	16.4
10,000	7	16.2
11,000	23	18.3
12,000	339	11.3
13,000	N/A	N/A
14,000	N/A	N/A
15,000	N/A	N/A
20,000	N/A	N/A
25,000	N/A	N/A
30,000	N/A	N/A

(a)

(b)
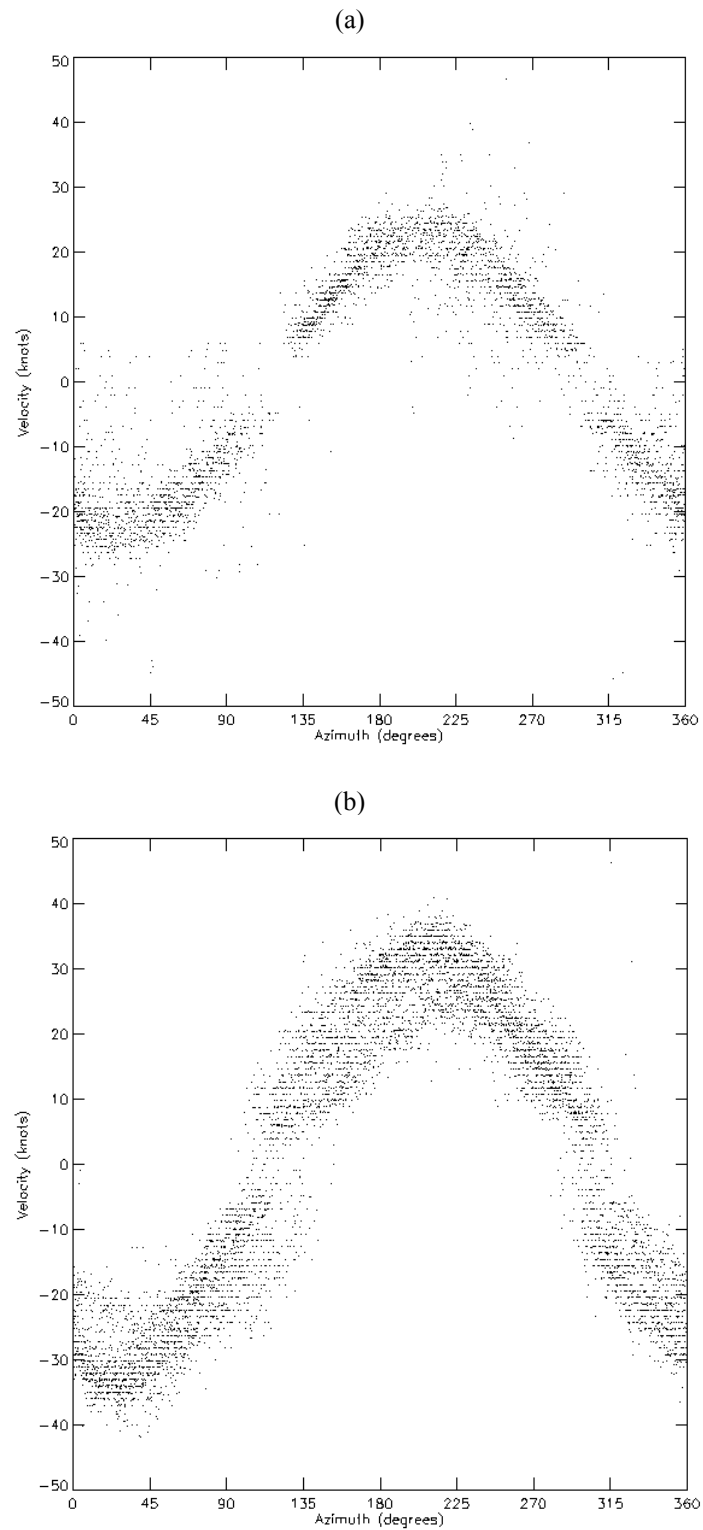
Fig. 64. VAD plots for 4,000 feet for (a) September 5, 2000 at 23:39Z and (b) September 6, 2000 at 1:39Z. Axes and data are plotted in the same manner as Fig. 44 (page 98).

Fig. 65a is the VAD plot for 5,000 feet for September 5, 2000 at 23:39Z, and Fig. 65b is

the VAD plot for September 6, 2000 at 1:39 Z. As with Fig. 64b, two clusters can be

seen in Fig. 65b. In addition, one of the clusters in Fig. 65b is similar to the one cluster

in Fig. 65a. The amplitude and phase shift of the similar clusters are consistent with the

observed wind for this height shown in Table 7, so those clusters must represent the

wind. The second cluster in Fig. 65b has a greater amplitude (higher speed) than the

wind curve, so this cluster must represent the migrating birds.

Fig. 66a is the VAD plot for 4,000 feet on September 6, 2000 at 2:39Z, just one

hour later than Fig. 64b. The two VAD clusters visible in Fig. 64b have become much

less noticeable in Fig. 66a. Fig. 66b is the VAD plot for 5,000 feet on September 6,

2000 at 2:39Z, and it shows that the two clusters for this level are also less noticeable

than they was an hour before in Fig. 65b. These observations support the fact

determined in the previous section that double VAD curves could disappear from view

with time.

While Table 8 suggests that two VAD clusters might be seen at 6,000 feet and

7,000 feet, Fig. 67a and Fig. 67b show that any second cluster for these levels are very

weak, just two hours after sunset. The conclusion that can be drawn from this

observation is that, while migrating birds may be contaminating the VWP at a particular

level, there may be insufficient radar sample volumes containing only wind-borne

targets to allow a second VAD cluster (from wind-borne targets) to be observed.

(a)

(b)
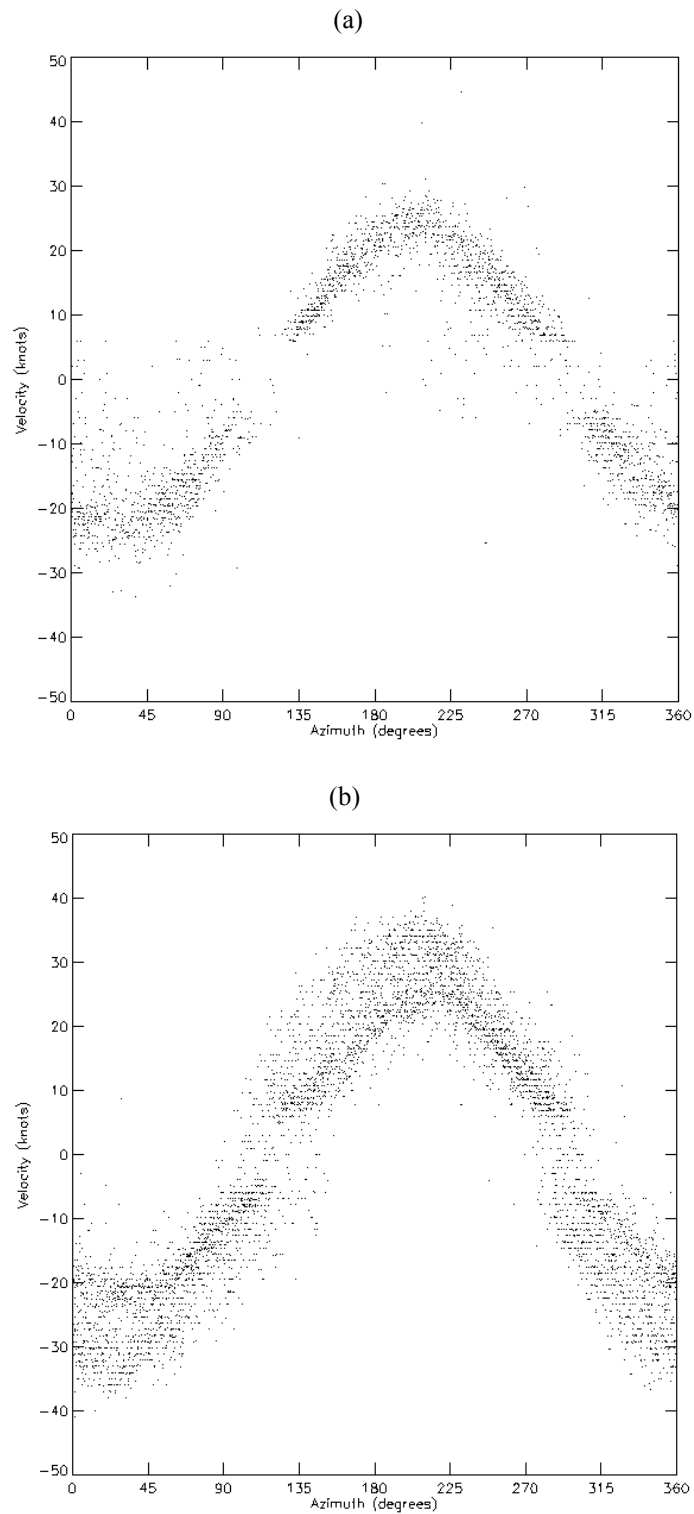
Fig. 65. VAD plots for 5,000 feet for (a) September 5, 2000 at 23:39Z and (b) September 6, 2000 at 1:39Z. Axes and data are plotted in the same manner as Fig. 44 (page 98).

(a)

(b)
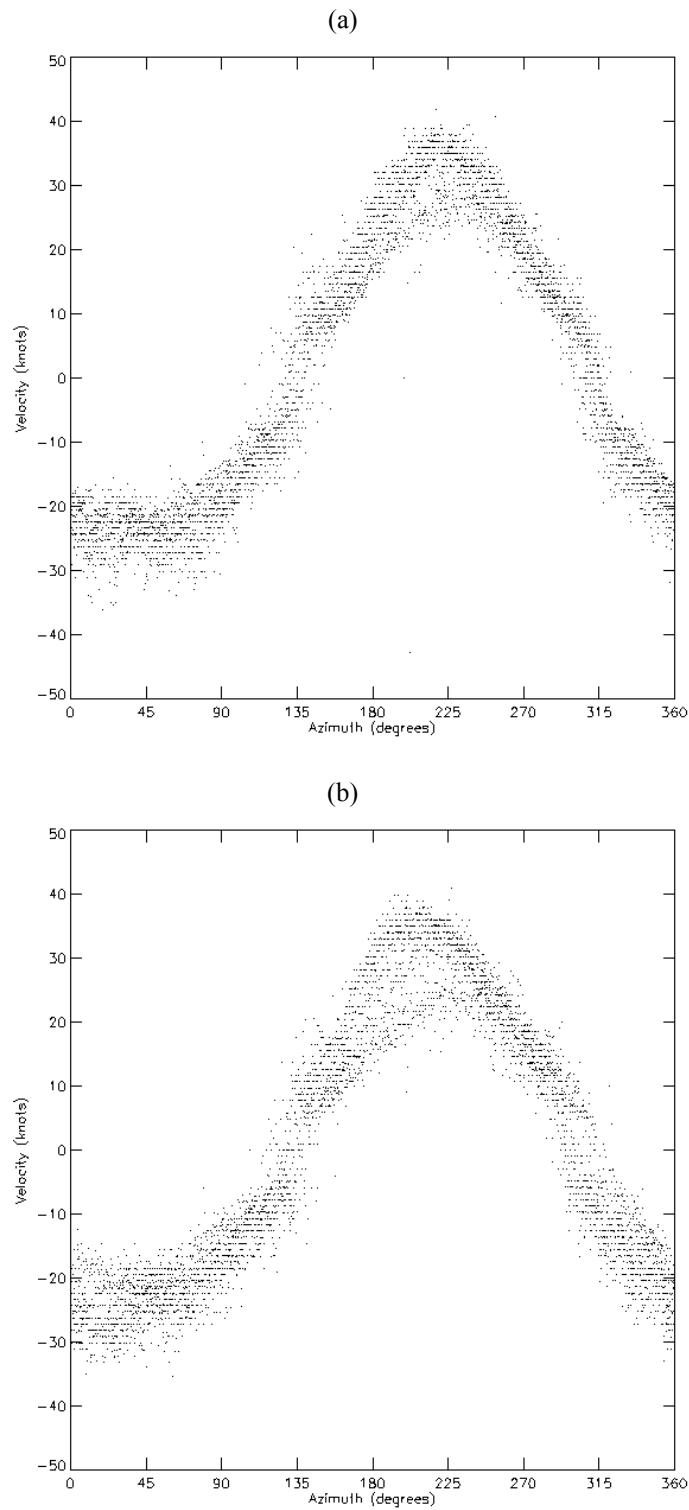
Fig. 66. VAD plots on September 6, 2000 at 2:39Z for (a) 4,000 feet and (b) 5,000 feet. Axes and data are plotted in the same manner as Fig. 44 (page 98).

(a)

(b)
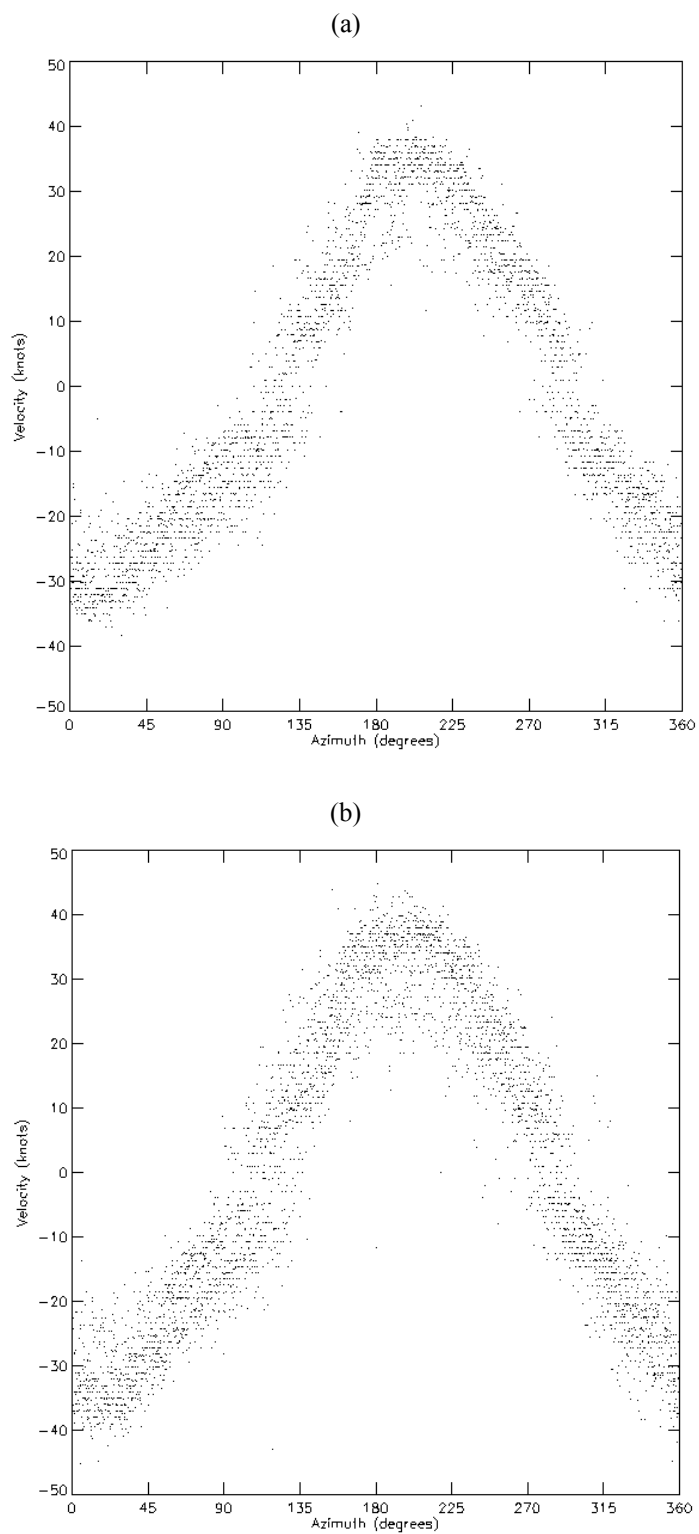
Fig. 67. VAD plots on September 6, 2000 at 2:39Z for (a) 6,000 feet and (b) 7,000 feet. Axes and data are plotted in the same manner as Fig. 44 (page 98).

d. September 6-7, 2000

For the third night in a row, winds were favorable for nocturnal bird migration along the Texas coastline towards Mexico. Unfortunately, weather balloon data from Wharton, TX for this evening failed to record the wind direction and speed. In lieu of these data, weather charts will need to be consulted in order to compare the observed wind with the VWP output.

Fig. 68 is the surface chart from 0Z on September 7, 2000. The winds were favorable near Houston for flying southwest along the coast. Near Corpus Christi, the winds blow more from the east-southeast, resulting in a crosswind more than a tailwind for birds flying along the coast. Forsyth and James (1971) found that onshore winds are also favorable for migration because they prevent birds from drifting out over water.

Fig. 69 is the 850-mb chart, and Fig. 70 is the 700-mb chart for the same time as the surface chart. Both Fig. 69 and Fig. 70 continue to show the favorable tailwinds present on this evening for bird migration towards Mexico. The wind speeds are 15-20 knots at 850-mb, and 20 knots at 700-mb.

Fig. 71 is the WATADS VWP output from around sunset, and Fig. 72 is a continuation of the VWP data, centered about an hour after sunset. In the time between Fig. 71 and Fig. 72, winds appear blowing from the northeast between 4,000 and 7,000 feet. The magnitude of the wind speed is 10-15 knots faster than the upper-air charts indicate, so contamination of the VWP by migrating birds is certainly possible for this evening.
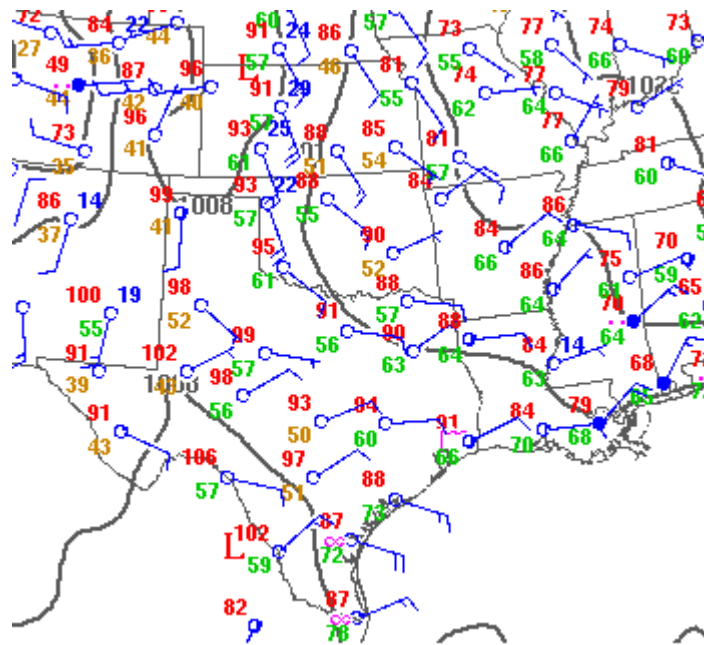
Fig. 68. Surface chart for 0Z on September 7, 2000. Data are in a similar format to Fig. 4, except this chart is in color. Red numbers are temperatures, dew points are green (greater than or equal to 55 degrees) or brown (less than 55 degrees). Blue numbers denote the wind gusts (in knots). Pressure is not plotted next to each station circle, but the pressure contours (isobars) are drawn with black lines.
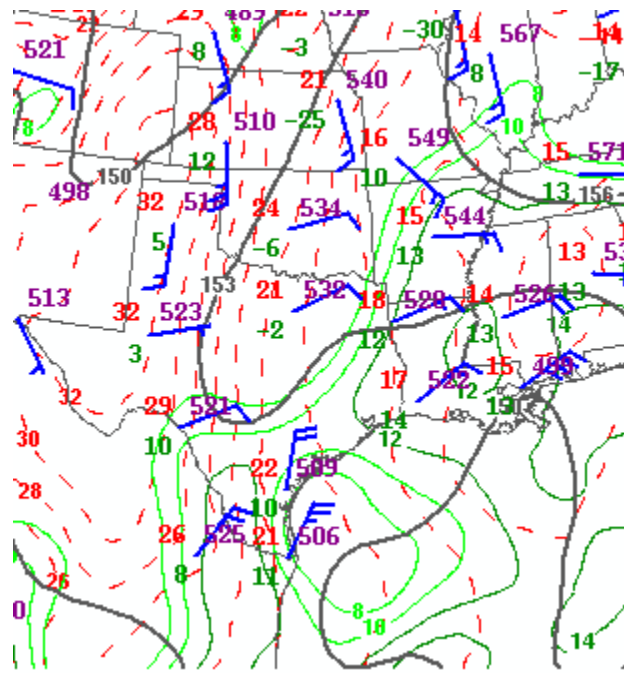
Fig. 69. 850-mb chart at 0Z on September 7, 2000. Data are in a similar format to Fig. 5a, except the red dashed lines are temperature contours (drawn every 2 degrees Celsius) and the green solid lines are dew point contours above 8 degrees Celsius (drawn every 2 degrees Celsius).

Fig. 70. 700-mb chart at 0Z on September 7, 2000. Data are in a similar format to Fig. 5b, except the red dashed lines are temperature contours (drawn every 2 degrees Celsius) for temperatures above freezing and blue dashed lines are temperature contours (drawn every 2 degrees Celsius) for temperatures below freezing. The green solid lines are dew point contours above -4 degrees Celsius (drawn every 2 degrees Celsius).

Fig. 71. WATADS VWP output for KHGX on September 7, 2000 between 0:09Z and 0:54Z.
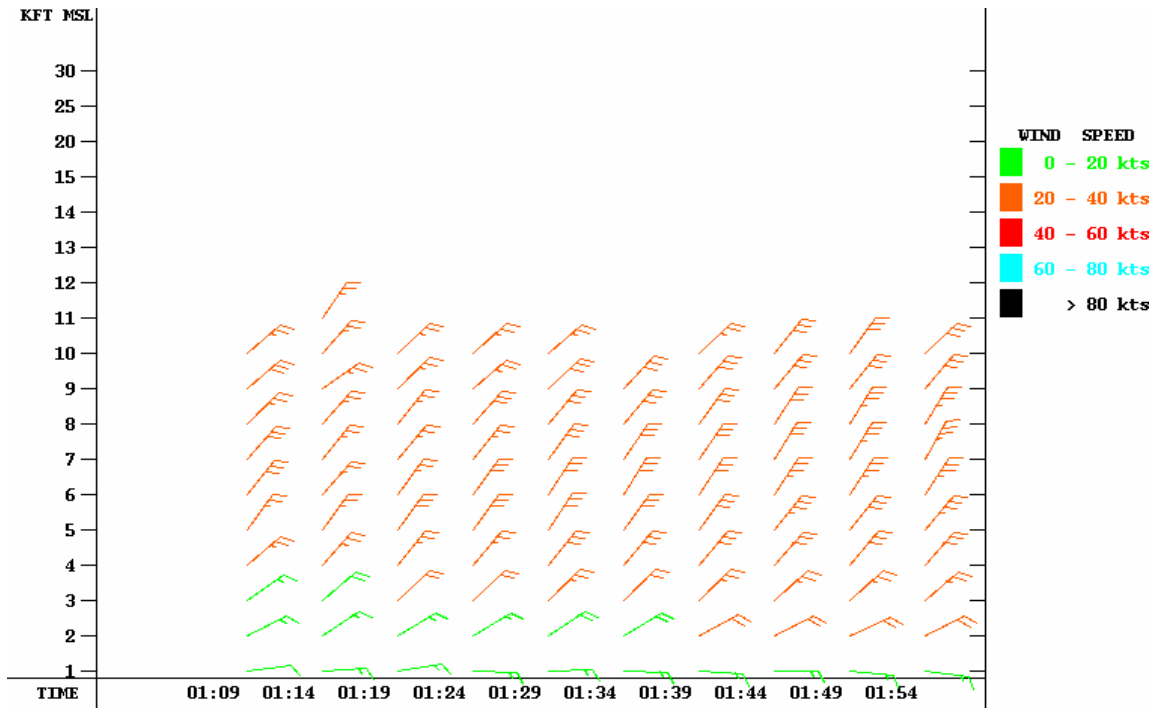
Fig. 72. WATADS VWP output for KHGX on September 7, 2000 from 1:09Z to 1:54Z.

Fig. 73a is a VAD plot for 3,000 feet at sunset, and Fig. 73b is the VAD plot an hour later for the same level. Two clusters are very apparent in Fig. 73b. The cluster with the smallest amplitude in Fig. 73b matches closely the single cluster in Fig. 73a, therefore this cluster is assumed to be the cluster due to wind-borne targets only (assuming no change in the wind). The cluster with the larger amplitude appears to be a result of migrating birds (it differs from the wind-borne cluster with a speed difference of 10-15 knots, consistent with bird flight speeds).

Fig. 74a is a VAD plot for 4,000 feet at sunset, and Fig. 74b is the VAD plot an hour later at the same level. As with the 3,000 foot level, two clusters are apparent an hour after sunset in Fig. 74b. Again, one cluster in Fig. 74b matches closely with the single cluster in Fig. 74a. Assuming no change in the wind within the hour time difference, the cluster in Fig. 74b that matches closely with the cluster in Fig. 74a must be the cluster due to the wind-borne targets only. The second cluster in Fig. 74b has a higher amplitude than the first cluster (greater speed), therefore this cluster can be assumed to be that caused by migrating birds.

For this evening, a second cluster could be observed on the VAD plots from 2,000 feet through 6,000 feet one hour after sunset. However, changes in the clusters became apparent as time progressed. Fig. 75a is the VAD plot for 3,000 feet two hours after sunset, and Fig. 75b is the VAD plot for 4,000 feet at the same time. Both Fig. 75a and Fig. 75b suggest that two clusters exist. However, the one cluster attributable to the wind no longer has the same amplitude it had just an hour earlier; the difference in magnitude between the two clusters has diminished to approximately 10 knots.

(a)

(b)
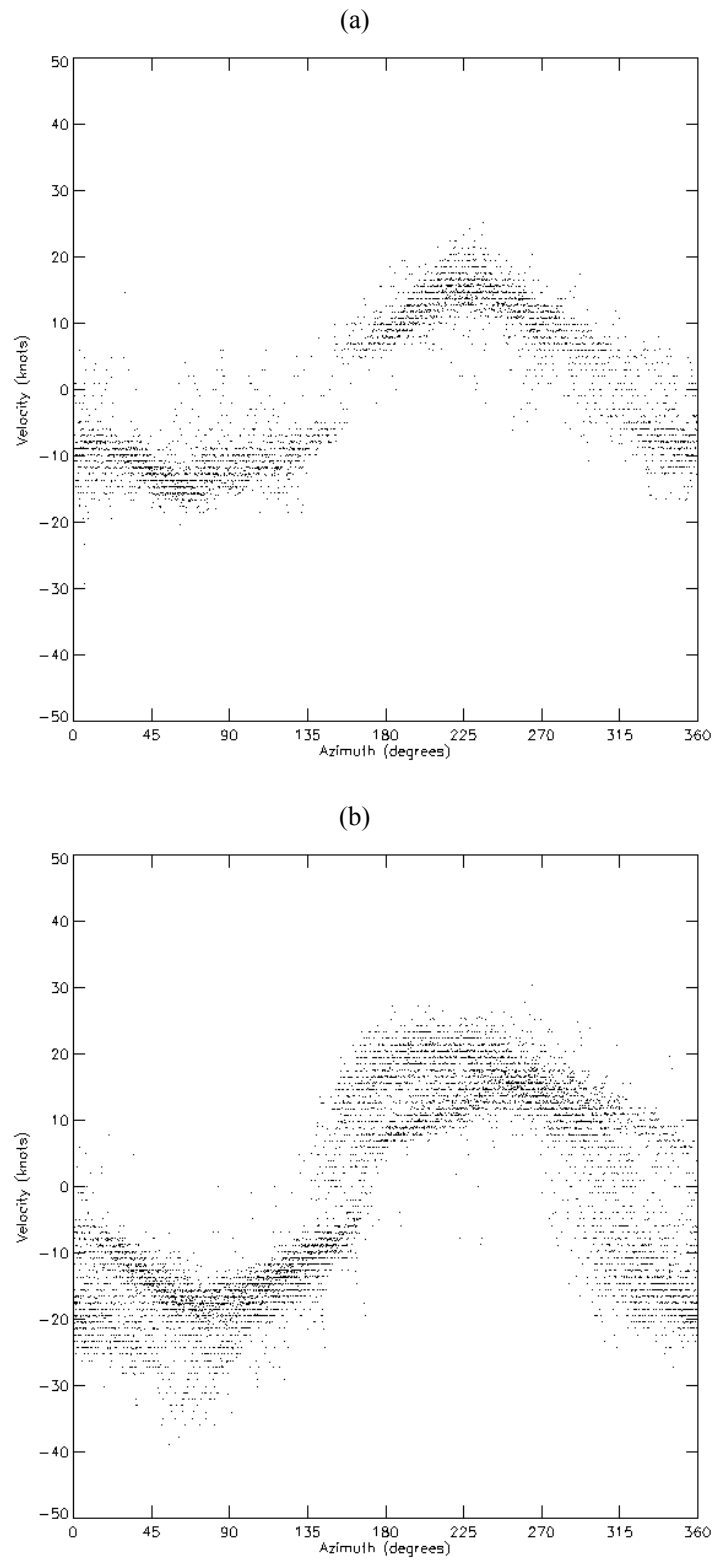
Fig. 73. VAD plots for 3,000 feet on September 7, 2000 at (a) sunset and (b) one hour after sunset. Axes and data are plotted in the same manner as Fig. 44 (page 98).

(a)

(b)
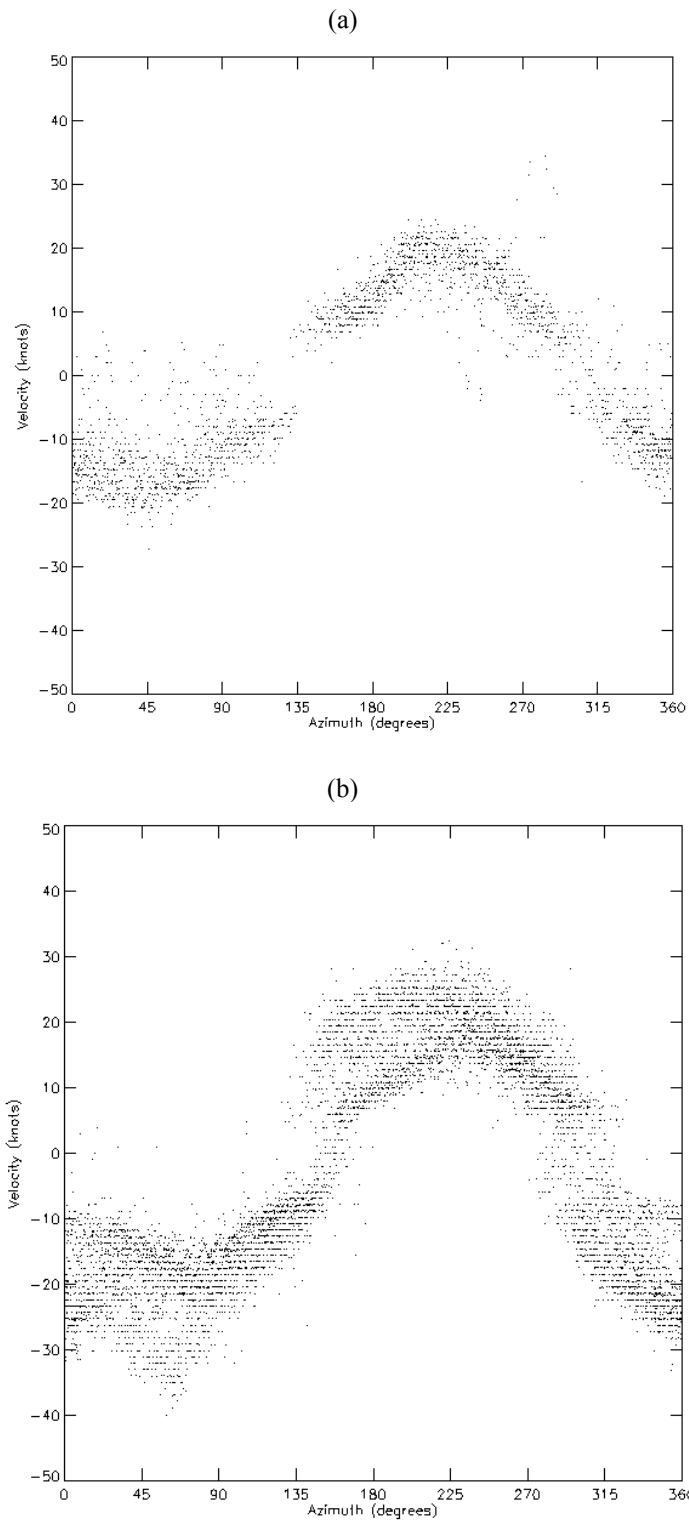
Fig. 74. VAD plots for 4,000 feet on September 7, 2000 at (a) sunset and (b) one hour after sunset. Axes and data are plotted in the same manner as Fig. 44 (page 98).

(a)

(b)
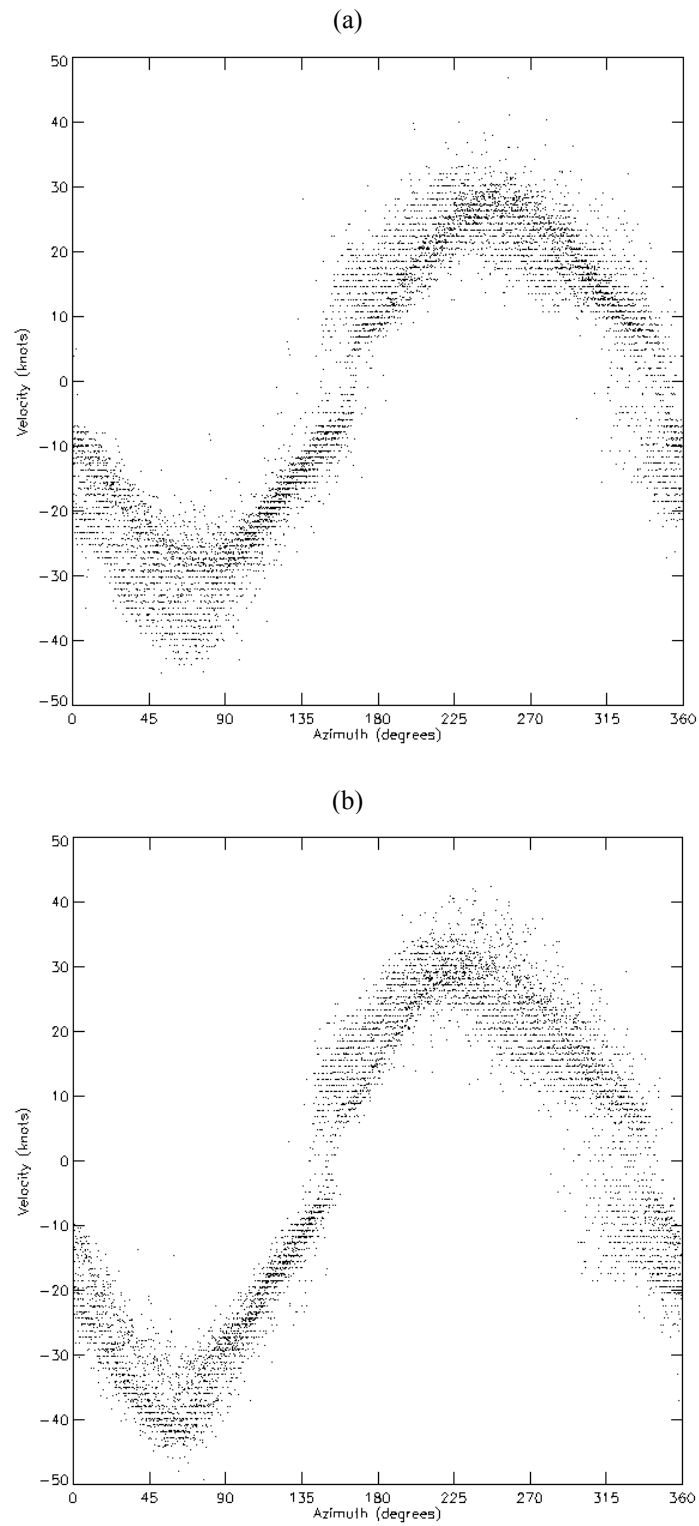
Fig. 75. VAD plots two hours after sunset on September 7, 2000 for (a) 3,000 feet and (b) 4,000 feet. Axes and data are plotted in the same manner as Fig. 44 (page 98).

Because no balloon data exist for this date and time, I can only offer one possible explanation: one cluster represents migrating insects and the other represents migrating birds. If the wind did not accelerate overnight, the radar sample volumes containing only passive wind-borne targets must no longer remain, each filled with either insects or birds. Fig. 76 is the 700-mb chart for the following morning (12Z). The wind speed and direction has not changed appreciably at this level in the 12 hours since 0Z.

4. Attempted Remedies

The human eye can see quite readily when two separate clusters of points exist in a VAD plot. Logic and human reasoning also allow one to infer fairly quickly which cluster of points is due to radar volumes containing wind-borne targets only, and which cluster must be the result of migrating birds.

The current VAD algorithm is only able to calculate a best-fit curve for a single cluster of points in the data. Having determined that two clusters of points exist (at certain levels and at certain times) when birds are migrating, a new objective numerical technique must be developed in order for the current algorithm to ingest data with two clusters of points, identify which one is due to migrating birds, remove that data so that they are not included in the calculation of the winds, and report what the true wind for that level is.

Unfortunately, there are limitations on how complicated the numerical technique under development can be: the computing speed and memory of the Radar Product Generator (RPG). The RPG is the computer that runs all the radar algorithms and
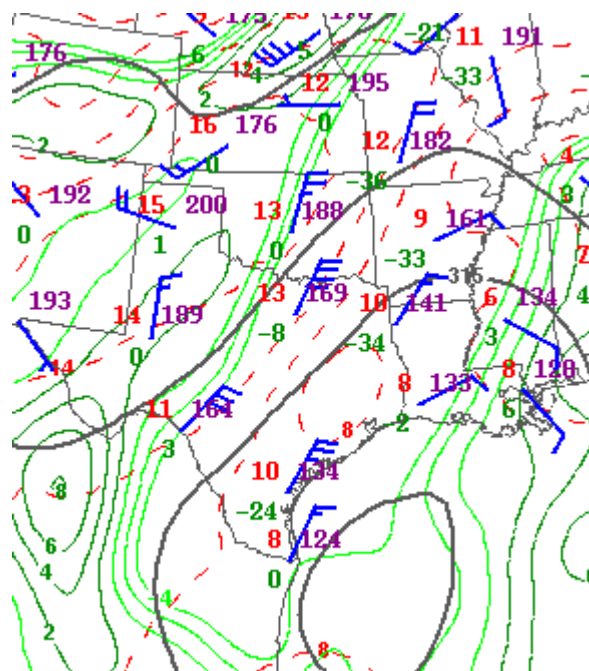
Fig. 76. 700-mb chart for September 7, 2000 at 12Z. Data are similar in format to Fig. 65.

creates all the products for the WSR-88D. Currently, the RPG is a Sun workstation, and

it does not have much extra memory or computing time (O'Bannon 2003, personal

communication). The entire suite of algorithms and products for each volume scan must

be completed prior to the start of the next radar volume scan, and this time is only 5 to

10 minutes (depending on the operating mode of the radar).

Two techniques were developed and tested to see if they could objectively

determine whether two clusters of points exist and identify the cluster not associated

with migrating birds. Details regarding these two techniques, and the results of the

testing, follow below.

a. Curve Isolation Technique

Because the current VAD algorithm can only handle one cluster of points about a

curve, the first idea involves isolating the two clusters from each other and having the

VAD technique analyze each cluster separately. The first step is to locate the first

cluster. To do this, an assumption is made that the wind does not change markedly

between radar volume scans. Using the past result of the VAD algorithm for a given

altitude, this technique would obtain and remove from the current VAD plot all data that

would fit the prior VAD curve within certain tolerances that would allow for slight

changes in the wind velocity.

Illustrating how this step in the technique works, data from September 5, 2000 at

1:39Z for 4,000 feet will be used. Fig. 56a shows the VAD for this level, prior to the

onset of bird migration (at 0:36Z). Removing similar data found in Fig. 56a from the

current VAD plot for this level (Fig. 57a) results in the plot shown in Fig. 77a. The data actually removed during this process are shown in Fig. 77b. In order to ensure optimum performance of this step, the curve selected to remove the data, as well as the tolerance, was done by visually and adjusted as needed to collect most of the first cluster present in Fig. 57a.

Inspection of Fig. 77b reveals that a considerable amount of data removed could be part of either cluster, and therefore some data points removed are not due to the wind. These "intersection" data must be removed so that only the data representing the wind-borne targets are included in any subsequent wind calculation. Failure to do so could result in a false-positive for two curves. For example, should the wind speed change significantly and the primary assumption for this technique fail, the VAD could assign a best-fit curve using just the intersection data alone. Then, upon finding a second curve with the remaining wind data, the algorithm will report bird contamination that isn't present. Before we can remove these data, however, the best-fit curve for the second cluster has to be determined.

The second step in this technique is to run the VAD algorithm on the remaining data (Fig. 77a) to determine if a second curve exists, and if so, to return the best-fit curve to the data. It is clearly apparent that a second curve exists and should be found by the VAD algorithm.

However, upon closer inspection, the second cluster does not have a smooth trigonometric curve shape. The maximum point of the second cluster is located at approximately 200 degrees azimuth, while the minimum point of the second cluster is

(a)

(b)
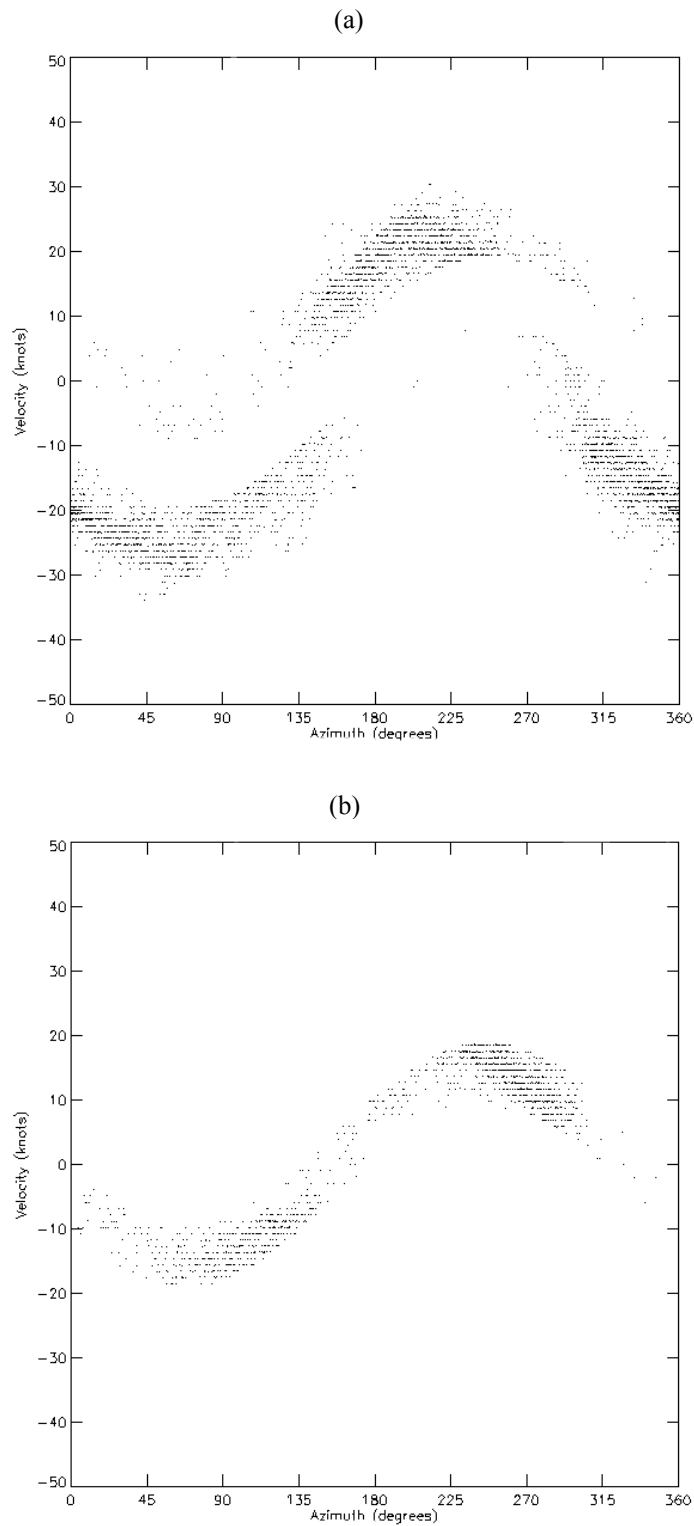
Fig. 77. VAD plots for September 5, 2000 at 1:36Z for 4,000 feet (a) after removing data matching the previous wind estimate for this level, and (b) the actual data removed. Axes and data are plotted in the same manner as Fig. 44 (page 98).

located near 60 degrees. The difference between the maximum and minimum points of the cluster is only 140 degrees, whereas a sine curve would have both points separated by a distance of 180 degrees. Consultation with Fig. 57a verifies that this finding is not a result of the separation process; the second cluster naturally has this anomalous shape. There is also a difference in amplitude between the maximum point (approximately 23 knots) and the minimum point (approximately 28 knots). Therefore, the bird cluster on the VAD is distorted in amplitude and phase.

One fundamental flaw with the curve-isolation technique that would prohibit this technique from being used operationally is that migrating birds do not always create perfect curves on the VAD. The shape of the birds' VAD cluster is a result of how the birds, mostly flying independently of each another, happen to be flying as a dissociated group at that particular moment. Fig. 66a shows that the bird cluster at 4,000 feet, just an hour later, is distorted in a different manner: the maximum point of the cluster now has a higher amplitude than the minimum point, and the distortion azimuthally is not as pronounced as it was at 1:36Z. Therefore, changes in the bird cluster can be quite dynamic and difficult to predict.

The failure of the bird cluster to follow a perfect curve results in too much data from the bird cluster being included with the wind cluster removed in step one. Fig. 78 shows the problem when trying to assign a specific best-fit curve to a distorted bird cluster. The curve in Fig. 78a is designed to capture the data closer to the maximum point. Too many data from birds still are present, especially between approximately 90 degrees and 150 degrees azimuth, and approximately between 270 degrees and 300

degrees. The results of trying a curve that best matches the minimum point of the bird cluster is shown in Fig. 78b. Once again, remaining bird data exist, particularly between 225 degrees azimuth and 280 degrees azimuth. Using the best-fit curve for the entire bird cluster would yield a mixture of the intersection data contained in Fig. 78a and 78b.

The failure to completely remove intersection data at times is not the only failure with this particular technique. When I first devised this technique, I envisioned two clusters of points separated to a much greater extent than the data in the previous section show. For example, Fig. 60b shows two curves visible with the naked eye. Unfortunately, the separation between the two clusters is not sufficient to guarantee that the curve-isolation technique could obtain enough wind-borne data to assign a wind estimate.

Finally, the discovery that the two clusters are visible for only a limited number of altitudes, and only for a limited period of time, suggests that this technique may have limited benefits. It may not be worth the additional computing and memory resources to perform this technique in real-time to have limited results. A better technique to somehow detect two VAD clusters needs to be found.

b. Minimum Variance Technique

The second technique that was attempted for finding two clusters involved calculating the local variance of the data. Where a VAD cluster exists, a relative minimum in the variance of the best-fitting data points should also exist. While the best-fit curve for data containing two clusters will be the absolute minimum for both clusters
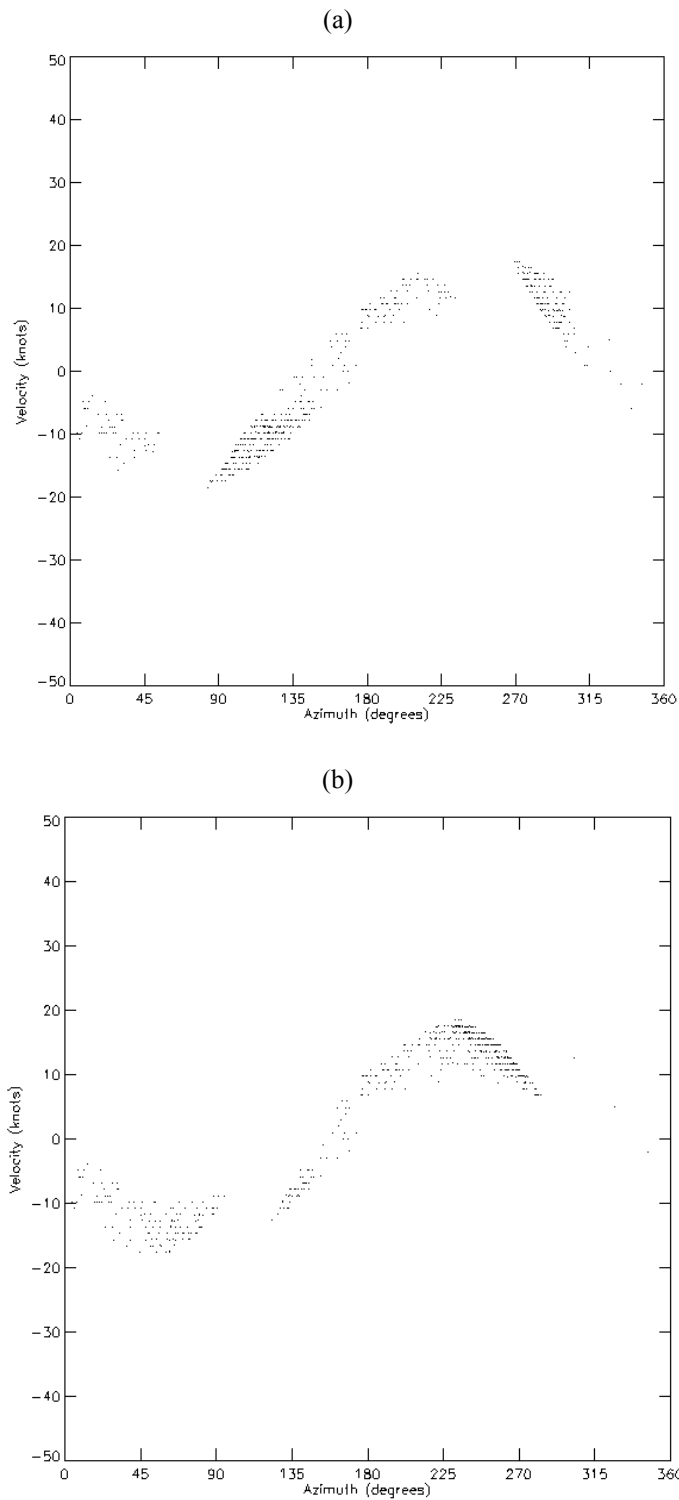
Fig. 78. VAD plots after an attempt to remove the bird cluster using (a) the minimum bird cluster amplitude and (b) the maximum bird cluster amplitude. Axes and data are plotted in the same manner as Fig. 44 (page 98).

combined, one could instead look for minimum values of variance around best-fit curves for a subset of the data. Limiting the data to a local subset will ensure that the data belonging to the other cluster do not cause the variance to increase.

The results of the case studies earlier in the chapter showed that the two clusters are more distinct where the radial velocity is a maximum and minimum. Therefore, this method begins by looking for the azimuth where the maximum and minimum radial velocity points exist. Because the clusters are most distinct at the maximum and minimum radial velocity values, the results of this technique will overestimate the viability of this technique.

Once the azimuth where the radial velocity values are a maximum and minimum are found, all data within 15 degrees azimuth of these points are retrieved. Because the difference between the sine of 90 degrees and 75 degrees is very small (approximately 3% difference), we can approximate the entire value of the sine curve with just a single value (straight line on the VAD) and reduce the amount of calculations required.

For the testing of this technique, the variance of all the data was computed for velocity values in 1 knot increments. Because the velocity data is recorded in level-II format to the nearest 0.5 meters per second, this velocity increment provides the highest resolution possible. The IDL program was amended to sort the variances in increasing order, then the nearest 20% (or N/5 variances, where N is the number of data) was summed and divided by N/5. The result for each velocity value was written to a output data file.

The first test of this technique was done on the VAD plot for 5,000 feet on September 6, 2000 at 1:39Z (Fig. 60b). The results of calculating the local variance between 10 degrees and 40 degrees azimuth are contained in Table 9. Only the variance between -40 knots and -10 knots are listed in Table 9 because it is the range of radial velocity values where the two minima in variance exist. From Table 9, the two minima are located at -30 knots and -21 knots. Consulting Fig. 60b, these results match closely with where each of the two clusters are found between 10 degrees and 40 degrees azimuth.

The second test of this technique was done on the VAD plot for 5,000 feet on September 5, 2000 at 1:36Z (Fig. 53a). The results of calculating the local variance between 30 degrees and 60 degrees azimuth are contained in Table 10. Only the variance between -35 knots and -5 knots are listed in Table 10 because it is the range of radial velocity values where the two minima in variance exist. From Table 10, the two minima are located at -26 knots and -14 knots. Consulting Figure 53a, these results match closely where each of the two clusters are found within 30 degrees and 60 degrees azimuth. While two minima can be found in the variance results for this second test, the minimum in variance located at -14 knots represents only a slight decrease in the variance from adjacent values (0.5 to 0.6 knots squared).

Further testing of this technique is required in order to determine how reliable it can detect two VAD clusters. In particular, an investigation whether secondary minima

Table 9. Variance of data from velocity values on September 6, 2000 at 1:39Z for 5,000 feet.

Velocity (knots)	Variance (knots squared)
-40	33.97265
-39	23.7642
-38	15.58014
-37	9.420466
-36	5.259259
-35	2.761658
-34	1.684798
-33	1.418876
-32	1.313019
-31	0.703837
-30	0.605068
-29	0.854718
-28	1.292594
-27	1.991463
-26	2.816244
-25	2.89338
-24	2.055883
-23	1.349595
-22	1.015827
-21	0.710251
-20	0.911959
-19	2.062741
-18	4.275799
-17	7.811769
-16	13.08279
-15	19.86374
-14	28.37353
-13	38.43814
-12	49.92352
-11	63.26683
-10	78.63452

Table 10. Variance of data from velocity values on September 5, 2000 at 1:36Z for 5,000 feet.

Velocity (knots)	Variance (knots squared)
-35	43.81469
-34	31.90894
-33	22.05653
-32	14.25745
-31	8.511702
-30	4.819289
-29	2.834296
-28	1.41577
-27	0.860703
-26	0.54585
-25	0.619004
-24	0.815924
-23	0.982105
-22	1.242782
-21	1.811553
-20	2.66884
-19	3.452779
-18	4.415261
-17	5.000686
-16	4.196584
-15	3.304724
-14	2.813898
-13	2.444514
-12	2.947908
-11	4.497387
-10	6.864046
-9	10.55425
-8	16.29779
-7	23.77601
-6	32.9348
-5	42.68211

can be found in instances where two VAD clusters do not exist needs to be performed. It is conceivable that points on a VAD plot can be randomly clustered near two points and result in two minima in the variance without the existence of birds.

CHAPTER V

CONCLUSIONS

The WSR-88D's VAD Wind Profile (VWP) product has been recognized to have errors when bird migration is taking place (Haro and Gauthreaux 1997). Direct observations of birds in flight (using a moon-watching technique developed by Lowery (1951)) confirmed this on evenings when VWP errors were suspected.

The type of bird migration that has the greatest impact on VWP contamination is nocturnal passerine migration. Because passerines are found to fly alone at night, and because a single songbird can produce a 10 dBZ echo at a range of 30 km, thousands of migrating birds can easily occupy a large amount of space on the PPI. Because the velocity measured by the radar is heavily weighted towards the velocity of the target with the strongest return for that sample volume, a single bird can contaminate the velocity for the radar sample volume that it occupies.

The primary time for passerine bird migration in the spring is from late-February through mid-June; in the fall, the primary time for passerine migration is July through the end of November (O'Bannon 1985). It has been discovered that the number of birds migrating on any particular evening is dependent on weather conditions (Richardson 1978). The primary weather concern appears to be wind; birds prefer to migrate with tailwinds. A second primary concern is precipitation; birds will not fly in precipitation. Therefore, migration is possible during those times of year when tailwinds are present and the weather is fair.

VWP data are used frequently by meteorologists, and are included in some computer models such as the RUC. Therefore, bird contamination of the VWP data is a serious concern since it can lead to errors in weather forecasts. Up until the paper by Zhang et al. (2002), no correction algorithm using current WSR-88D technology has been proposed to warn for the presence of birds, or to remove the birds from the data.

While the method by Zhang et al. (2002) has shown an ability to differentiate biological targets from precipitation, their method might not allow for the true wind to be determined in the presence of birds. By computing a seven-point running mean and computing each radar sample volume's variance to that mean, the likelihood that valid meteorological data will be removed is high; should the number of radar sample volumes with valid targets be small compared with the number of nearby sample volumes with birds, the velocity of the valid sample volume would be at greater odds with the birds' higher velocities. This could result in the valid radar volume having a greater variance from the mean, and result in its exclusion. A better method would allow for the valid meteorological data to be retained, and thereby allow the VWP to report the true wind.

On three consecutive days in early September of 2000, the winds at the surface and aloft were from the northeast. While passerines will migrate across the Gulf of Mexico in the spring, fall migration usually takes place over land. Therefore, the wind conditions from September 4-7, 2000 were ideal for bird migration along the Texas coastline towards Mexico. On these evenings, the Houston WSR-88D VWP was in error when compared with weather balloon launches (from Wharton Power Plant, northwest of downtown Houston) and/or consultation with weather maps.

The current VAD algorithm only uses one specific radar elevation angle at a single specific slant range to obtain the data for its wind calculation. Because of the angular beam width of the radar beam, the radar sample volume size increases with range; at 57 kilometers, it is one kilometer in diameter. The thickness of the radar sample volume along a radial is 250 meters. Therefore, the odds of having a migrating bird, randomly distributed in space, in a radar sample volume increases with range.

To reduce the influence of migrating birds in the data, it is vital to obtain as many radar sample volumes that contain wind-borne targets only as possible. Because of beam spreading, the range of the data being investigated must be limited to nearby ranges only. In addition, including all data adjacent to the reporting altitude in question (altitude thickness) can increase the number of data. Finally, by including all data from every elevation angle within the range limit, a large amount of data with small radar sample volumes is attained.

Should the number of sample volumes containing wind-borne data only be comparable to the number of radar sample volumes containing birds, two clusters should be visible when one looks at the VAD plot for that altitude. One cluster will represent the wind-borne sample volumes, and the other will represent the volumes containing birds.

Looking at the raw VAD plots using the new technique discussed above, two clusters were observed immediately after sunset. One cluster had a shape consistent with the wind velocity being reported and could be assumed to be the cluster due to wind-borne targets only. The second cluster always had a greater amplitude, which

suggested those targets were engaging in powered flight and could reasonably be identified as birds. These two clusters were most apparent at altitudes of 3,000 feet to 7,000 feet, when using all radar sample volumes within a range limit of 80,000 feet and within 100 feet of the reporting altitude. These two clusters remained apparent for at least a couple of hours, but became less apparent with time.

An earlier case with winds not favorable for migration resulted in no two clusters being observed. The existence of two clusters was found to be present only when the VWP was in error (and therefore, when birds were flying). Therefore, the two clusters are a unique feature on the VAD plot when birds are migrating. Because one of the clusters is due to the wind, the VAD could report the actual wind if it were able to determine which cluster is due to the wind.

Because the current VAD algorithm can only calculate one best-fit curve to all the data, a new technique is required. A primary limitation exists on any new algorithm: it must be simple and fast enough for the current Radar Product Generator to handle the additional duties. This computer is charged with processing all the incoming radar data and creating the entire suite of products and algorithms. This task must be completed in the five to ten minute time window between radar volume scans.

One method that involved separating the two clusters of points and running the current VAD algorithm on each curve separately was tested. This method was found to be less than ideal, due to a necessary assumption that the wind cannot change appreciably between volume scans, and because of the inclusion of intersection points from the two clusters. Removing the intersection points proved to be difficult, since the

bird cluster does not always have to have perfect trigonometric shape. Therefore, this method does not appear to be ideal in handling the two clusters.

A second method involves computing the variance in a range of azimuths near the maximum and minimum points on the VAD clusters. The amount of separation between clusters is greatest at these points, since the difference between the bird's radial velocity (vector sum of the wind velocity and the bird's velocity relative to the air) and the wind target's radial velocity is the most at this point. When the radar is pointed orthogonal to the orientation of the birds, the radial velocity for both targets is identical and results in no separation between clusters.

The thickness of the altitude layer being included in the VAD plot needs to be as small as possible. Should a frontal zone or shear zone exist within the thickness level being investigated, two clusters of points will be created due to the two different winds. This would result in a false alarm for migrating birds.

The variance technique has some promise as a warning algorithm, but further testing of its performance is required. The benefits of using this technique to detect two VAD clusters are that it is fairly simple and easy to run. Because the greatest separation between VAD clusters are most often at the relative maximum and minimum points in the VAD curve, the algorithm can use the result of the VAD calculation to know where to look. This detection algorithm can be run after the wind calculation to determine the existence of two clusters. Because two clusters are not visible at all levels and at all times, the detection of two clusters at one level should warn the user of data contamination at all levels until sunrise.

Although an objective detection algorithm remains elusive at the present time, the wind can easily be estimated visually. A radar operator that suspects contamination by migrating birds will be able to visually inspect the VAD plot and determine the existence of birds, and possibly the wind direction and speed, subjectively. As the Radar Product Generator becomes more advanced and more memory is added, the potential exists to develop a more complicated algorithm to detect two curves and calculate the true wind.

The possibility of using reflectivity to differentiate between the two clusters was envisioned towards the end of this work. Because birds return more radar energy than passive clear-air targets, it is possible that the bird cluster will be comprised of radar sample volumes with higher reflectivity values than the wind cluster. Unfortunately, due to time and technical constraints, this possibility could not be explored here.

Future improvements with the WSR-88D, such as dual-polarization, might allow biological data to be removed very easily. Zrnic and Ryzhkov (1997) have shown that birds and insects have unique attributes when looking at polarimetric radar data, such as a lower differential reflectivity and a larger backscatter differential phase. However, this upgrade to the WSR-88D is still some time away. A technique is required not only to work on current and future data prior to the dual-polarization upgrade, but also to run on the large amount of archived radar data that exists.

REFERENCES

Alerstam, T., 1990: *Bird Migration*. Cambridge University Press, 420 pp.

Allen, S., cited 1996: Impacts of optimum slant range on 88D VAD wind profiles. [Available online at http://www.srh.noaa.gov/FTPROOT/HGX/HTML/projects/vad2/main.htm.]

Benjamin, S., K. Brundage, P. Miller, T. Smith, G. Grell, D. Kim, J. Brown, T. Schlatter, and L. Morone, 1994: The rapid update cycle at NMC. Preprints, *10th Conf. on Numerical Weather Prediction*, Portland, OR, Amer. Meteor. Soc., 566-568.

Berthold, P., 1996: *Control of Bird Migration*. Chapman and Hall, 355 pp.

Blokpoel, H. and J. Burton, 1975: Weather and height of nocturnal migration in eastcentral Alberta: A radar study. *Bird Banding*, **46**, 311-328.

Bruderer, B., 1997a: The study of bird migration by radar. Part I: The technical basis. *Naturwissenschaften*, **84**, 1-8.

Bruderer, B., 1997b: The study of bird migration by radar. Part II: Major achievements. *Naturwissenschaften*, **84**, 45-54.

Davis, J.L., R.R. Lee and J.L. Ingram, 1995: Comparing rawinsonde and WSR-88D wind profiles. Preprints, *27th Conf. on Radar Meteorology*, Vail, CO, Amer. Meteor. Soc., 409-411.

Drake, V.A., and R.A. Farrow, 1988: The influence of atmospheric structure and motions on insect migration. *Ann. Rev. Entomol.*, **33**, 183-210.

Eastwood, E., 1967: *Radar Ornithology*. Methuen Co., Ltd., 278 pp.

Edwards, J., and E.W. Houghton, 1959: Radar echoing area polar diagrams of birds. *Nature*, **184**, 1059.

Forsyth, B.J., and D. James, 1971: Springtime movements of transient nocturnally migrating landbirds in the Gulf coastal bend region of Texas. *Condor*, **73**, 193-207.

Gauthreaux, S.A., Jr., 1969: A portable ceilometer technique for studying low-level nocturnal migration. *Bird-Banding*, **40**, 309-320.

———, 1970: Weather radar quantification of bird migration. *BioScience*, **20**, 17-20.

———, and K.P. Able, 1970: Wind and the direction of nocturnal songbird migration. *Nature*, **228**, 476-477.

———, 1971: A radar and direct visual study of passerine spring migration in southern Louisiana. *Auk*, **88**, 343-365.

———, 1972: Behavioral responses of migrating birds to daylight and darkness: A radar and direct visual study. *Wilson Bull.*, **84**, 343-365.

———, 1991: The flight behavior of migrating birds in changing wind fields: Radar and visual analyses. *Amer. Zool.*, **31**, 187-204.

———, and C.G. Belser, 1998: Displays of Bird Movements on the WSR-88D: Patterns and Quantification. *Wea. Forecasting*, **13**, 453-464.

———, D.S. Mizrahi, and C.G. Belser, 1998: Bird migration and bias of WSR-88D wind estimates. *Wea. Forecasting*, **13**, 465-481.

Haro, J., and S. Gauthreaux, 1997: WSR-88D VAD wind profile data influenced by bird migration over the southwest United States. NOAA Tech. Memo. NWS WR-244, 26 pp. [Available from National Technical Information Service, U.S. Dept. of Commerce, 5285 Port Royal Rd., Springfield, VA 22161.]

Hassler, S.S, R.R.Graber, and F.C. Bellrose, 1963: Fall migration and weather, a radar study. *Wilson Bull.*, **75**, 56-77.

Jungbluth, K., J. Belles, and M. Schumacher, 1995: Velocity contamination of WSR-88D and wind profiler data due to migrating birds. Preprints, *27th Conf. on Radar Meteorology*, Vail, CO, Amer. Meteor. Soc., 666-668.

Kaufman, K., 1996: *Lives of North American Birds*. Houghton Mifflin, 675 pp.

Kerlinger, P., 1995: *How Birds Migrate*. Stackpole Books, 228 pp.

Klazura, G.E., and D.A. Imy, 1993: A description of the initial set of analysis products available from the NEXRAD WSR-88D system. *Bull. Amer. Meteor. Soc.*, **74**, 1293-1311.

Larkin, R.P., 1990: Flight speeds observed with radar, a correction: Slow "birds" are insects. *Behav. Ecol. Sociolbiol.*, **29**, 221-224.

———, 1991: Sensitivity of NEXRAD algorithms to echoes from birds and insects. Preprints, *25th Conf. on Radar Meteorology*, Paris, France, Amer. Meteor. Soc., 203-205.

Lhermitte, R.M., and Atlas, D., 1961: Precipitation motion by pulse Doppler radar. *Proc. Ninth Wea. Radar Conf.*, Boston, MA., Amer. Meteor. Soc., 218-223.

Liechti, F., B. Bruderer, and H. Paproth, 1995: Quantification of nocturnal bird migration by moonwatching: Comparison with radar and infrared observations. *J. Field Ornithology*, **66**, 457-468.

Lowery, G.H., Jr., 1951: A quantitative study of the nocturnal migration of birds. *Univ. Kansas Publ. Mus. Nat. Hist.*, **3**, 361-472.

NCDC, cited 2003: WSR-88D visualization software. [Available online at ftp.ncdc.noaa.gov.]

Nisbet, I.C.T., 1959: Calculation of flight directions of birds observed crossing the face of the moon. *Wilson Bull.*, **71**, 237-243.

NOAA, 1991a: Doppler radar meteorological observations. Part B, Doppler radar theory and meteorology. Federal Meteorological Handbook 11, Rep. FCM-H11B-1991, Office of the Federal Coordinator for Meteorological Services and Supporting Research, 228 pp. [Available from National Climatic Data Center, 151 Patton Ave., Rm. 120, Asheville, NC 28801-5001.]

———, 1991b: Doppler radar meteorological observations. Part C, WSR-88D products and algorithms. Federal Meteorological Handbook 11, Rep. FCM-H11C-1991, Office of the Federal Coordinator for Meteorological Services and Supporting Research, 210 pp. [Available from National Climatic Data Center, 151 Patton Ave., Rm. 120, Asheville, NC 28801-5001.]

———, 1991c: Doppler radar meteorological observations. Part D, WSR-88D unit description and operational applications. Federal Meteorological Handbook 11, Rep. FCM-H11D-1991, Office of the Federal Coordinator for Meteorological Services and Supporting Research, 208 pp. [Available from National Climatic Data Center, 151 Patton Ave., Rm. 120, Asheville, NC 28801-5001.]

NSSL, cited 1997: WSR-88D algorithm testing and display software. [Available online at ftp://nssl.nssl.noaa.gov.]

O'Bannon, T., 1995: Anomalous WSR-88D wind profiles - migrating birds? Preprints, *27th Conf. on Radar Meteorology*, Vail, CO, Amer. Meteor. Soc., 663-665.

Richardson, W.J., 1978: Timing and amount of bird migration in relation to weather: A review. *Oikos*, **30**, 224-272.

Rinehart, R.E., 1999: *Radar for Meteorologists*. Rinehart Publications, 428 pp.

Simpson, J.E., 1994: *Sea Breeze and Local Wind*. Cambridge University Press, 234 pp.

USNO, cited 1997: U.S. Naval Observatory Astronomical Applications Department. [Available online at http://aa.usno.navy.mil/data/docs/AltAz.html.]

Wilczak, J.M., R.G. Strauch, F.M. Ralph, B.L. Weber, D.A. Merritt, J.R. Jordan, D.E. Wolfe, L.K. Lewis, D.B. Wuertz, J.E. Gaynor, S.A. McLaughlin, R.R. Rogers, A.C. Riddle, and T.S. Dye, 1995: Contamination of wind profiler data by migrating birds: Characteristics of corrupted data and potential solutions. *J. Atmos. Oceanic Technol.*, **12**, 449-467.

Zhang, P., Q. Xu, and A. Ryzhkov, 2002: Identification of biological scatterers and radar data quality control. Preprints, *21st Conf. on Severe Local Storms*, San Antonio, TX, Amer. Meteor. Soc., 208-209.

Zrnic, D.S, and A.V. Ryzhkov, 1997: Recognition of nonmeteorological echoes with a dual-polarization radar. Preprints, *28th Conf. on Radar Meteorology*, Austin, TX, Amer. Meteor. Soc., 5-6.

VITA

Karl Werner Schulze was born to Werner and Mary Schulze on June 27, 1969 in Waukegan, Illinois. He lived his first 5 years in North Chicago, Illinois before moving to Waukegan, Illinois, where he lived until graduating from Waukegan East High School in January, 1987. Karl obtained his B.S. degree in Meteorology from Northern Illinois University in May, 1996, after attending flight school in Wisconsin (no degree earned).

In August, 1996, Karl moved to Texas to obtain his Masters degree at Texas A&M University. In addition to his own research, he also took part as a radar operator in the TEFLUN-A project in 1997, and as a forecaster in the TexAQS 2000 project in 2000. During the fall semester of 1999, Karl was the instructor of record for METR 151 and enjoyed this experience very much. In January 2001, he was asked by the Texas A&M Student Chapter of the American Meteorological Society to run the student-run storm chasing organization, the Texas A&M Mobile Severe Storms Data Acquisition (TAMMSSDA). While the coordinator for TAMMSSDA, he rewrote the organization's rules and procedures and led a group of students to intercept the first TAMMSSDA tornado on May 1, 2001 near Cordell, Oklahoma.

Karl enjoys traveling and has spent significant time away from Texas as well, traveling to 15 countries on 5 continents, most of them on more than one occasion.

Mr. Schulze can be reached at the following permanent address:

1950 North Avenue

Waukegan, Illinois 60087